Scuola Internazionale Superiore di Studi Avanzati - SISSA
International School for Advanced Studies

Neurobiology Group
Trieste, Italy

Spontaneous and stimulus-evoked spiking activities in olfactory sensory neurons from Kir2.1 knock-in and TMEM16B knock-out mouse models.

Thesis submitted for the degree of “Doctor Philosophiae”

Academic Year 2014/2015

CANDIDATE

Pietra Gianluca

SUPERVISORS

Prof. Anna Menini
Dr. Anna Boccaccio

DECLARATION

The original work presented in this Thesis was carried out at the International School for Advances Studies, SISSA, Trieste, between November 2011 and October 2015 under the supervision of Dr. Anna Boccaccio and Prof. Anna Menini.

I performed and analyzed all the electrophysiological experiments from OSNs in loose patch.

ABSTRACT

The sense of smell enables animals to detect myriads of different odors carrying information about the quality of food, the presence of pathogens, prey, predators, or potential mates. Olfactory sensory neurons (OSNs) in the nasal cavity are the interface of the main olfactory system with the external environment. The binding of an odorant molecule to specific olfactory receptors (OR) located in the cilia of these neurons triggers a transduction cascade that transduces the chemical signal into action potentials which travel along the axon of the OSNs to the olfactory bulb. Here, the odor information is processed and conveyed to higher brain centers, ultimately leading to the perception of smell.
In this Thesis I studied the effect of two genetic manipulations on the firing activity of the OSNs: the ectopic overexpression of the inward rectifier potassium channel Kir2.1 and the deletion of the *TMEM16b/Ano2* gene, that codes for the Ca^{2+}- activated chloride channel TMEM16B.

The overexpression of Kir2.1 reduces the excitability of the neurons, and when expressed in OSNs, mice show a general disorganization of the glomerular map in the olfactory bulb. Since spontaneous and sensory-evoked electrical activity play important roles in the formation of several sensory circuits, including the olfactory system, in the first part of this Thesis, I investigated how the spiking activity of mouse OSNs is influenced by the Kir2.1 overexpression, using loose-patch recordings from the OSNs knobs. I found that the overexpression of Kir2.1 caused a decrease in the spontaneous firing activity of OSNs but did not influence the evoked firing properties induced by odorant stimulation, indicating that the olfactory bulb disorganization was caused by a reduced spontaneous firing activity.

Ca^{2+}-activated Cl^- current (CaCC) is an important component of the transduction current evoked by odor stimulation in OSNs. Binding of odorants to their specific receptor on the cilia of OSNs causes the activation of adenylyl cyclase with a relative increase of intracellular cAMP, activating cyclic nucleotide-gated (CNG) channels. Ca^{2+} entry through CNG channels increases the open probability of Ca^{2+}-activated Cl^- channels. The molecular identity of these channels has been elusive for a long time, but recently it has been shown that the olfactory CaCC are mediated by the membrane protein TMEM16B/Anoctamin2. However, the physiological role of olfactory CaCC is still unclear, and the first description of TMEM16B knockout (KO) mice reported no clear olfactory deficits.
In the second part of this Thesis, I studied basal firing properties and stimulus-evoked responses with loose-patch recordings in OSNs from TMEM16B KO or WT mice. OSNs responded to a stimulus with a transient burst of action potentials. Responses of OSNs from TMEM16B KO mice showed an increased number of action potentials compared to responses from WT mice, both in OSNs expressing a random or I7 OR.

The basal spiking activity of individual OSNs is correlated with the expressed OR that drives basal transduction activity. I measured a reduced basal activity in TMEM16B KO OSNs expressing the I7 OR compared to WT OSNs. Moreover, axonal targeting was altered and TMEM16B KO had supernumerary I7 glomeruli compared to WT. These results show that the expression of TMEM16B affects OSNs firing properties and contributes to the glomerular formation and refinement of I7-expressing OSNs in the olfactory bulb, suggesting a crucial role for TMEM16B in normal olfaction.

INDEX

PAG.

PICTURE INDEX

PAG.

TABLE INDEX

PAG.

ABBREVIATIONS

(ACIII) type III adenylyl cyclase

(ACSF) artificial cerebro spinal fluid

(CaCC) Ca^{2+}-activated Cl^- current

(cAMP) cyclic AMP

(CNG) cyclic nucleotide gate

(DMSO) dimethyl sulfoxide

(EOG) electroolfactogram

(GFP) green fluorescent protein

(GPCR) G-protein coupled receptor

($G_{\alpha olf}$) olfactory α subunit of the coupled G protein

(IBMX) isobutyl-1-methylxanthine

(IF) instantaneous frequency

(IRES) internal ribosome entry site

(ISI) inter-spike interval

(ISO) isoamyl acetate

(Kir2.1) OMP-IRES-tTA/Teto X Kir2.1-IRES-tau-LacZ

(KO) knock-out

(MOB) main olfactory bulb

(MOE) main olfactory epithelium

(NKCC1) $Na^+K^+/2Cl^-$ cotransporter

(OB) olfactory bulb

(OE) olfactory epithelium

(OMP) olfactory marker protein

(OSN) olfactory sensory neuron

(OR) olfactory receptor

(PDE) phosphodiesterase

(tauGFP) tau-green fluorescent protein

(WT) wild type

1 INTRODUCTION

1.1 - The olfactory system

1.1.1 - Chemosensation and Olfaction

Chemosensation is used to analyze some of the chemical stimuli of the external environment and is an essential survival tool in the animal world, providing information regarding food, mates, danger, predators and pathogens. In mammals, chemosensation is composed of two distinct senses, olfaction and taste, and I will focus on the description of olfaction. In rodents, olfaction is mediated by the main olfactory system (described in section 1.1.2) and by three additional olfactory subsystems (Fig. 1): the vomeronasal organ, detecting pheromones, which are chemical cues important for social behavior, the Grueneberg ganglion, which is composed of two small patches of neurons involved in the detection of alarm pheromones, the septal organ of Masera, situated in the air path, possibly also involved in pheromone detection (Munger *et al.*, 2009; Tirindelli *et al.,* 2009; Ma, 2010; Francia *et al.*, 2014).

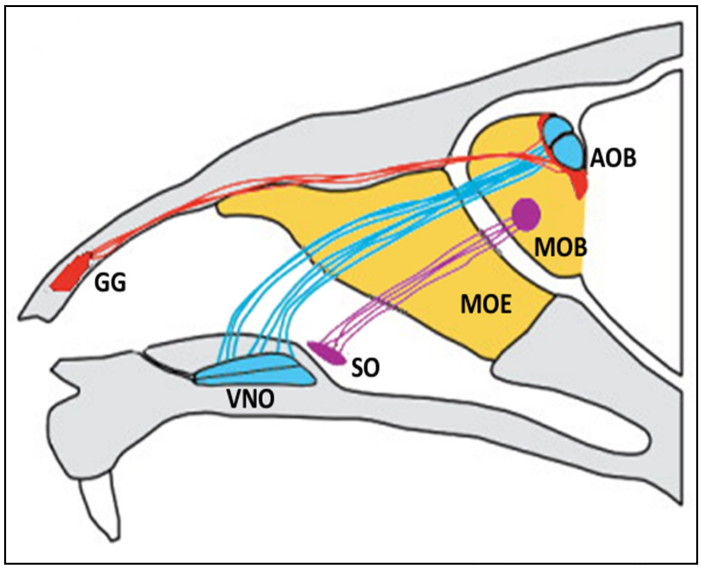

Figure 1 – Olfactory systems
Sagittal view of the mouse nose showing the olfactory systems organization. Each olfactory subsystem is represented by a different color. In yellow the main olfactory epithelium (MOE) and main olfactory bulb (MOB). In blue the vomeronasal organ (VNO) which projects to the accessory olfactory bulb (AOB). In purple the septal organ of Masera (SO) subsystem and its axonal projections to the olfactory bulb. In red the Grueneberg ganglion (GG) and its projections to the olfactory bulb. [modified from Munger *et al.*, 2009]

In this Thesis, I have focused on the main olfactory system, which detects and discriminates thousands of volatile molecules with different structures across a wide range of concentrations.

1.1.2 - Organization of the main olfactory system in mice

The main olfactory system mainly carries information about volatile molecules in the external environment, the quality of food, the presence of pathogens, prey, predators, or potential mates (Firestein, 2001). The main olfactory system is composed by the main olfactory epithelium (MOE), the main olfactory bulb (MOB), and higher olfactory centers. The MOE is located in the ventral dorsal section of the nasal cavity and is the interface of the main olfactory system with the external environment (Fig. 1). Indeed, volatile molecules reach the MOE when air is inhaled, and bind to olfactory receptors (ORs) expressed by olfactory sensory neurons (OSNs). The binding of molecules to ORs is transduced in action potentials that travel across the

axons of OSNs throughout the cribriform plate to reach the MOB, which is located in the ventral part of the forebrain. Axons of OSNs synapse with second order neurons (mitral or tufted cells) in the MOB, which in turn project to several cortical areas collectively named “primary olfactory cortex”, including the piriform cortex and the cortical amygdala. Differently from other sensory systems, the olfactory system sends signals directly to the cortex without first connecting to the thalamus. Neurons of the primary olfactory cortex directly project to the orbitofrontal cortex and also to the hippocampus, hypothalamus and mediodorsal nucleus of the thalamus. (Munger *et al.*, 2009; Tirindelli *et al.*, 2009; Pifferi and Menini, 2015).

1.1.2.1 - The main olfactory epithelium

The MOE is a pseudostratified sensory epithelium located in the nasal cavity. It covers the dorsal-posterior part of the nasal septum bone and turbinates and is flanked ventrally by the respiratory epithelium (Fig. 2A). It is composed of cell types with distinct morphology and function: the OSNs (described in section 1.2), the supporting cells, the basal cells and a small heterogeneous population of microvillar cells. In addition, the epithelium is traversed by secretory ducts of the Bowman’s glands, whose acini reside in the lamina propria (Fig. 2B).

The supporting cells are aligned almost in a single layer at the apical part of the epithelium. They are columnar epithelial cells with broad apical cell bodies and basal branched projections towards the lamina propria. Their apical membrane is structured in a series of microvilli which protrude into the nasal cavity and are intermixed with the OSN cilia (Nomura *et al.*, 2004). Although the physiological function of supporting cells in mammals is still unknown, some studies suggest that these cells have a supporting role similar to glial cells in the brain, and also metabolize the inhaled xenobiotic molecules (Dahl and Hadley, 1991; Ling *et al.*, 2004). Additionally, they regulate the ionic composition of the mucus (Menco *et al.,* 1998; Rochelle *et al.*, 2000) and electrically isolate the OSNs (Breipohl *et al.*, 1974).

Basal cells are located in the basal part of the MOE and can be divided into two types, horizontal and globose basal cells. Some basal cells are stem cells, capable of regenerating OSNs in the MOE throughout life (Carter, 2004; Huard *et al.*, 1998). Indeed, this continued process of neurogenesis cyclically renews the entire OSN population (Brann *et al.*, 2014), which in any time of an adult mouse is composed of mature OSNs located in the apical part of the MOE, with immature OSNs found in lower parts of the epithelium (Graziadei and Graziadei, 1978).

Mature OSNs are the first order bipolar neurons of the main olfactory system, devoted to detecting the presence of odors in the nasal cavity and transduce them into electrical signals (Kleene, 2008; Pifferi *et al.*, 2010; Schild and Restrepo, 1998). They have a bipolar morphology with a single dendrite, soma and axon. The axon of each OSN passes through the cribriform plate and synapses with the dendrites of MOB second order cells. The apical section is constituted of dendrite which protrudes toward the luminal surface of the epithelium and terminates with a knob with several cilia exposing their membrane to the external

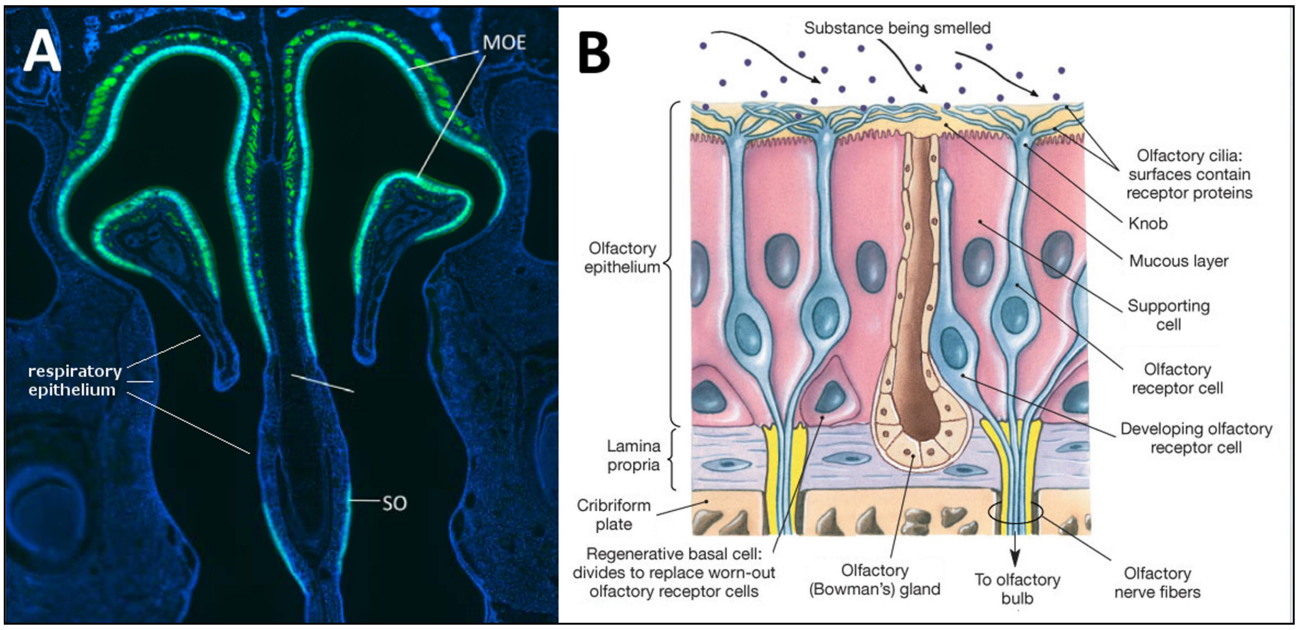

Figure 2 – Olfactory epithelium
(A): Coronal section of nasal cavity from an OMP-GFP mouse at the level of septal organ (SO). The mouse strain is engineered to express green fluorescent protein (GFP) instead of olfactory marker protein (OMP) a cytosolic protein highly expressed in OSNs. The signal in the dorsal section represents MOE flanked ventrally by respiratory epithelium. [Unpublished image of Maurya and Menini with permission from the authors]
(B): Schematic representation of the MOE showing the organization of the different cell types in the tissue [modified from Anatomy and Physiology Laboratory Manual, Marieb *et al.*, 2013]

environment to contact odorant molecules. ORs and other proteins involved in olfactory transduction are expressed in the cilia.

Each OSN expresses one OR type among ~1000 possibilities. In rat, ORs are spatially distributed into four zones along the MOE antero-posterior axis. Each OR gene is expressed in only one zone, but within it, the OSNs expressing the OR gene are randomly scattered (Ressler *et al.*, 1993; Sullivan *et al.*, 1993; Vassar *et al.*, 1993; Strotmann *et al.*, 1992). In mice, the OR zonal organization has not been found, although localization of specific ORs in defined areas of the sensory epithelium have been shown (Mombaerts *et al.*, 1996, Bozza *et al.*, 2002).

A minor cell population in the MOE is constituted of microvillar cells whose physiological role is unclear (Menco and Morrison, 2003; Elsaesser and Paysan, 2007). Microvillar cells are not a homogenous population of cells but they include different cellular subsets expressing distinct signal transduction molecules (Elsaesser *et al.*, 2005). It is unclear whether they project an axon to the olfactory bulb (Asan and Drenckhalm, 2005; Rowley *et al.*, 1989).

1.1.2.2 - The main olfactory bulb

The MOB is the first integration center of the olfactory information mediated by the main olfactory system (Munger *et al.*, 2009). In mice, it is localized in the frontal lobe of the brain, dorso-posterior of the nasal cavity and immediately above the cribriform plate. Axons from OSNs of the MOE pass through the

cribriform plate and innervate the olfactory bulbs. Histologically, the MOB is structured in four different layers composed of morphologically distinct cell types (Fig. 3B) (Shepherd *et al.*, 2011): glomerular layer, the most external layer that receives input from OSNs; external plexiform layer; mitral cell layer and inner plexiform layer. The glomerular layer contains the glomeruli, spherical neuropil conglomerates of 50–100 µm in diameter composed of the OSN axon terminals and the apical dendrites of the mitral and tufted cells.

The OSN axon terminals expressing the same OR coalesce and form one medial and one lateral glomeruli, creating two mirror-image maps within each olfactory bulb (Fig. 3A) (Mombaerts *et al.*, 1996). Glomeruli are the MOB functional units. They integrate afferent signals from thousands of OSNs, and relay output via several dozen mitral/tufted cells.

Inside a glomerulus, the OSN axons synapse directly with inhibitory interneurons and with tufted cells and mitral cells. The inhibitory interneurons are located in the glomerular layer and modulate the incoming olfactory information. They are divided into short axon cells, innervating lateral glomeruli, and periglomerular cells, inhibiting the same glomerulus from which they are stimulated (Fig.3B) (Murphy *et al.*, 2005). Instead, tufted and mitral cells are housed in the external plexiform layer and in the mitral cell layer respectively (Shepherd *et al.*, 2011). Each tufted and mitral cell targets its primary dendrite to only one glomerulus and sends its axon through the lateral olfactory tract to various areas of the olfactory cortex (Sosulski *et al.*, 2011).

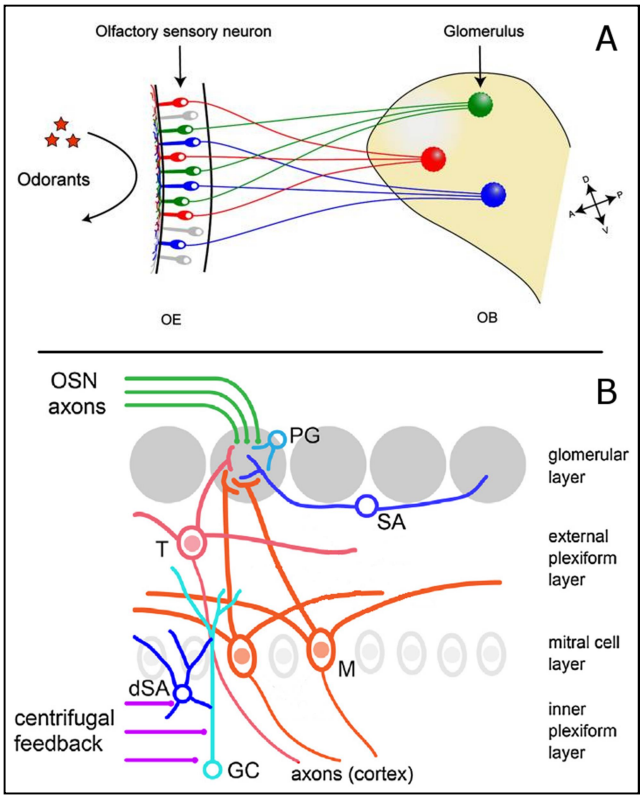

Figure 3 – Main olfactory bulb
Schemes of the MOB organization (A): OSN axonal targeting from MOE to the MOB. OSNs expressing the same OR are represented with the same color and converge on the same glomerulus in the MOB
(B): Schematic representation of layer organization in MOB. OSN axons synapse in a glomerulus with tufted (T), mitral (M), periglomerular (PG), and short axon cells (SA). Granule cells (GC) and deep short axon cells (dSA) receive centrifugal feedback from olfactory cortex, leading to inhibition or disinhibition of mitral/tufted cells. [modified from Takeuchi and Sakano, 2014 (A) and Imai, 2014 (B)]

An important feature in maximizing the discriminatory power of the olfactory system is the combination of the convergence of axons of OSNs expressing the same OR to a glomerulus and the targeting of the main dendrites of mitral and tufted cells to one glomerulus (Imai, 2014).

Additionally, olfactory cortex manipulates the information which flows through the MOB by feedback fibers which reach the inner plexiform layer and modulate the activity of two types of inhibitory interneurons: deep short axon cells and granule cells (Markopoulos *et al.*, 2012). The projections of these cells interact

with secondary lateral dendrites of mitral and tufted cells in the external plexiform layer producing a later inhibition which modulates the activity of the mitral and tufted cells (Egger *et al.*, 2003).

Each glomerulus integrates afferent signals from thousands of OSNs, and relays output through several dozen mitral and tufted cells. The projections of these cells are distributed via the lateral olfactory tract to several areas of the brain like the piriform cortex, olfactory tubercle, anterior olfactory nucleus and specific parts of the amygdala and entorhinal cortex. These areas are collectively named the olfactory cortex (Imai, 2014).

1.2 - The olfactory sensory neurons

OSNs are first order neurons of the main olfactory system. In rodents, the cell body has a spindle-like shape with a diameter of 5-8 µm that is located in the lower two-thirds of the MOE and flanked by the supporting cells (Fig. 2B and 4A). The basal part is composed of an axon which synapses with second order neurons in the MOB. The apical part is a dendrite ending in a spherical swelling of 1-2 µm diameter named knob, from which departs the cilia - columnar structures of 0.1-0.3 µm in diameter and 15-60 µm in length (Fig. 4B). Each OSN in rodents has tens of non-motile cilia, completely immerged in the mucus produced by the Bowman's glands. Since the cilia are dedicated to odor detection, their morphology is optimized for maximization of their surface exposed to the external environment. It has been estimated that the cilia increase the knob surface by ~40 times in mouse OSNs (Menco, 1997). Volatile molecules are detected by specific ORs expressed in the cilia and each OSN expresses only one type of OR among ~1000 functional ones identified in the mouse genome (Buck and Axel, 1991; Adipietro *et al.*, 2012). Moreover, ultrastructural and immunohistochemistry studies have shown that all the key proteins of the olfactory

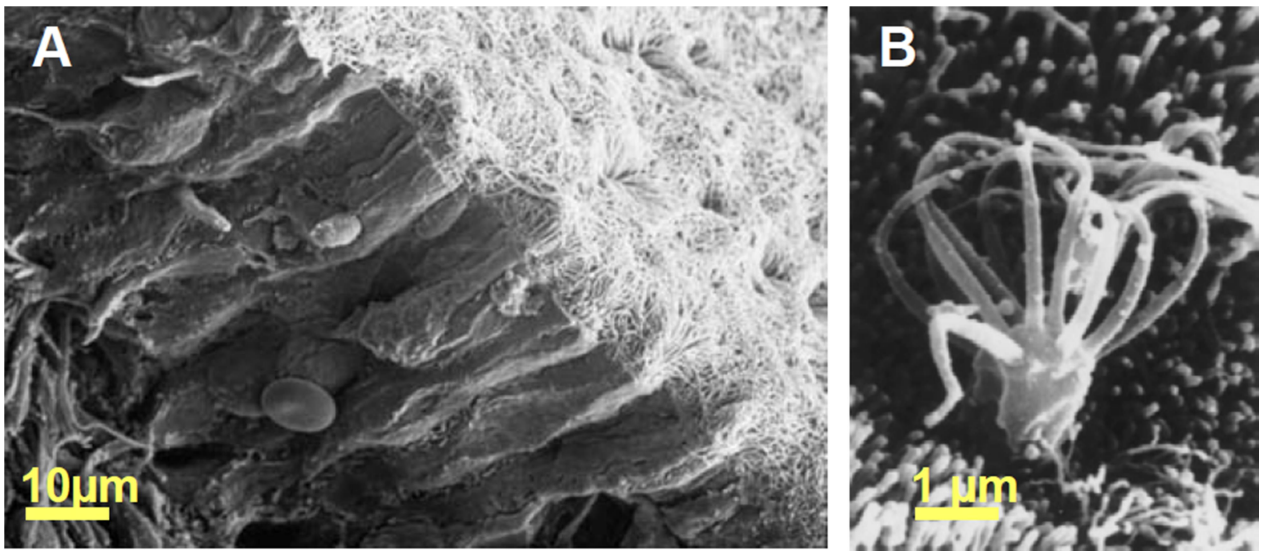

Figure 4 – Olfactory sensory neurons
(A) Microphotograph of a sectioned human olfactory epithelium obtained by scanning electron microscopy. (B) Magnification of a single knob of olfactory sensory neuron where cilia are visible [modified from Morrison and Costanzo, 1990]

transduction are localized on the ciliary membrane *(*Menco *et al.*, 1992; Matsuzaki *et al.*, 1999, Flannery *et al.*, 2006; Maurya and Menini, 2014).

1.2.1 - Passive electrical properties and ionic environment of olfactory sensory neurons

The resting electrical properties of the OSN in mice as well as the ion environment of the ciliary membrane play fundamental roles in shaping both the spontaneous and evoked electrical activity. OSNs in mice are characterized by a high input resistance measured around the 4 GΩ (Ma *et al.*, 1999). This feature implies that small receptor currents are sufficient to depolarize OSNs and to trigger action potentials. Studies performed with OSNs in rats, which have very similar electrical properties to mice (Ma *et al.*, 1999), reported that the opening of a single channel was enough to induce a generation of action potentials (Lynch and Barry, 1989). The resting potential of an OSN recorded in whole-cell, cell-attached and perforated patch configurations is variable; it is estimated to range from -40 to -90 mV with an average of around -55 mV (in whole-cells, Lagostena and Menini, 2003; cell-attached, Maue and Dionne, 1987; and perforated patch, Ma *et al.*, 1999; for a review, Schild and Restrepo, 1998). However, given the high input-resistance of OSNs, measurements of the resting potential are probably underestimated and the real potential is about -75 mV (Pun and Kleene, 2004). To have a reliable measurement of the membrane resting potential, it is necessary that the resistance of the seal between the patch pipette and the cell membrane is much higher than the resistance of the cell membrane, which is unusually high in OSNs (Lynch and Barry, 1989).

The OSN ionic environment is another important feature that affects the electrical activity of OSNs (Table 1), because it determines the driving force for the various ions. The cilia and knobs are exposed to the mucus whose ionic composition is unclear and probably variable, while the dendrite and soma are exposed to interstitial and baso-lateral fluids.

	$[Ion]_{in}$ (mM)	$[Ion]_{mucus}$ (mM)	E_{Nernst} (mV)
Na^+	53 ± 31	55 ± 12	+1
K^+	172 ± 23	69 ± 10	-24
Free Ca^{2+}	40 ± 9 *10^{-6}	4.8	+156
Cl^-	54 ± 4	55 ± 11	0

Table 1 – Resting electrochemical gradients at the apical part of olfactory sensory neurons
Most of the ionic concentrations shown were measured by energy-dispersive X-ray microanalysis in dendritic knobs of rat OSNs (Reuter *et al.*, 1998). Those values represent total rather than free ionic concentrations. Three of the concentrations were measured by other methods, as follows. Intraciliary [Ca^{2+}] was measured in salamander cilia with a Ca^{2+}-sensitive fluorescent dye (Leinders-Zufall *et al.*, 1997). Extracellular [Ca^{2+}] was determined with a Ca^{2+}-sensitive microelectrode in olfactory mucus of rat (Crumling and Gold 1998); the value shown is the midpoint of the reported range (2.6–7.1 mM). $[Cl^-]_{in}$ was measured in the dendritic knobs of rat OSNs with a Cl^--sensitive fluorescent dye (Kaneko *et al.*, 2004). [Table modified from Kleene, 2008].

Few studies have addressed the ionic composition of the mucus, in which the cilia of the OSNs are embedded, and there is no consistency among them, which is likely caused by cytosol or interstitial fluid contamination and the use of different species and techniques (Reuters *et al.*, 1998; Joshi *et al.*, 1987; Bronshtein and Leontev, 1972). Interstitial fluid is characterized by 100-120 mM for Cl^- and 2-5 mM for K^+. Additionally, estimations of 55 mM for Cl^-, 55 mM for Na^+ and 69 mM for K^+ have been obtained applying energy-dispersive x-ray microanalysis to samples of rat mucus (Reuters *et al.*, 1998). Ca^{2+} extracellular concentration has been estimated to range from 2.6–7.1 mM when measured with a Ca^{2+}-sensitive microelectrode in olfactory mucus of rats (Crumling and Gold, 1998). Moreover, Reuter *et al.,* (1998) measured the ionic composition of the cytoplasm in the dendritic knobs, estimating an unusually high Cl^- concentration of 69 mM. This finding has important consequences and will be discussed in detail in paragraph 1.4.1.

1.2.2 - Spontaneous activity in mouse olfactory sensory neurons

Mouse OSNs show heterogeneous spontaneous firing activity in the absence of any molecule which may induce stimulation, when measured with extracellular electrophysiological recordings on dissociated OSNs with suction electrodes (Reisert and Matthews, 2001a; Reisert, 2010), or in cell-attached and perforated-patch configuration from intact epithelium (Connelly *et al.*, 2013; Jarriault and Grosmaitre, 2015). The mean firing frequency ranges from 0 - 3 Hz in dissociated cells (Reisert, 2010) and from and 0 - 9 Hz in intact epithelium (Connelly *et al.*, 2013). The firing pattern is heterogeneous and is composed of single action potentials and bursts of spikes with a duration of few milliseconds with a large variability amongst different neurons (Fig. 5A) (Connelly *et al.*, 2013). Recently, it has been reported that OSN spontaneous activity is related to the expression of a specific OR (Fig. 5B) (Reisert, 2010, in dissociated neurons; Connelly *et al.*, 2013, in intact epithelium). ORs can activate spontaneously the transduction molecular cascade, producing a basal firing activity. Different ORs may have different

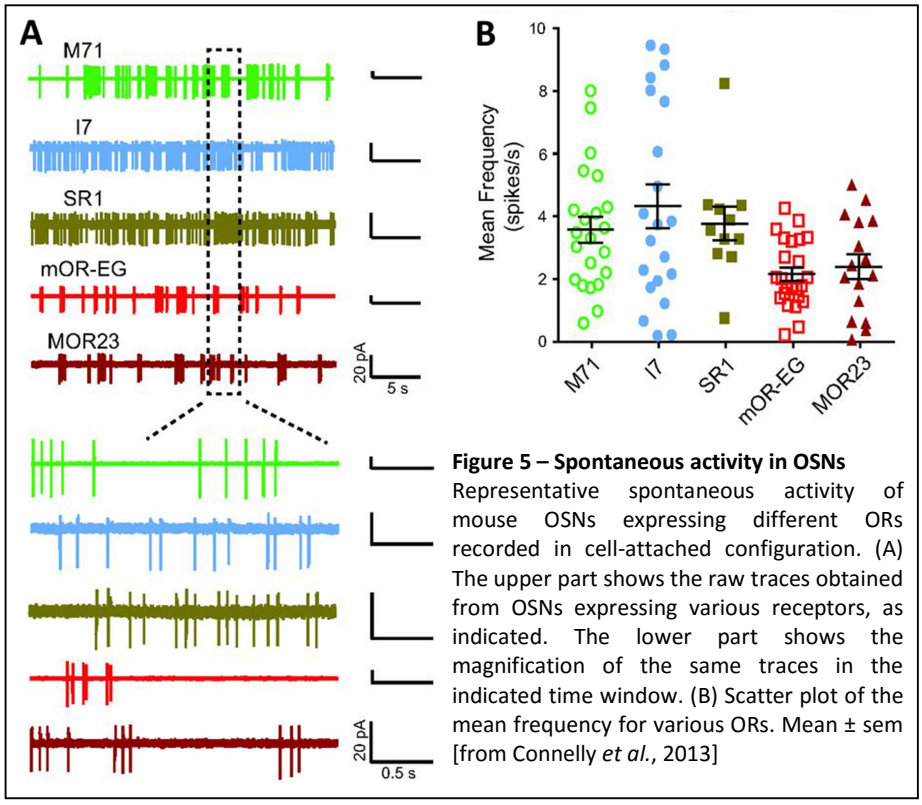

Figure 5 – Spontaneous activity in OSNs
Representative spontaneous activity of mouse OSNs expressing different ORs recorded in cell-attached configuration. (A) The upper part shows the raw traces obtained from OSNs expressing various receptors, as indicated. The lower part shows the magnification of the same traces in the indicated time window. (B) Scatter plot of the mean frequency for various ORs. Mean ± sem [from Connelly *et al.*, 2013]

molecular properties to trigger the cascade. Despite the expression of different ORs produces a different basal activity, a large variability of the spontaneous activity has also been observed within a population of OSNs expressing the same OR (Fig. 5B) (Connelly *et al.*, 2013; Reisert, 2010). The function and reason of the high variability of the spontaneous activity in OSNs have not yet been addressed.

It is well known that in other sensory systems, such as hearing and vision, spontaneous activity during the first phases of development is essential in shaping and organizing higher sensory centers (reviews; MacVicar, 2015; Kirkby *et al.*, 2013). The role of basal activity in olfaction is much less understood. A genetic approach indicated that spontaneous activity in OSNs is essential for correct wiring of OSNs to target glomeruli in the MOB, although a thorough electrophysiological analysis of spontaneous spiking activity was missing (Yu *et al.*, 2004). This phenomenon has important consequences and will be discussed in detail in the following paragraph (1.2.3).

1.2.3 - Axonal targeting of olfactory sensory neurons to olfactory bulb glomeruli

In the nervous system, the connection specificity is essential to translate electrical activity into meaningful neuronal code. In olfaction, OSNs send axonal projections to the MOB and, although there are hundreds of glomeruli in the external layer of the MOB, all OSNs expressing the same OR converge only to two glomeruli, one in the medial and one in the lateral side of each bulb (Mombaerts *et al.*, 1996). Additionally, each glomerulus receives afferences only from the OSNs expressing the same OR. This draws a sensory map, where the glomerulus is the functional unit and the information coming from a single type of OR is segregated (Fig. 3A). However, new OSNs differentiate continually from basal cells replacing the old neurons and therefore a precise mechanism of wiring is necessary throughout the mouse life span in order to maintain a correct bulb organization (Mori and Sakano, 2011).

Neuronal activity of primary neurons is essential in shaping and organizing higher sensory centers in the visual system, for example the thalamus and primary visual cortex (Berardi *et al.*, 2003, Spolidoro *et al.*, 2009). In olfaction, genetic approaches indicated that spontaneous activity of OSNs play a role in the wiring process to the MOB (Yu *et al.*, 2004). This study used a mouse strain genetically modified to overexpress the inwardly rectifying potassium channel Kir2.1 in the OSNs, a channel that should hyperpolarize the neurons and considerably reduce the spontaneous firing activity. This condition delayed the development of a MOB sensory map and induced a general mis-targeting of OSNs axons on the glomeruli, producing a general disorganization of the bulbs (Yu *et al.*, 2004).

Using a similar genetic approach where the overexpression of Kir2.1 in OSNs can be conditionally silenced using doxycycline, a recent study has shown the presence of a critical period in olfaction (Ma *et al.*, 2014). They reported that it was possible to reestablish the right connections to the olfactory bulb only within postnatal day 21 (P21) in mice. After this critical period, any perturbation of the OSN axonal targets was not reversible, suggesting the possibility that two distinct mechanisms for targeting are used before and after

P21 (Ma *et al.*, 2014). Nevertheless, a general inhibition of the OSN synaptic release, induced by the expression of light chains of tetanus protein in 70% of the OSNs did not influence the development and maintenance of the bulb sensory map (Yu *et al.*, 2004).

1.3 - Olfactory transduction

1.3.1 - The molecular cascade of the olfactory transduction

The olfactory transduction is a chain of molecular events which occurs in the cilia of the OSNs following the binding of an odor to a specific OR (Fig. 6) (Malnic, 2007). It translates a chemical signal into an electrical one. In other words, the binding of odor molecules to an OR is transduced in a ciliary inward current which depolarizes the OSN leading to the generation of action potentials that convey the chemosensory information to the olfactory bulb. ORs belong to the family of G-protein coupled receptors with seven transmembrane domains (Buck and Axel, 1991). About 1400 OR genes have been found in mouse genome, but only ~1000 are expressed; the remaining are pseudogenes (Zhang and Firestein, 2002; Godfrey *et al.*, 2004; Nimura and Nei, 2005). OR expression is monoallelic and each OSN is able to express only one type of OR. Mechanisms of single OR expression are under study but they have not been completely clarified yet (for review, Monahan and Lomvardas, 2015).

In vertebrates, the odor binding induces a conformational change of the OR which in turn activates the specific olfactory α subunit of the coupled G protein ($G_{\alpha olf}$) (Strader *et al.*, 1995). The activation of the G-protein increases the activity of type III adenylyl cyclase (ACIII), which converts ATP in cyclic AMP (cAMP), increasing its intraciliar concentration. Both $G_{\alpha olf}$ and ACIII have a crucial role in the transduction process and indeed KO mice for these proteins are anosmic (respectively, Belluscio *et al.,* 1998; Wong *et al.*, 2000).

Low micromolar cAMP concentrations in the cilia open the cyclic nucleotide-gated (CNG) channel (Nakamura and Gold, 1987; Dhallan *et al.*, 1990). The channel is permeable to sodium, potassium and calcium, producing a net inward current which depolarizes the cell. Ca^{2+} entry has a negative feedback on the CNG channel since, upon binding to calmodulin, it decreases its sensitivity to cAMP, and therefore closes the channel (Chen and Yau, 1994; Bradley *et al.*, 2004; Pifferi *et al.*, 2006a).

Yet Ca^{2+} entry has a secondary effect, directly activating a chloride current. The unusually high chloride concentration inside the cilia (Reuter *et al.*, 1998; Kaneko *et al.*, 2004; Nickell *et al.*, 2006; Reisert *et al.*, 2005; Restrepo, 2005) produces an efflux of Cl^- and a related inward current which further depolarizes the OSN. The depolarization due to Ca^{2+}, Na^+ influx and Cl^- efflux in the cilia spread to the dendrite and may trigger action potentials (Reisert *et al.,* 2005; Kurahashi and Yau, 1993).

Although Ca^{2+}-activated Cl^- currents (CaCCs) were first observed in the early nineties in the cilia of OSNs (Kleene and Gesteland, 1991; Kleene, 1993; Kurahashi and Yau, 1993; Lowe and Gold, 1993), their molecular counterpart has only recently been identified as TMEM16B/Anoctamin2 (Stephan *et al.*, 2009;

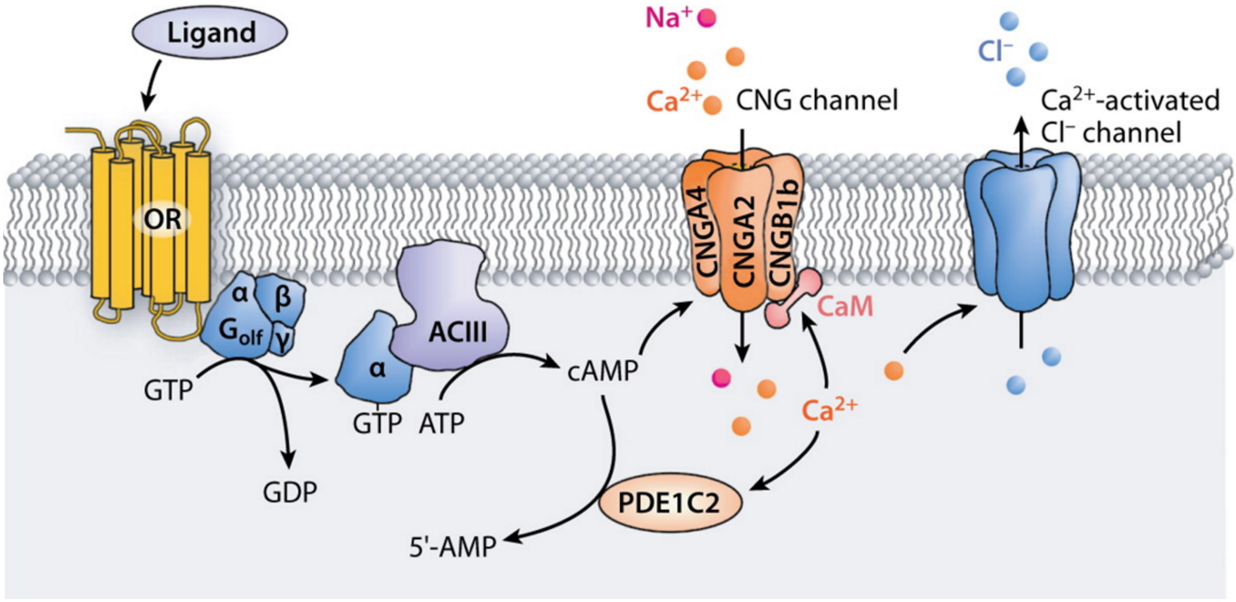

Figure 6 – Olfactory transduction
The binding of odorant molecules to an olfactory receptor (OR) induces the activation of $G_{\alpha olf}$ which mediates activation of adenylyl cyclase (ACIII). cAMP directly gates cyclic nucleotide channels (CNG) generating a depolarizing influx of Na^+ and Ca^{2+}. Intracellular Ca^{2+} increase mediates both excitatory and inhibitory events. Ca^{2+} gates Cl^- channels that produce a depolarizing efflux of Cl^-. On the other side Ca^{2+} negative feedback acts through Ca^{2+}-calmodulin reduction of cAMP sensitivity of CNG channels and Ca^{2+} activation of the phosphodiesterase (PDE1C2) that hydrolyzes cAMP to AMP. [modified from Munger *et al.*, 2009]

Pifferi *et al.*, 2009; Sagheddu *et al.*, 2010; Pifferi *et al.,* 2012), a member of the Anoctamin (TMEM16) family (Pedemonte and Galietta, 2014).

The falling phase of the transduction current triggered by odor stimulation is regulated by different mechanisms: (Kleene, 2008): G_{olf} inactivation is mediated by its intrinsic GTPase function (Trzaskowski *et al.*, 2012); Ca^{2+} calmodulin mediates phosphorylation of the ACIII, inhibiting its activity (Boekhoff *et al.*, 1996); decrease of the intraciliary cAMP concentration due to diffusion and phosphodiesterase activity; the above mentioned Ca^{2+}–calmodulin negative feedback on CNG channel activation; decrease of intraciliary Ca^{2+} concentration due to diffusion and extrusion mediated by Ca^{2+} active transporters. The phosphodiesterase activity on cAMP allows the use of isobutyl-1-methylxanthine (IBMX) as an alternative stimulus of OSNs. Indeed, application of IBMX inhibits basal phosphodiesterase activity, increases the intraciliar cAMP concentration and therefore emulates odor stimulation.

However, after a prolonged odor response, the intraciliary ionic condition can be altered, most likely with the accumulation of Ca^{2+} and a depletion of Cl^- and K^+ (Lindemann, 2001). The activity of different ionic transporters reestablishes the resting condition. The Ca^{2+} intraciliary concentration is recovered by a Na^+/Ca^{2+} exchanger and the plasma membrane calcium ATPase, while Cl^- and K^+ are equilibrated by $Na^+K^+/2Cl^-$ cotransporter (NKCC1) and other not yet identified transporters (Nickell *et al.*, 2007).

Besides the ionic environment alteration, strong stimulation induces a process of adaptation in OSNs. In prolonged stimulation the current response decreases with time, despite the continued presence of the

stimulus (Firestein *et al.*, 1990; Zufall *et al.*, 1991; Reisert and Matthews, 1999; Zufall and Leinders-Zufall, 2000). Similarly, in paired stimulations the amplitude of the second response is reduced if the interval between the pulses is sufficiently short. Ca^{2+} is involved in these phenomena, and at least the paired pulse adaptation is related to Ca^{2+}-calmodulin feedback modulation on CNG channels (Kurahashi and Menini, 1997). However, the calmodulin binding site on CNGB1b has been reported to not affect pulse adaptation (Song *et al.*, 2008).

1.3.2 - Odor-induced electrical response in olfactory sensory neurons

Ottoson (1956) was the first to measure an electroolfactogram (EOG), an odor-induced electrical activity from the surface of the olfactory epithelium. An extracellular recording electrode was placed on the surface of the exposed olfactory epithelium at the level of the turbinates. The electrode measured the summated generator potential of a large population of OSNs, in response to an odor application (Fig. 7). EOG has often been used for evaluating the effects of genetic manipulations on olfactory response. For example, the EOG response was dramatically reduced or abolished in knock-out mice for some components of odor transduction cascade, such as ACIII, $G_{\alpha olf}$ subunit and CNG channel α subunit, (Wong *et al.*, 2000; Belluscio *et al.*, 1998; Brunet *et al.*, 1996; respectively). Although EOG recording represents one of the most physiological methods to study odor-induced responses, most of our knowledge about olfactory transduction has been accomplished by studies on single OSNs. .

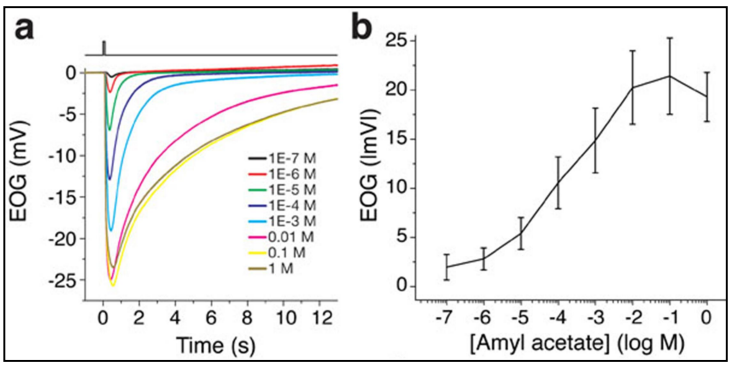

Figure 7 – Transduction responses in electroolfactogram recordings
Representative EOG signals from mouse under different stimulations. (A) Examples of EOGs in response to stimulations with increasing concentrations of amyl acetate. The black line at the top of the panel indicates the timing and duration of odorant stimulation. In the legend the concentration of amyl acetate applied. (B) Dose-response relationship averaged from five experiments [from Cygnar *et al.*, 2010]

Techniques used to record from individual OSNs include: patch-clamp, loose-patch, perforated patch, or suction electrode recordings. Spontaneous or evoked activity of individual OSNs has been measured from dissociated OSNs, slices of olfactory epithelium, or from intact olfactory epithelium preparations. OSNs respond to a suitable stimulus generating a transient inward current that depolarizes the cell. In mice, the current has a duration of generally up to 5 s with a latency between the application of the stimulus and response onset of 100-150 ms (Fig. 8) (Reisert and Matthews, 2001b; Grosmaitre *et al.*, 2006). Each OSN responds only to a small subset of odors (Firestein *et al.*, 1993; Bozza *et al.*, 2002; Lagostena and Menini, 2003; Grosmaitre *et al.*, 2006) depending on the expressed OR. By directing the odor stimulus to various parts of the cell, it has been shown that the sensitivity to odors is largely restricted to the cilia, where ORs

are localized (Kurahashi, 1989; Firestein *et al.*, 1990; Lowe and Gold, 1993; Takeuchi and Kurahashi, 2002). The expression of only one of the hundreds ORs in each OSNs dramatically decreases the success rate of a single odor stimulation. A mix of odors is often utilized as stimulus, in order to overcome this problem. As an alternative stimulus, isobutyl-1-methylxanthine (IBMX), an inhibitor of the basal phosphodiesterase activity which increases the intraciliary cAMP concentration, is often used. The OR cloning introduced the possibility to record from engineered mice where OSNs co-expressed a fluorescent marker protein with a specific OR, opening the possibility to measure the response of a specific OR.

The evoked current increases with the concentration or duration of the stimulus (Firestein *et al.*, 1993; Takeuchi and Kurahashi, 2002) until saturation is reached. The relationship between odor dose and amplitude of the receptor current is generally well fitted by a Hill equation:

$$I = I_{max}/(1 + (K_{½}/C)^{n})$$

where I_{max} is the maximum macroscopic current, C is the concentration of odor, $K_{½}$ is the half-maximal effective concentration, and n is the Hill coefficient (Hille, 2001; Kleene, 2008). Depending on the OR expressed by the OSNs, some odors have half maximal concentration in the micromolar range (Firestein *et al.*, 1993), others in the nanomolar and picomolar range (Frings and Lindemann, 1990; Grosmaitre *et al.*, 2006). In most cases saturating concentrations are measured in ranges from a few to hundreds µM in

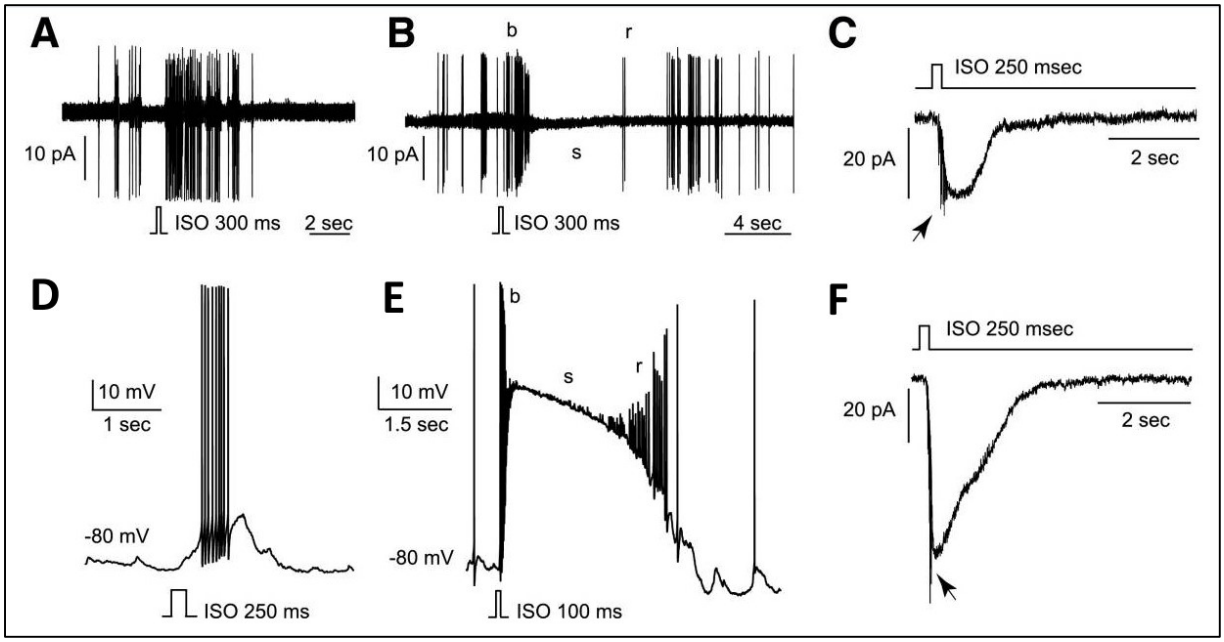

Figure 8 – Odor-evoked response recorded by different electrophysiological approaches
Representative odor-evoked responses in rat individual OSNs induced by 100 µM isoamyl acetate (ISO) and recorded in cell-attached (A, B) and perforated patch (C-F) from the intact olfactory epithelium. Odorant stimulation induces various activity patterns in individual OSNs. Two types of responses were frequently observed. In some neurons, brief puffs of odor elicited a non-decrementing amplitude burst both in in cell-attached and in perforated patch-clamp (A, D, respectively). In other neurons (E), an initial burst (b) is followed by a silence (s) and a firing rebound (r) (perforated patch-clamp in current-clamp mode).
(C, F) Transduction currents of different amplitude induced by the same stimulus in two neurons in perforated patch (voltage clamp mode V=-80 mV). Some action potentials occurred, despite the presence of 1 µM tetrodotoxin (TTX) in the bath perfusion. [from Savigner *et al.*, 2009]

mouse OSNs (Grosmaitre *et al.*, 2006). The "n" parameter in the Hill equation describes the slope of the dose–response relationship. A higher value corresponds to a smaller dynamic range, defined as the window of stimulus doses producing a change in the response. In amphibian, "n" was around 2-7 when recorded from dissociated OSNs under whole cell (Firestein *et al.*, 1993; Takeuchi and Kurahashi, 2005),, while in rats "n" was about 3-5 (Lowe and Gold, 1993). When the recordings were made on the epithelium "n" was smaller: 1.5 in rats (Ma *et al.*, 1999) and 0.3-0.8 in mice (Grosmaitre *et al.*, 2006, Grosmaitre *et al.*, 2009). However, dose response relationships for a given odor were highly variable among different OSNs (Tomaru and Kurahashi, 2005), even among neurons expressing the same OR (Grosmaiter *et al.*, 2006).

Single cell recordings of the odor-induced responses may be performed on slices or intact olfactory epithelium. Both loose patch and whole cell configurations have been used to record from OSNs in slice of olfactory epithelium (loose patch, Trotier, 1994; whole cell, Tomaru and Kurahashi, 2005). Techniques used on the intact olfactory epithelium include: cell attached (Fig. 8A and 8B) (Connelly *et al.*, 2013) and perforated patch (Fig. 8C-F) (Ma *et al.*, 1999; Grosmaitre *et al.,* 2006; Savigner *et al.,* 2009; Jarriault and Grosmaitre, 2015) and whole cell (Ma *et al.*, 1999). The perforated patch technique allows the use of voltage/current-clamp configurations while leaving a rather physiological internal environment (Ma *et al.*, 1999; Grosmaitre *et al.*, 2006) compared to whole-cell patch-clamp. These techniques allow the recording of both spontaneous and evoked firing activity of the OSN (Fig. 5 and 8, respectively).

The OSNs respond to odor stimulation with a burst of action potentials. Low and medium strength stimuli induce a continued burst which reflects the duration of the depolarization. Strong stimuli induce a robust depolarization that inactivates voltage dependent sodium channels saturating the firing activity and producing a silencing period which sometimes is followed by a second burst of action potentials corresponding to the falling part of the response (Fig. 8E) (Rospar *et al.*, 2003; Savigner *et al.*, 2009).

In addition, it has been reported that mechanical stimulation can trigger a response in OSNs (Grosmaitre *et al.*, 2007). This response engages the activation of the transduction cascade in which genetic ablation of key proteins of olfactory transduction cancel the mechanical response. However, mechanoresponse does not involve all ORs. OSNs expressing different ORs showed varying degrees of mechanosensitivity. The mechanical response can be minimized by drifting apart or distancing the stimulus dispenser (Connelly *et al.*, 2014).

1.4 - Calcium-activated chloride current in olfactory sensory neurons

1.4.1 - Chloride accumulation in olfactory sensory neurons

The Cl^- equilibrium potential is important information in understanding the role of the CaCC in olfactory transduction. It determines the direction and size of Cl^- flux across the ciliary membrane. Studies on various animal species reported an unusually high intracellular Cl^- concentration for OSNs (Reuter *et al.*, 1998; Kaneko *et al.*, 2001; Kaneko *et al.*, 2004). Unfortunately, few studies addressed the ionic composition of the

mucus, in which cilia of the OSN are embedded, and there is no consistency among them (Reuter *et al.*, 1998; Chao *et al.*, 1989). Energy dispersive X-ray micro analysis on cryosections of rat olfactory epithelium estimated a Cl^- concentration inside the cells of 69 mM and an olfactory mucus concentration of 55 mM, with a calculated equilibrium potential for Cl^- of +6 mV (Reuter *et al.*, 1998). In another study Cl^- concentration was estimated from intact olfactory epithelium of mice and rats using two-photon fluorescence lifetime imaging of the Cl^- sensitive dye MQAE technique. A maximal concentration up to 70 mM was found within the dendritic knob that decreased to 55 mM along the dendrite in the presence of a high extracellular Cl^- concentration (Kaneko *et al.*, 2004). For a lower extracellular Cl^- concentration of 50 mM the gradient disappeared, suggesting the presence of an apical Cl^- uptake system (Kaneko *et al.*, 2004). This data support the view that a Cl^- accumulation process charges the resting cilia prompting an excitatory Cl^- efflux in the olfactory transduction (Kleene, 2008).

The NKCC1 has been shown to be implied in Cl^- accumulation (Kaneko, 2004; Reisert *et al.*, 2005). The NKCC1 pharmacological block or genetic suppression abolishes the chloride component of the odor-induced current, recorded with the suction electrode technique in isolated mouse OSNs (Reisert *et al.*, 2005). The localization of NKCC1 is not completely clear, although more recent proteomic and immunohistochemistry data suggested a ciliary localization (Stephan *et al.*, 2009; Mayer *et al.*, 2009, Hengl *et al.*, 2010). However, NKCC1 may not be the only player of the Cl^- accumulation (Nickell *et al.*, 2006; 2007). $NKCC1^{-/-}$ genetic deletion or pharmacological block reduced by only ~30–50% the evoked response recorded by EOG (Nickell *et al.*, 2006, 2007), and $NKCC1^{-/-}$ did not show a reduced olfactory sensitivity (Smith *et al.*, 2008).

1.4.2 - Features of olfactory calcium-activated chloride current

Evidence that CaCC is involved in olfactory transduction was first reported in isolated frog olfactory cilia (Kleene and Gesteland, 1991; Kleene, 1993) where the current was induced by an influx of Ca^{2+} through CNG channels (Kleene, 1993). The CaCC was described as part of the current response to odorant stimulation in isolated OSNs from amphibians (Kurahashi and Yau, 1993; Firestein and Shepherd, 1995; Zhainazarov and Ache, 1995), rats and mice (Lowe and Gold, 1993; Reisert *et al.*, 2003). In mouse OSNs, CaCC is constituted of an efflux of Cl^- due to the unusually high concentration of this anion in the cilia. Studies on the activation of the CaCC at different Ca^{2+} concentrations reported Ca^{2+} sensitivity for the current is in the low micromolar range, with half maximal concentration of 2.2-4.8 μM and a Hill coefficient of about 2-3 (Reisert *et al.*, 2003, Pifferi *et al.*, 2006a; Stephan *et al.*, 2009).

Single channel recordings have shown a very small current, preventing direct recordings of single-channel opening events. Experiments of noise-analysis of macroscopic currents give an estimate in the pS range, specifically: 0.8 pS in frogs (Larsson *et al.,* 1997), 1.5 pS in rats (Reisert *et al.*, 2003) and 1.6 pS in mice (Pifferi *et al.*, 2006b). Such a low conductance implies an amplification of the receptor current through CNG

channels with no significant increase in noise (Kleene, 1997). Finally in mice, CaCC mediated up to 90% of the odor-induced inward current of dissociated OSNs when recorded in symmetrical Cl^- condition (Lowe and Gold, 1993; Reisert *et al.*, 2005; Boccaccio and Menini, 2007).

1.4.3 - Hypothesis on the physiological role of TMEM16B in olfactory sensory neurons

After its discovery in the excised cilia of frog OSNs (Kleene and Gesteland, 1991; Kleene, 1993), CaCCs have been shown to contribute to the response of odorant stimulation in OSNs from newt and tiger salamander (Kurahashi and Yau, 1993). In amphibians the presence of both cationic and anionic currents in olfactory transduction was interpreted as an adaptation to allow depolarizing current responses in a variety of extracellular ionic environments (Kurahashi and Yau, 1993; Kleene and Pun, 1996). However the discovery of the CaCC in rat OSNs (Lowe and Gold, 1993) opened the possibility for a current of a more general function in olfactory transduction. It has been suggested that CaCC served to amplify suprathreshold responses relative to basal transduction noise (Lowe and Gold, 1993). The features of nonlinear Ca^{2+}-dependence, together with the small single channel conductance may contribute to a high-gain and low-noise amplification of the primary CNG current in olfactory transduction (Kleene, 1997). As well, transduction amplification by nonlinear transduction current contributes in narrowing the dynamic range of OSNs response to stimulus (Boccaccio *et al.*, 2006), tuning the sensitivity of OSNs in a smaller range. However, since neurons have a high input resistance and few pAs are sufficient to generate action potentials a large amplification of the sensory current is not essential to transduce the signal (Lynch and Barry, 1989).

1.4.4 - TMEM16B is the olfactory calcium-activated chloride channel

CaCCs have been described in various tissues and cell types (Hartzell *et al.*, 2005; Duran and Hartzell, 2011; Huang *et al.*, 2012) and their functional role has been widely studied for more than 25 years. Their molecular identity has been controversial until 2008, when two members of the TMEM16/anoctamin gene family, TMEM16a/anoctamin1 and TMEM16b/anoctamin2, were shown to mediate CaCCs (Caputo *et al.*, 2008; Schroeder *et al.*, 2008; Yang *et al.*, 2008). The TMEM16 protein family is composed of ten members, but only TMEM16A and TMEM16B are currently well characterized. The function of the other members is controversial or not clear. The level of sequence similarity among the members suggests that all of them have a similar structure which has been recently clarified by the crystallization of the fungal homologous N. haematococca TMEM16 (Brunner *et al.*, 2014). The nHTMME16 is a dimeric membrane protein with ten transmembrane domains with intracellular N- and C- terminals. The Ca^{2+}-binding site is formed by six negatively charged aminoacids from different protein regions that come close to the tertiary structure and coordinate two Ca^{2+} ions. The nHTMME16 did not show any ion transport activity; it works as scramblase,

translocating phospholipids between the sides of the membrane, much like at least one other member of the family TMEM16F/anoctamin6 (Yang *et al.,* 2012).

Before its identification as an ion channel, Yu *et al.,* (2005) used in situ hybridization to show that TMEM16B was expressed in mature sensory neurons of mouse olfactory epithelium. After identification of TMEM16A and TMEM16B as CaCCs, TMEM16B was found in the olfactory ciliary proteome (Mayer *et al.,* 2009; Stephan *et al.,* 2009). Immunohistochemistry experiments showed its expression in the ciliary layer of the olfactory epithelium together with other protein involved in olfactory transduction (Hengl *et al.,* 2010; Rasche *et al.,* 2010; Sagheddu *et al.,* 2010; Billig *et al.,* 2011; Maurya and Menini, 2014). Additionally, when a TMEM16B/EGFP fusion protein was expressed in vivo in the mouse olfactory epithelium using an adenoviral vector, localized in the OSN cilia (Stephan *et al.*, 2009).

A side-by-side comparison was made between the electrophysiological properties measured from the native olfactory current and the TMEM16B-induced current in HEK cells in excised inside-out patches and in whole-cell configuration. It showed remarkable similarities in Ca^{2+}-sensitivity, anion selectivity, and pharmacology (Stephan *et al.*, 2009, Pifferi *et al.*, 2009, Sagheddu *et al.*, 2010). Both the native channel and TMEM16B showed a characteristic change with time of the reversal potential in the presence of large permeant anions in the extracellular bath, as if permeability changes with time. Although unusual, this dynamic selectivity is not unique to TMEM16B and has been observed in TMEM16A (Schroeder *et al.*, 2008) and in cation channels such as TRPV1 and P2X (Chung *et al.*, 2008; Khakh and Lester, 1999).

The role of TMEM16B as CaCC in OSNs was confirmed by the development of a KO mouse strain for TMEM16B. Electrophysiological experiments performed in whole cell configuration on dissociated OSNs of KO mice showed the absence of CaCCs, while the cationic current mediated by CNG channels was still present (Billig *et al.*, 2011).

TMEM16B shows alternative splicing. In particular, in the olfactory epithelium, TMEM16B transcripts lack exon 14 (Stephan *et al.*, 2009). Alternative splicing occurs at the starting exon, affecting N-terminal length, and at exon 4, involving 33 amino acids in the N-terminal (Ponissery Saidu *et al.*, 2013). The functional significance of such alternative splicing is unknown, but the native channel properties are better recapitulated by the co-expression of the predominant isoforms, with shorter N terminal, one with and one without the exon 4 sequence (Ponissery Saidu *et al.*, 2013).

A CaCC has also been recorded in mouse vomeronasal sensory neurons (Yang and Delay, 2010; Kim *et al.*, 2011; Dibattista *et al.*, 2012) and contributes to the response to urine (Yang and Delay, 2010; Kim *et al.*, 2011). Both TMEM16A and TMEM16B have been shown to be expressed in the microvilli of vomeronasals sensory neurons (Dibattista *et al.*, 2012). Very recent data suggest that TMEM16A contributes primarily to the CaCC in vomeronasal sensory neurons (Amjad *et al.*, 2015).

1.4.4.1 - TMEM16B KO mouse model

The initial evidence suggested TMEM16B as a CaCC in OSNs (Stephan *et al.*, 2009, Pifferi *et al.*, 2009, Sagheddu *et al.*, 2010), but a study on an animal model KO for the gene was needed to confirm its role of chloride current in olfaction. In 2011 the Thomas Jentsch laboratory in Berlin published a paper where they reported the development of a KO mouse strain for TMEM16B (Billig *et al.*, 2011). The disruption of the TMEM16B gene was induced by crossing Cre-recombinase expressing mice (Schwenk *et al.*, 1995) with engineered mice with exon 12 of TMEM16B flanked by LoxP sequences. Western blot and immunohistochemistry analysis with different antibodies did not show any TMEM16B presence in the main expressing tissues, such as the MOE, the vomeronasal organ, the olfactory bulb and the eye. However, the lack of TMEM16B did not modify the morphology of tissues and OSNs in adult mice. Crossing TMEM16B KO mice with two mouse strains where OSNs expressing OR M72 or P2 were labeled by LacZ expression did not report any alteration of anatomical organization of the glomeruli in the MOB.

Electrophysiological experiments in whole cell configuration on dissociated OSNs showed that CaCC was not present in these neurons. However, field recording from the surface of olfactory epithelium of transduction current induced by odor stimulation using EOG reported controversial results. They did not observe a difference between TMEM16B KO and WT mice for air-phase EOG recordings. While in submerged conditions they recorded the evoked response in KO mice was reduced by ~40% in respect of the WT (Billig *et al*., 2011).

The TMEM16B KO mice lacked an immediately apparent olfactory phenotype. The basic behavioral experiments did not show any impairment in olfactory ability. KO and control animals performed equally well in associative olfactory tasks aiming to test odor discrimination ability and odor sensitivity (Billig *et al.*, 2011). The minor reduction in EOG response, together with the lack of olfactory phenotype questions a crucial role of CaCCs in olfactory transduction (Billig *et al.*, 2011).

2- AIM

The study of OSNs firing properties is an essential step to decode the information processing in the olfactory system. Genetically modified mice with altered OSNs firing properties are a useful tool to investigate in detail the physiological roles of both evoked and spontaneous OSNs firing activities.

In the absence of stimuli, OSNs have an OR-dependent spontaneous firing activity that plays a fundamental role in axonal targeting to the glomeruli in the MOB. A previous study has shown that mouse OSNs overexpressing Kir2.1 induced a general mis-targeting of OSNs axons to glomeruli, producing a general disorganization of the MOBs. This effect was attributed to a decrease in OSN spontaneous firing activity, although a thorough electrophysiological analysis of spiking activity was missing.

The aim of the first part of this Thesis was to perform a first detailed study of the spontaneous and odor-evoked firing activity in mouse OSNs overexpressing Kir2.1 to contribute to the understanding of how OSNs spiking activity influences circuit formation in the MOB. The characterization of the OSN firing activity in Kir2.1 mice may detect if specific features of the spontaneous activity induce the alteration of the axonal targeting of the OSNs to the glomeruli into the MOB. Moreover, it could reveal if the overexpression of Kir2.1 alters the firing evoked activity opening alternative interpretation to the molecular mechanism of the OSN axonal targeting.

Mouse models knock-out for key proteins of the olfactory transduction show an alteration of the firing properties of the OSNs. A previous study has suggested that the Ca^{2+}-activated Cl^- channel plays a role in OR-dependent spontaneous firing activity, as this activity was greatly suppressed by blocking CaCCs. The recent availability of KO mice for the Ca^{2+}-activated Cl^- channel TMEM16B allows a direct analysis of spiking activity in the absence of TMEM16B.

The aim of the second part of this Thesis was to obtain the first characterization of spiking activity in OSNs from TMEM16B KO mice, to unveil a possible role of TMEM16B in the generation or modulation of spontaneous and stimulus-evoked firing of OSNs. This study could explain why TMEM16B KO mice did not show at first analysis any obvious impairment in ethological tasks mediated by olfaction.

3 - MATERIALS AND METHODS

3.1 - Animals

To study the influence of firing activity on the circuit formation in the olfactory bulb we obtained the OMP-IRES-tTA/Teto X Kir2.1-IRES-tau-LacZ (following as Kir2.1) mouse strain from the laboratory of Dr. Claudia Lodovichi, Neuroscience Institute, CNR, Padova, originally generated in the Center of Neurobiology and Behavior of the Columbia University in New York (Yu *et al.*, 2004). This mouse strain was developed to express Kir2.1 in 80% of the cells expressing OMP, a protein expressed exclusively in mature OSNs.

To study the physiological function of TMEM16B in OSNs, we obtained the TMEM16B knock-out (KO) mouse strain from Prof. Thomas J. Jentsch (Billig *et al.*, 2011). TMEM16B KO mice were crossed with I7-IRES-tauGFP, a mouse line where cells expressing the OR I7 can be identified with GFP-fluorescence, since they are tagged with tau-green fluorescent protein (tauGFP) (Bozza *et al.*, 2002). As wild type (WT) control for TMEM16B KO mice we used animals with the same genetic background, while for TMEM16B KO X I7-IRES-tauGFP mice we used I7-IRES-tauGFP mice. I7-IRES-tauGFP mouse strain was a generous gift from Prof. Peter Mombaerts (Max Planck Research Unit for Neurogenetics, Frankfurt).

All animals were handled in accordance with the Italian Guidelines for the Use of Laboratory Animals (Decreto Legislativo 27/01/1992, no. 116) and European Union guidelines on animal research (No. 86/609/EEC). Moreover, all animal procedures were performed under a protocol approved by the ethic committee of SISSA.

3.1.1 - Genotyping

Mice overexpressing Kir2.1 channel and control animals were provided directly from the laboratory of Dott. Claudia Lodovichi in Padova, where they were previously genotyped. A biological sample was lysed to obtain the DNA: a piece of tail and a finger of mouse pups were added to: 88 µl of autoclaved water; 10 µl of TRIS-HCl, pH 7.5, 1M; 2 µl of proteinase K (Invitrogen, California, USA). The lysis was performed at 57°C for 90 minutes in a Thermomixer (Eppendorf, Milano, Italy). Samples were kept in ice and then at 99°C for 5 minutes to inactivate the proteinase K. PCR was performed on a volume of 50 µl. After 3 initial minutes at 94°C, thermocycler ran 35 cycles, organized in the following steps: 94°C for 30 sec; 57°C for45 sec; 72°C for 45 sec. Kir2.1 genotyping was performed in three PCRs detecting the presence of tTA, LacZ and OMP sequences. For tTA were used two primers (tTA, forward primers 5'-AATTACGGGTCTACCATCGAGGGC-3', reverse 5'-GTCAATTCCAAGGGCATCGGTAAAC-3'; LacZ, forward primers 5'-CATCTGGTCGCTGGGGAATGAATC-3', reverse 5'-GCAACTGGAAAAACTGCTGCTGGTG-3'; OMP; forward primers 5'-CCTCGATTTCATCCAGCAGCAG-3'; reverse 5'-CAGGGGGCCCATCCATCTTCC-3').

In mice overexpressing Kir2.1 tTA and LacZ primers yielded a sequence of 300 bp and 500bp respectively and no sequence was yielded by OMP primers. In WT mice tTA and LacZ primers yielded no sequence contrarily to OMP primers which yielded a sequence of 680bp.

TMEM16B KO and I7-IRES-tauGFP strain were genotyped in SISSA by biomolecular technician Jessica Franzot. Genomic DNA was extracted from the mouse tails by using 5'PRIME Kit (Eppendorf, Milano, Italy), according to manufacturer's protocol. PCR was performed on a volume of 25 µl repeating for 40 times the following cycle: 94°C for 5 min (only in the first cycle), 94°C for 30 sec, 60°C for 30 sec and 72°C for 30 sec.

For TMEM16B KO strain were used primes flanking the LoxP site of TMEM16B allele (forward primers 5'-GGACACCCCGTACTTGAAGA-3'; reverse 5'-AGCACAATGCAGACCAAGTT-3'), the protocol require a single PCR which yielding a sequence of 163-bp for KO and 1051-pb for WT.

For I7-IRES-tauGFP two different forward primers were used (WT 5'- CATGCACTGACATGTCCA-3'; KI 5'-GAGAAGCGCGATCACATGGTCCT-3') giving the possibility to perform the PCR with the single forward primers or both in case of heterozygosis. The third reverse primer is common for both (5'-TTTATATTATCA ACTGCTCCC-3'). The presence of I7-IRES-tauGFP construct produces a band of 200-bp contrarily, for WT mice PCR yields a band of 520-bp.

3.2 - Tissue Preparation

3.2.1 - Intact olfactory epitheliun preparation

Mice (4 to 12 weeks) were anesthetized with CO_2 inhalation, decapitated and the head was immediately put in ice-cold artificial cerebrospinal fluid (ACSF) bubbled with 95% O_2 and 5% CO_2. ACSF contained (in mM): 120 NaCl, 5 KCl, 1 $MgSO_4$, 1 $CaCl_2$, 25 $NaHCO_3$, 10 glucose, 10 HEPES; osmolarity pre oxygenation 310 mOsm, pH = 7.2. The nasal septum was quickly dissected en bloc cutting out the turbinates and the vomeronasal organ. The septum bone with the two attached epithelia was placed in a recording chamber at room temperature (21-24 °C) continually perfused by bubbled ACSF (Fig. 9).

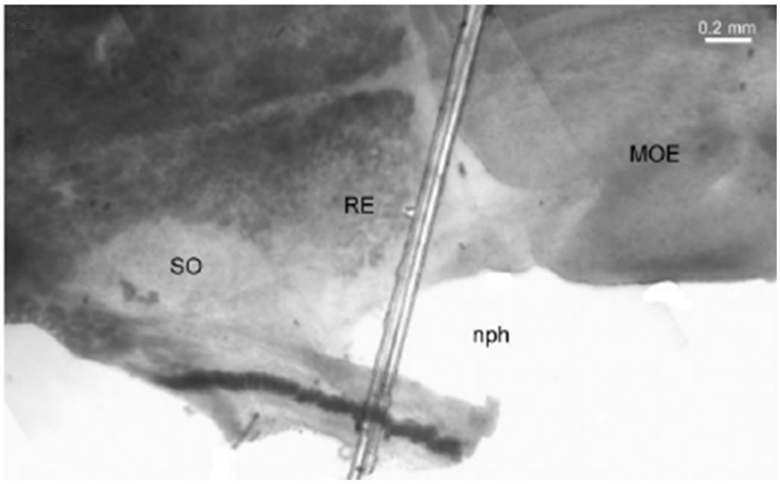

Figure 9 - Intact olfactory epithelium preparation
View of the tissue attached to the septum. SO, septal organ of Masera, RE, respiratory epithelium, MOE the main olfactory epithelium (modified from Ma *et al.*, 2003).

3.2.2 - Mouse nose coronal slice preparation

Since OSNs expressing I7 OR are not present in the MOE portion attached to septum bone, but are mostly expressed in the ventro-lateral zone (zone 1) of the MOE, we developed a coronal slice preparation from pups, which include the epithelium attached to the turbinates. In this region I7-IRES-tauGFP OSNs are highly present. P0-P4 mice were decapitated and the nose was dissected en bloc. The skin and the eyes were removed and the remaining preparation was glued inside a small hole obtained in a cube of boiled carrot. A vibratome 1000 Plus (Sectioning System, St. Louis) and classic double edge blades (Wilkinson, United Kindom) were used to cut coronal slices of 250-300 μm thickness (Fig. 10). During the cutting procedure, the tissue was completely submerged in a bath of ACSF continuously oxygenated and kept near 0° C. After sectioning, coronal slices were let to recover in ACSF oxygenated and kept near 0° C at least 30 minutes before recording. Slices could be used up to 4-6 hours after dissection. For experiments, a slice was transferred to the recording chamber and anchored using flattened pieces of pure silver placed on the carrot support, thereby holding down the slice without touching it.

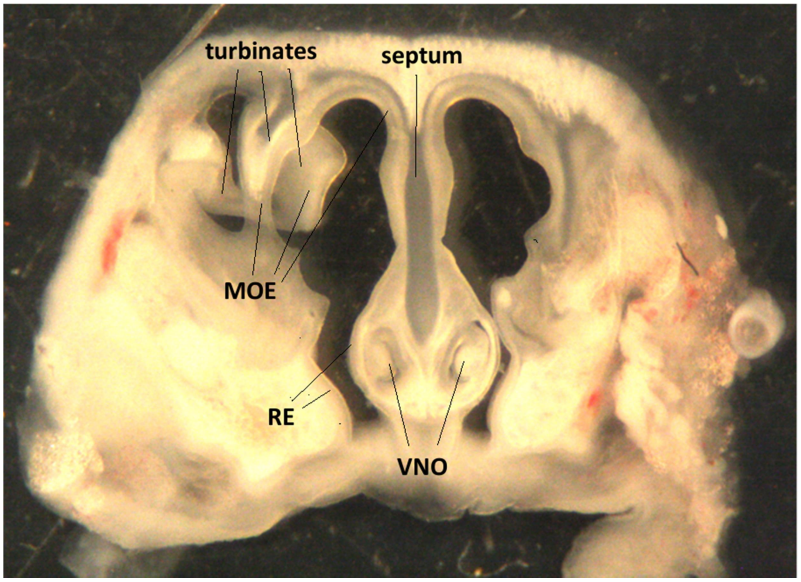

Figure 10 – Mouse nose coronal slice preparation
Nose coronal slice of 250 μm thickness from a P2 mouse at level of the vomero-nasal organ (VNO). The two nasal cavities are separated by the septum and lined ventrally by the respiratory epithelium (RE) and dorsally by the main olfactory epithelium (MOE).

3.3 - Electrophysiology

Electrophysiological experiments were performed on dendritic knobs of individual OSNs present in the MOE using the loose patch technique.

Dendritic knobs were viewed using an upright microscope (Olympus BX51WI, Japan) by differential contrast optics equipped with a DFK 72BUC02 camera (Imagingsource, Germany) and a 40X water-immersion objective (Fig. 11A-B). An additional X2 auxiliary lens was used to further increase the magnification of the tissue.

The microscope was placed on an antivibration table (TMC, USA) and a homemade Faraday cage provided adequate electrical shielding. A mercury lamp provided the fluorescent light to detect OSNs expressing I7 OR in I7-IRES-tauGFP mice.

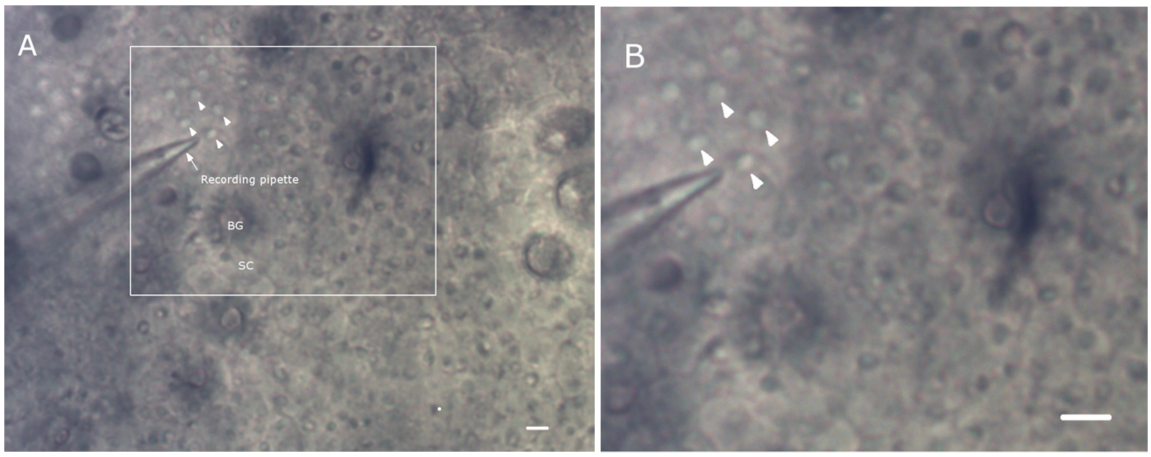

Figure 11 – Olfactory epithelium magnification
(A-B): Intact olfactory epithelium observed under bright field condition at 40X magnification (Scale bar: 5 µm). OSN dendritic knobs (white arrow heads) are enclosed in a mesh of microvilli of supporting cells (SC). BG, Bowman glands. (B): Enlarged view of region indicated by the white rectangle in A.

The recording chamber was continuously perfused with oxygenated Ringer solution by gravity flow (1.5 ml/min) and the experiments were performed at room temperature (20-24°C) using a Multiclamp 700B amplifier controlled by Clampex 9.2 via a Digidata 1322A (Molecular Devices, USA).

Borosilicate capillaries (outer diameter, 1.65 mm; inner diameter, 1.1 mm; WPI, USA) were pulled by a PC-10 puller (Narishige, Japan) in order to produce patch pipettes with a resistance of about 5-10 MΩ for loose patch configuration. Pipettes were mounted on a pipette holder with an Ag/AgCl electrode for electrical recordings and its movements were controlled by an electronic SM5 micromanipulator (Luigs & Neumann, Germany).

3.3.1 - Loose patch recordings

Extracellular recordings from dendritic knobs of OSNs were obtained in the loose patch configuration with seal resistances of 20-40 MΩ (Nunemaker *et al.*, 2003; Delay and Restrepo, 2004) in both coronal slices and entire septum preparations. Pipette was filled with ACSF (Table 2), the same solution present in the bath. The recordings were made in voltage-clamp configuration with a holding potential of 0 mV. Data were low-pass filtered at 1 kHz and sampled at 5 kHz.

Patch stability was checked recording at least 2 minutes of spontaneous activity before application of chemical stimulation.

Bath solution (ACSF)	**Electrode Solution (ACSF)**
120mMNaCl	120mMNaCl
25mM $NaHCO_3$	25mM $NaHCO_3$
5mM KCl	5mM KCl
10mM Glucose	10mM Glucose
10mM HEPES	10mM HEPES
1mM $MgSO_4$	1mM $MgSO_4$
1mM $CaCl_2$	1mM $CaCl_2$
(pH 7.2)	(pH 7.2)
310 mOsm	310 mOsm

Table 2 – Electrophysiological solutions

3.3.2 - Stimulus application

A pipette mounted on a secondary holder was used to deliver chemical stimulations by pressure injection (10-15 psi) produced by Picospritzer II (Parker, USA) controlled by Clampex 9.2 via a Digidata 1322A (Molecular Devices, USA). The puff pipette was pulled from the borosilicate capillaries (outer diameter, 1.65 mm; inner diameter, 1.1 mm; WPI, USA) by a PC-10 puller (Narishige, Japan) to have a tip of 2-3 µm. Puff duration was changed in order to modulate the stimulation intensity. Puffing pipette was placed more than 25 µm far from the knob of the recorded OSN to avoid any mechanical response (Grosmaitre *et al.*, 2007). Fluorescein was added to stimulus solution (approximate concentration 1-1.5 nM) to visually control the lack of solution leakage and efficacy of the stimulation. The holder movements were controlled by an electronic SM5 micromanipulator (Luigs & Neumann, Germany).

Heptanal, one of the main ligands of I7 receptor (Krautwurst *et al.*, 1998), was used as odor stimulation for OSNs expressing I7 OR in the nose coronal slices of I7-IRES-tauGFP mice. Alternatively, OSNs expressing an unidentified OR were stimulated by 100 µM 3-isobutyl-1-methylxanthine (IBMX) diluted in ACSF or, for the experiments on the mouse strain overexpressing Kir2.1 channel, a mix of odor. IBMX is an inhibitor of the phosphodiesterase activity, used to increase the intracellular cAMP concentration, thereby activating the CNG channels. The odor mix was composed by 19 odors diluted in ASCF 1mM composed by: hexanal, benzilic alcohol, eptanoic acid, propionic alcohol, benzaldehyde, 3-isobutyl-2-methoxypyrazine (IBMP), citralva, R-carvon, S-carvon, citronellol, geraniol, acetophenone, eugeniol, menthone, butyraldehyde, benzyl acetate, heptanol, hexanol, butanol.

3.4 - Chemicals

ACSF solution was stocked 10X without $CaCl_2$ and glucose and stored a 4°C. Fresh solution was renewed every 3 days.

IBMX was pre-dissolved in DMSO and diluted in ACSF to reach a concentration of 20 mM with 5% DMSO. Before the experiments it was diluted in ACSF to the final concentration and vortexed for 2 minutes.

Heptanal was dissolved at 100 mM in DMSO and kept at -20°C. Before the use it was diluted in ACSF to the final concentration vortexed for 2 minutes.

The 19 odors compounds of the odor mix (see paragraph 3.3.2 for complete list) were stocked at room temperature in an aspirated closet. During odor mix preparation the compounds were directly diluted to 1 mM in ACSF, sonicated for 40 minutes and stored at -20° C. Before each experiment the odor mix was defrosted and sonicated again for 10 minutes.

All stimulus solutions were refreshed weekly starting from specific stock solutions, except odor mix that was renewed every 2 days.

All compounds and chemicals were obtained from Sigma-Aldrich (St. Louis, Missouri, USA) if not otherwise reported.

3.5 - Data Analysis

Clampfit 10.2 software (Molecular Devices, USA) was used to filter raw data in the window 5-700 Hz and to detect action potentials on the electrical noise. Further, results were imported on Igor 6.0 (Wavemetrics, USA) and the spontaneous and evoked activities were differently analyzed using self-written procedures.

3.5.1 – Spontaneous activity

Spontaneous firing activity was evaluated in a time window of 2 to 5 minutes and was characterized as mean firing frequencies, inter-spike interval (ISI) and the instantaneous frequency (IF). Mean firing frequency was calculated for each OSN as the number of spikes divided by the duration of the recording (#AP/time). Alternatively, ISI was calculated for each spike as the time occurrence of a spike less the time occurrence of the previous spike ($ISI = T_n - T_{n-1}$) (second to first, third to second, and so forth). Moreover, instantaneous frequency (IF) of each spike was calculated as the inverse of ISI.

Sometimes very high frequency spontaneous firing activity followed by complete silencing of the recorded OSN showed clear evidence of neural damage or loss of cell integrity, such units were routinely discarded.

Mean firing frequency data were presented as a scatter plot. In the box plots, the inner square represents the mean, lines represent the median, upper and lower box boundaries represent the 25th and 75th percentile, upper and lower whiskers represent the 5th and 95th percentiles. IF data were averaged on each OSN and it was presented with the same method used for mean frequency.

Data from ISI were used to create an ISI distribution histogram evaluating the frequency components of each studied group.

Mean firing frequency and IF data were not always normally distributed (tested with Kolmogorov-Smirnov) and statistical significance was determined using one tail Mann-Whitney U-test. P-values < 0.05 were considered statistically significant.

3.5.2 – Evoked activity

Odor or IBMX-evoked firing activity were detected on top of the spontaneous background activity using an established protocol for OSN response analysis (Rospar *et al.*, 2003, Savigner *et al.*, 2009). Briefly, neuronal spiking activity was defined as a presumptive response to odor when, within 1.25 s after stimulus presentation, at least 3 consecutive spikes presented an instantaneous frequency (IF, 1/ISI) higher than the mean instantaneous frequency plus 1.5 Hz in the 30 s before stimulation (IF > avgIF + 1.5 Hz). If a presumptive response was detected, its instantaneous firing frequency distribution was compared using the Mann-Whitney U-test with the instantaneous firing frequency distribution occurring before stimulation.

When the two distributions were found significantly different at a level of 1% the presumptive response was considered a true response, otherwise it was discarded.

Strong increase of the firing frequency response was correlated with a decrease of the action potential amplitude. We defined a response as saturating when it was composed by action potentials which decreased their amplitude progressively up to baseline, saturating the possibility of the neuron of to fire again in the short term and producing a silencing period which sometimes was followed by a further high frequency burst. During the rebound burst the amplitude of the action potentials increased and the frequency progressively decreased towards the spontaneous firing activity level (similarly to Rospar *et al.,* 2003, Savigner *et al.*, 2009).

To characterize an evoked-response, the firing rate of the responses was estimated as the average of ISI of the first four spikes of the response. Moreover, the response duration and the silencing duration were measured differently. For saturating responses the response duration referred to the time between the first and last spike recognized as part of the response, including the silent period and the firing rebound.

Finaly, difference in firing response was evaluated using the spike distribution histogram. In this graph the time was divided in bins (bin size = 100 ms). To each bin correspond a bar reporting the average number of spikes occurred in the bin time window.

Each tested features was compared with the Mann-Whitney U-test, if no-parametric, or Student's t-test if parametric.

4.1 - Circuit formation and function in the olfactory bulb of mice with reduced spontaneous afferent activity

Paolo Lorenzon, Nelly Redolfi, Michael J. Podolsky, Ilaria Zamparo, Sira Angela Franchi, **Gianluca Pietra**, Anna Boccaccio, Anna Menini, Venkatesh N. Murthy, and Claudia Lodovichi

The Journal of Neuroscience, January 7, 2015 • 35(1):146 –160

Systems/Circuits

Circuit Formation and Function in the Olfactory Bulb of Mice with Reduced Spontaneous Afferent Activity

Paolo Lorenzon,[1]* Nelly Redolfi,[1]* Michael J. Podolsky,[2] Ilaria Zamparo,[1] Sira Angela Franchi,[1] Gianluca Pietra,[3] Anna Boccaccio,[4] Anna Menini,[3] Venkatesh N. Murthy,[5] and Claudia Lodovichi [1,6]

[1]Venetian Institute of Molecular Medicine (VIMM), 35129 Padua, Italy, [2]Department of Medicine, Massachusetts General Hospital, Boston, Massachusetts 02114, [3]Neurobiology Group, SISSA, International School for Advanced Studies, 34136 Trieste, Italy, [4]Biophysics Institute, CNR, 16149 Genova, Italy, [5]Department of Molecular and Cellular Biology and Center for Brain Science, Harvard University, Cambridge, Massachusetts 02138, and [6]Neuroscience Institute, CNR, 35129 Padua, Italy

The type of neuronal activity required for circuit development is a matter of significant debate. We addressed this issue by analyzing the topographic organization of the olfactory bulb in transgenic mice engineered to have very little afferent spontaneous activity due to the overexpression of the inwardly rectifying potassium channel Kir2.1 in the olfactory sensory neurons (Kir2.1 mice). In these conditions, the topography of the olfactory bulb was unrefined. Odor-evoked responses were readily recorded in glomeruli with reduced spontaneous afferent activity, although the functional maps were coarser than in controls and contributed to altered olfactory discrimination behavior. In addition, overexpression of Kir2.1 in adults induced a regression of the already refined connectivity to an immature (i.e., coarser) status. Our data suggest that spontaneous activity plays a critical role not only in the development but also in the maintenance of the topography of the olfactory bulb and in sensory information processing.

Key words: **behavior; functional imaging; olfactory bulb; olfactory system; sensory map; topography**

Introduction

Specificity of connectivity in the CNS is essential for normal brain function. In sensory systems, peripheral neurons project axons to precise loci in the brain to generate topographic maps that define the quality and the location of environmental stimuli. In the olfactory bulb (OB) a sensory map is generated by the convergence of olfactory sensory neurons (OSNs) expressing the same odorant receptor (OR) to form glomeruli (homogeneous glomeruli) in specific loci on the medial and on the lateral side of each OB (Ressler et al., 1994; Vassar et al., 1994; Mombaerts, 1996).

A glomerulus defines a functional unit, i.e., an odor column, consisting of the tufted and the mitral cells, receiving inputs from a specific group of sensory neurons, along with the granule cells connected to them (Shepherd, 2004). A second level of topographic organization is provided by the intrabulbar associational system (Schoenfeld et al., 1985), which connects specifically and reciprocally homologous glomeruli (Belluscio et al., 2002; Lodovichi et al., 2003; i.e., homologous odor columns).

Received Feb. 12, 2014; revised Oct. 15, 2014; accepted Nov. 4, 2014.

Author contributions: C.L. designed research; P.L., N.R., M.J.P., I.Z., S.A.F., and G.P. performed research; P.L., N.R., M.J.P., I.Z., S.A.F., G.P., A.B., A.M., V.N.M., and C.L. analyzed data; A.B., A.M., V.N.M., and C.L. wrote the paper.

This work was supported by an Armenise–Harvard Career Developmental Award and by the Cariparo Grant to C.L. We are grateful to J.A. Gogos for generously providing the P2-IRES-GFP and the tet_o-Kir2.1-IRES-tauLacZ mice. We thank Luca Dall'Arche for helping with behavioral experiments.

*P.L. and N.R. contributed equally to this work.

The authors declare no competing financial interests.

Correspondence should be addressed to Claudia Lodovichi, Neuroscience Institute–CNR and VIMM, Via Orus 2-35129 Padova, Italy. E-mail: claudia.lodovichi@unipd.it.

DOI:10.1523/JNEUROSCI.0613-14.2015

 0270-6474/15/350146-15$15.00/0

The development of sensory maps is regulated by the complex interaction between spatially and temporally regulated axon guidance molecules and neuronal activity (Huberman et al., 2008; Feldheim and O'Leary, 2010). Spontaneous and sensory-evoked activity play important roles in the formation of sensory circuits (Zhang and Poo, 2001). The exact contribution provided by each type of activity remains, however, largely to be understood.

The topographic organization of the OB hinges on the OR identity that defines the organization of homogeneous glomeruli and of the related odor columns (Sakano, 2010; Murthy, 2011). Odor-evoked activity does not affect significantly the organization of the sensory map (Belluscio et al., 1998; Lin et al., 2000; C. Zheng et al., 2000), although it perturbs the intrabulbar projections (Marks et al., 2006). However, spontaneous activity may play a role. OSNs exhibit spontaneous firing (Hallem and Carlson, 2004; Reisert, 2010) that could originate from the spontaneous activity of the odorant receptor (Connelly et al., 2013). Spontaneous firing in the OSNs has been shown to be required for the formation of the sensory map (Yu et al., 2004). Whether the spontaneous firing of OSNs can modulate the whole topographic organization of the OB, namely the organization of glomeruli, their intrabulbar connections and the related functional maps, remains unknown.

To address these critical issues, we took advantage of a line of mice genetically modified to have very little afferent spontaneous activity due to the overexpression of the inwardly rectifying potassium channel Kir2.1 in the OSNs (Yu et al., 2004). Using a combination of anatomical tracing, functional imaging, and behavioral analysis, we found that the olfactory bulb of Kir2.1 mice

exhibited unrefined connectivity that in turn could contribute to the altered olfactory information processing and olfactory behavior. In addition, we found that overexpression of Kir2.1 in adults induces a regression of the already mature neural circuits. These data suggest that spontaneous afferent activity is required for the development and for the maintenance of neural circuits in the olfactory bulb.

Materials and Methods

All animal procedures were performed under a protocol approved by the ethic committee of the University of Padua, of the University of Trieste, and the institutional guidelines of Harvard University.

Mutant mouse lines. Experiments were performed on the following genetically modified lines of mice: OMP-IRES-tTA/Tet_o (RRDI: MGI:3721403)-Kir2.1-IRES-tau-LacZ (Kir2.1, RRDI: MGI:3723462), P2-IRES-GFP (P2-GFP), and M71-IRES-GFP (M71-GFP, RRDI: IMSR_JAX:006676). The OMP-IRES-tTA/Tet_o-Kir2.1-IRES- tau-LacZ (Kir2.1) and the P2-IRES-GFP (P2-GFP), generously provided by J.A. Gogos (Columbia University, New York, NY), were described in detail previously (Gogos et al., 2000; Yu et al., 2004). The M71-IRES-GFP (M71-GFP) mice, described in detail previously (Feinstein et al., 2004), were purchased from the The Jackson Laboratory.

Ca^{2+} imaging. Procedures were modified from those in Maritan et al., 2009. Briefly, the olfactory epithelium was harvested from P25–P30 control and Kir2.1 mice in ice-cold HBSS (Invitrogen). Tissue was enzymatically dissociated and the resultant cell suspension was plated on 24 mm coverslip coated with poly-L-lysine (Sigma) and maintained in culture medium [D-Val Mem; 10% FBS, 5% Nu Serum, Penstrep L-glutamine, 100 U/ml (Invitrogen), 10 μM Ara-C (Sigma), and 25 ng/ml NGF (BD Biosciences) under standard conditions for 1–2 h (Ronnett et al., 1991). Neurons were then loaded with 8 μM fura-2 AM, 80 μg/ml Pluronic F127, and 250 μM sulfinpyrazone (Invitrogen) at 37°C for 30–40 min. Dissociated preparations were constantly perfused (3 ml/min) except during stimulus presentation (4–10 s, bath applied).

The odorant stimuli were represented by mixtures of several compounds including: citralva, citronellal, menthone, carvone, eugenol, geraniol, acethophenone, hexanal, benzyl alcohol, heptanoic acid, propionic acid, benzaldehyde, and IBMP (all from Sigma) prepared as 1 mM stock in Ringer's solution and diluted to the final concentration of 1 μM and 10 and 200 μM for each odorant in the bath. This stimulus concentration is well within the range (1 nM to 1 mM) of those used in previous imaging (Bozza and Kauer, 1998; Maritan et al., 2009; Pietrobon et al., 2011) and electrophysiological studies (Reisert, 2010, Connelly et al., 2013, Tan et al., 2010) on OSNs.

Ca^{2+} imaging experiments were performed on an inverted microscope (Olympus IX 81 with a 40 × NA 1.3 oil-immersion objective). The microscope was equipped with a CCD camera (SIS-F View) and an illumination system (MT 20; Olympus). Images were acquired every 3 s using Cell software using 380/15 and 340/15 nm excitation filters and a 510/40 nm emission filter. Images were processed off-line using ImageJ software (NIH). Changes in fluorescence (340 nm/380 nm) were expressed as R/R_0, where R is the ratio (340 nm/380 nm) at time t and R_0 is the ratio at time = 0 s. Response amplitude (%) was evaluated as $\Delta R/R_0 \times 100$, where $\Delta R = R - R_0$. The duration of the calcium response was calculated as the time (s) between the onset of the calcium rise and the return to baseline of the calcium signal.

Electrophysiology. Kir2.1 and wild-type control mice (4–8 weeks) were anesthetized with CO_2 inhalation and decapitated and the head was immediately put in ice-cold ACSF bubbled with 95% O_2 and 5% CO_2. ACSF contained the following (in mM): 120 NaCl, 5 KCl, 1 $MgSO_4$, 1 $CaCl_2$, 25 $NaHCO_3$, 10 glucose, and 10 HEPES, pH 7.2. The nasal septum was dissected en bloc and the tissue was placed in a recording chamber continually perfused by bubbled ACSF. Dendritic knobs of OSNs present in the main olfactory epithelium were viewed using an upright microscope (Olympus BX51WI) by infrared differential contrast optics with a 40× water-immersion objective and a 2× lens.

Extracellular recordings from dendritic knobs of OSNs were obtained in the loose-patch configuration with seal resistances of 20–40 MΩ (Nunemaker et al., 2003; Delay and Restrepo, 2004). The pipette solution was the same as the bath solution. Patch pipettes, pulled from borosilicate capillaries (WPI) with a Narishige PC-10 puller, had a resistance of ~5–10 MΩ. Recordings were made in voltage-clamp mode with a holding potential of 0 mV using a Multiclamp 700B amplifier controlled by Clampex 9.2 via a Digidata 1322A (Molecular Devices). Data were low-pass filtered at 1 kHz and sampled at 5 kHz. Experiments were performed at room temperature (20–25°C).

The odorant mixture had the same compounds (each at 1 mM in ACSF solution) of the odor mixture used in the Ca^{2+} imaging experiments (see above). The odorant stimulus was delivered by pressure ejection (4–8 psi), 150 ms duration, using a Picospritzer II (Parker).

Spontaneous firing activity was defined as the mean firing frequency recorded in a time window of 2–5 min. For spike detection raw data were filtered in the window of 5–700 Hz. Odor-evoked firing activity was detected on the spontaneous background activity using an established protocol for OSN response analysis (Rospars et al., 2003). Briefly, neuronal spiking activity was defined as a response to odor when, within 1.25 s after stimulus presentation, at least three consecutive spikes presented an instant frequency (IF; 1/interspike interval) higher than the mean instant frequency in the 30 s before stimulus presentation plus 1.5 Hz (IF > avgIF + 1.5 Hz). We defined saturating the responses consisting in an initial burst of firing activity, followed by a silent period, and by a firing rebound (Rospars et al., 2003; Savigner et al., 2009). The firing rate of the odor-evoked saturating responses was estimated as an interspike interval (ISI) of the first four spikes (Rospars et al., 2003).

Data from spontaneous firing frequency are presented as mean value ± SEM and number of neurons (n). Spontaneous firing frequency data were not normally distributed (Kolmogorov–Smirnov test) and statistical significance was determined using Mann–Whitney U test. P values <0.05 were considered statistically significant.

Optical imaging of intrinsic signal. Recordings of intrinsic optical signals from the olfactory bulb were made as reported previously (Rubin and Katz, 1999; Meister and Bonhoeffer, 2001; Soucy et al., 2009). Briefly, mice (P26–P30) were anesthetized lightly (ketamine/xylazine) and a window was made in the dorsal surface of the skull over the olfactory bulbs. The exposed tissue was covered with 1% agarose and a glass coverslip. Images were captured using a 35,000 electron/well CCD camera (CCD 1300-F; Vosskuhler) with a NIKON 55 mm f/2.8 microlens (NI5528M) via an NI frame grabber board (NI PCI-1422). Two 60-LEDs chips (780 nm and 500mW; Roithner Laser Technik) were attached to articulating arms (Edmund Optics) to illuminate the olfactory bulbs. Data acquisition software was developed in Igor (WaveMetrics) and LabView (National Instruments) by E. Soucy and A. Fantana (Soucy et al., 2009). A custom-built odor robot was used to deliver a large set of chemically diverse stimuli (97 compounds in mineral oil) presented at low concentrations (~0.1% saturated vapor pressure). Each stimulus was delivered for 30 s and preceded by 30 s of fresh air and the 97 stimuli (and one fresh air control) were repeated three to five times. Images were captured at 25 Hz. Frames taken during fresh air were averaged for the baseline fluorescence (F) and frames taken during odor presentation were used for ΔF. $\Delta F/F$ images of the entire field of view were generated and repeated trials of the same stimulus were averaged, yielding 98 $\Delta F/F$ images, one for each of the stimuli and one for fresh air. Individual responding regions were selected and used for analysis. The size of the boxes used to demarcate responding regions was quantified as the radius of an ellipse circumscribed within the box. Thresholding for response amplitudes was determined as 1.5 SDs above threshold of the average light intensity change in each box for each odor. We used Kolmogorov–Smirnov tests as statistical tests of significance for distributions of statistics, reporting $p < 0.05$ as significant.

In vivo *tracer injections and imaging analysis.* Tracer injections were performed and analyzed as described previously (Lodovichi et al., 2003).

Briefly, wild-type (C57BL/6), M71-GFP, and Kir2.1 mice were anesthetized with a mixture of Zoletil 100 (a combination of zolazepam and tiletamine, 1:1, 10 mg/kg; Virbac) and Xilor (Xylazine 2%, 0.06 ml/kg; Bio98). The scalp was resected and the bone over the bulbs removed to provide access for tracer injections. Microinjections of tetramethylrhod-

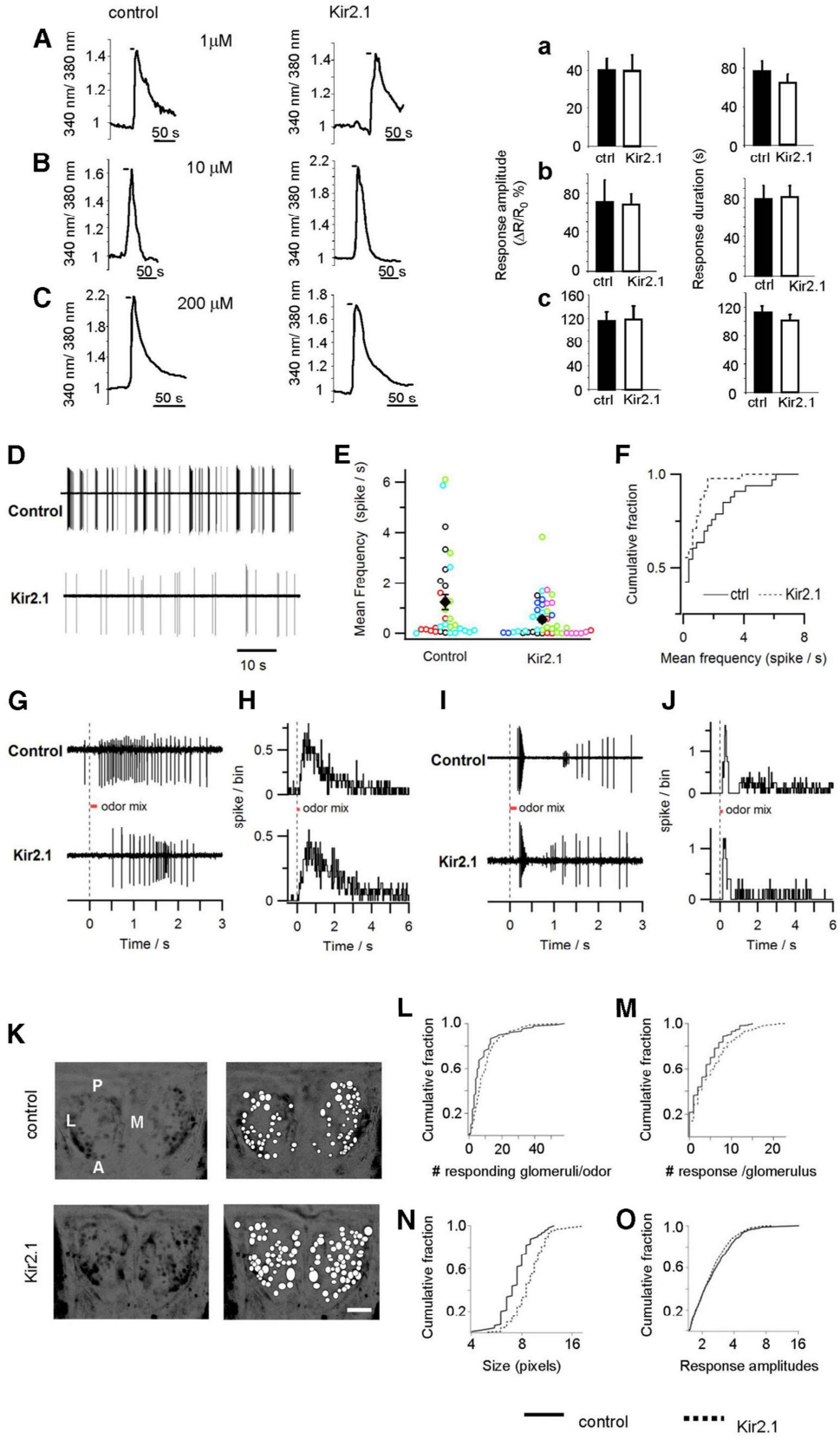

Figure 1. Spontaneous and odor-evoked activity in OSNs in Kir2.1 mice. ***A–C***, Normalized fluorescence ratio (340 nm/380 nm) changes in OSNs loaded with fura-2 and stimulated with a mixture of odors (***A***, 1 μM; ***B***, 10 μM; ***C***, 200 μM) in control (left) and Kir2.1 (right) OSNs. ***a–c***, Amplitude of the calcium response ($\Delta R/R_0$%) and duration of the calcium response (s). Data are presented as mean ± SEM. ***D***, Examples of traces of the spontaneous firing activity in OSNs, respectively, in control (top) and Kir2.1 mice (bottom). ***E***, Dispersion plot of spontaneous firing activity in OSNs in control and Kir2.1 mice. Each symbol indicates a single OSN. OSNs from the same mouse are indicated with symbols of the same color. Black diamond, mean ± SEM (*Figure legend continues.*)

amine dextran, 3000 MW (Invitrogen), were targeted to GFP-labeled glomeruli or to the glomerular layer, under an epifluorescent microscope (Leica MZ16). Tracer was iontophoresed (+2 μA, 50% duty cycle, 7 s pulses, for 2–3 min) into the olfactory bulb through a glass micropipette (4–5 μm tip diameter). Eight to twelve hours after injections, mice were killed by a Xilor–Zoletil overdose and transcardially perfused with 0.9% saline, followed by 4% paraformaldehyde in 1× PBS. Olfactory bulbs were removed, post fixed overnight, sectioned (60 μm horizontal sections) at the vibratome (Leica; VT 1000S), and mounted (Aqua-Poly/Mount; Polysciences).

In vitro *tracer injections.* P2-GFP and Kir2.1 × P2-GFP were deeply anesthetized with Xilor–Zoletil and decapitated. The bulbs were rapidly dissected in low Ca^{2+} ACSF (McQuiston and Katz, 2001) and bubbled with 95% O_2 and 5% CO_2. Under an epifluorescent microscope (Leica MZ16), targeted iontophoretic injections of tetramethylrhodamine dextran, 3000MW (Molecular Probes), were made in the medial P2-GFP glomerulus, using the same parameters used for the *in vivo* injections (above). Once injected, the bulbs were oxygenated in ACSF for 4–5 h, and then were fixed in 4% paraformaldehyde in 1× PBS and then processed as described above.

Confocal imaging acquisition and analysis. Sections were imaged on Leica SP5 confocal microscope with HC PL Fluotar 20×/0.50 NA objective (Leica). *Z*-stack series were collected in each section that contained any labeling related to the injection and the projection sites, respectively. The *Z*-stacks were then projected on the *XY* plane to obtain the maximum intensity projection, containing the entire reconstruction of the projection and of the injection sites, respectively.

Images were then analyzed using ImageJ software (NIH; RRID:nif-0000-30467). To quantify the extent of the injection and the projection sites, images were processed as follows: (1) a threshold was created for each image by clicking in a nonlabeled area; (2) images were then background subtracted and converted in binary files, and an object with clearly defined border was obtained; and (3) the distance between the borders of this object was measured. The ratio between the projection and the injection site was calculated. Ratios for each experimental and control group were averaged and presented as mean ± SD.

Immunohistochemistry. Mice were killed with an Xilor–Zoletil overdose and transcardially perfused with 0.9% saline followed by 4% paraformaldehyde in 1× PBS. Olfactory bulbs were removed, post fixed overnight, and sectioned (60 μm horizontal sections) at the vibratome (Leica; VT 1000S). Sections were blocked with 0.5% Triton X-100 + 5% normal donkey serum in 1× PBS for 60 min. Sections were then reacted with primary antibody against OMP (1:500; Wako Chemicals catalog #544-10001-WAKO RRID: AB_664696) at 4°C overnight. The primary antibody was visualized with Cy3-conjugated donkey anti-goat antibody (Jackson ImmunoResearch catalog #705-165-147, RRID: AB_2307351) after 2 h incubation at room temperature. DAPI (Invitrogen) was used as nuclear counterstain. Images were acquired at the confocal microscope (Leica SP 5) using an HC PL Fluotar 20×/0.50 NA objective (Leica).

Mitral cell labeling. Mice heterozygous for tet_o-Kir2.1-IRES-tauLacZ and wild-type C57BL/6 mice at P6–P8 were killed by decapitation. A small incision was made in the presumptive lateral olfactory tract and a small crystal of DiI_{18} (3) (Invitrogen) was applied. Brains were replaced in fixative and incubated at 37°C for 7–10 d. Brains were then sectioned (60 μm sections) at the vibratome (Leica; VT 1000S). Sections were imaged at a Leica SP 5 confocal microscope with an HC PL Fluotar 20×/0.50 NA objective (Leica). *Z*-stacks through selected mitral cells were performed and projected on the *XY* plane to obtain the maximum intensity projections, containing the reconstruction of the entire cells.

Olfactory discrimination test. Wild-type control and Kir2.1 male mice, age > P40, were trained and tested to assess their ability to discriminate between pairs of odors: fenchone (+) and (−), carvone (+) and (−), 2-heptanol (+) and (−), 2-methylbutyric acid (2MB), and cyclobutanecarboxylic acid (cb), all from Sigma-Aldrich. For each pair of odors a group of $n = 6$ control mice and a group of $n = 6$ Kir2.1 mice was used. The behavioral paradigm was slightly modified from that used previously (Schellinck et al., 2001). Briefly, 4 d before training the animals were put on a food restriction schedule to maintain 80–85% of their free-feeding weight. Water was available *ad libitum*. Mice were trained for 4 d in the following way. Each mouse was exposed in 4 × 10 min sessions to a conditional stimulus (CS+) contained in an odor pot hidden in the bedding of the cage, together with a piece of sugar (0.05 g). Each mouse was also exposed to the unconditioned stimulus (CS−) present in an odor pot hidden in the bedding of the cage, without the sugar. The CS+ and CS− were presented in different cages and each mouse was exposed randomly to CS+ or to CS− during the course of the training day. Odor concentrations were as follows: (+) carvone (6.4 M), (−) carvone (6.4 M), (−) fenchone (6.2 M), (+) fenchone (6.2 M), (−) 2-hepatonol (7.03 M), (+) 2-heptanol (7.01 M), 2-MB (9.1 M), cb acid (10.4 M). These odor concentrations are well within the range of those used in previous behavior experiments (Kobayakawa et al., 2007).

On the fifth day, mice were tested in a three-chamber apparatus. In the left and in the right compartment the CS+ and CS−, in odor pots, were hidden in the bedding. Sugar was not present in the testing phase. The animal was introduced in the chamber apparatus, without odors, for 5 min for habituation. After that the odors were hidden in the lateral chambers and the animal introduced in the central chamber having free access to the side compartments of the apparatus. The ability of the mice to discriminate CS+ versus CS− was assessed scoring the time spent investigating, digging, and sniffing around each odor pot, within a 2 min time window. The discrimination test was done blind to the conditioned odor. Differences between groups were evaluated using the Mann–Whitney test, $*p < 0.05$; $**0.001 < p < 0.01$.

Modulation of Kir2.1 expression. To examine the effects of Kir2.1 expression only in adulthood, two experimental procedures were used. In the first one, animals were fed with doxycycline (Sigma-Aldrich; 6 mg/g pellet food) throughout gestation until P30 (to abolish Kir2.1 expression). At P30 the sensory map (i.e., organization of glomeruli; see above, Immunohistochemistry and main text) and the link between homologous glomeruli were studied. For the latter, focal tracer injections *in vivo* were performed as described above in Kir2.1 and control mice at P30. In the second experimental procedure, the doxycycline administration was suspended at P30 and the animals (Kir2.1 mice and controls) analyzed at P60. At P60, the sensory map and the link between homologous glomeruli were studied (see above). To assess the Kir2.1 expression, sections of the olfactory bulb of Kir2.1 and control animals at P30 and P60, respectively, were reacted with goat antibody specific for β-gal (1: 1000; MorphoSys catalog #4600-1409, RRID: AB_2307350). The primary bound antibody was then visualized using anti-goat Cy3 conjugated (Jackson ImmunoResearch catalog #705-165-147, RRID: AB_2307351).

←

(*Figure legend continued.*) (1.23 ± 0.29 Hz, $n = 33$ in control mice and 0.54 ± 0.11 Hz, $n = 45$ in Kir2.1 mice). ***F***, Cumulative plot of spontaneous firing frequency, bin of 0.25 Hz (Mann–Whitney *U* test, one-tail, $*p = 0.02$). ***G***, Representative recordings of nonsaturating responses to odors (150 ms) in control (top) and Kir2.1 OSNs (bottom). ***H***, Cumulative response to an odor puff (150 ms) normalized to the number of neurons ($n = 13$ in control mice, $n = 22$ in Kir2.1 mice; bin 30 ms). ***I***, Examples of saturating responses to odors (150 ms) in control (top) and Kir2.1 OSNs (bottom). ***J***, Cumulative response to an odor puff (150 ms) normalized to the number of neurons ($n = 8$ in control mice, $n = 5$ in Kir2.1 mice; bin 30 ms). ***K***, Maximum intensity projection images of all odor responses collected in optical imaging of intrinsic signal experiments in glomeruli of the olfactory bulb of control (top) and in Kir2.1 mice (bottom). Darker regions indicate responding areas. Right, The responding spots are shown as white ellipses in control (top right) and in Kir2.1 mice (bottom right). Scale bar, 500 μm. M, medial; L, lateral; A, anterior; P, posterior. ***L***, Cumulative distribution of the number of glomeruli activated by the same odorants. ***M***, Cumulative distribution of the number of responses recorded in each glomerulus. ***N***, Cumulative distribution of the size of responding glomeruli upon odor stimulation. ***O***, Cumulative distribution of amplitude of the odor-evoked responses elicited in the glomeruli. Responses are shown as multiples of the SD of noise, with a threshold of 1.5 used to define a response. Cumulative fraction = total number of events. Solid line, controls; dashed line, Kir2.1 mice.

Results

Spontaneous and odor-evoked activity in OSNs overexpressing Kir2.1

The overexpression of Kir2.1 channel is supposed to dramatically reduce the spontaneous firing in OSNs (Yu et al., 2004), although its effect on odor-evoked activity remained to be clarified. To address this point we analyzed the calcium dynamics in response to a mixture of odors in isolated OSNs loaded with the Ca^{2+} indicator fura-2. OSNs exhibited a fast onset, rapidly recovering Ca^{2+} signal in response to all the concentrations of odors tested (1, 10, and 200 μM), which was not significantly different in Kir2.1 and in control mice (1 μM, controls: $n = 16$, Kir2.1: $n = 17$, amplitude of calcium response, $\Delta R/R_0$ (%) controls = 39.7 ± 6.2, Kir2.1 = 39.8 ± 8.2, t test, $p = 0.95$; duration of calcium response, controls = 75.6 ± 10.8 s, Kir2.1 = 64.2 ± 8.5 s, t test, $p = 0.4$; 10 μM, controls: $n = 12$, Kir2.1: $n = 19$, amplitude of calcium response, $\Delta R/R_0$ (%) controls 70.7 ± 23, Kir2.1 = 68.6 ± 10.4, t test, $p = 0.9$; duration of calcium response, controls 79 ± 13.6 s, Kir2.1 = 81.2 ± 11.4 s, t test, $p = 0.9$; 200 μM, controls: $n = 17$; Kir2.1: $n = 20$; amplitude of calcium response, $\Delta R/R_0$ (%) controls 115.3 ± 15.3; Kir2.1 = 117.1 ± 23.5; t test, $p = 0.95$; duration of calcium response, controls = 111.5 ± 9.1 s; Kir2.1 = 100.8 ± 8.3 s; t test, $p = 0.4$; Figure 1*A–C*). These results indicated the Ca^{2+} dynamics in response to odors was very similar in Kir2.1 and in control mice.

Ca^{2+} imaging is widely used to analyze neuronal activity (Cossart et al., 2005; Kerr et al., 2005; Grienberger and Konnerth, 2012). In our experimental conditions, however, Ca^{2+} imaging did not have the temporal resolution required to extract the temporal firing patter (i.e., single action potential resolution) of neurons. To overcome this limitation and thoroughly dissect the effect of Kir2.1 expression on the spiking activity of OSNs, using the loose-patch configuration, we recorded spontaneous and odor-evoked activity from dendritic knobs of OSNs, in the intact epithelium.

The spontaneous firing activity of OSNs was recorded for 2–5 min. We found that basal activity exhibited some variability in the firing rate among neurons both in control and in Kir2.1 mice (respectively, four and six mice, 33 and 45 neurons, 4–11 neurons for each animal; Fig. 1*E*). These data are in agreement with previous studies reporting a consistent variability in the basal firing activity of

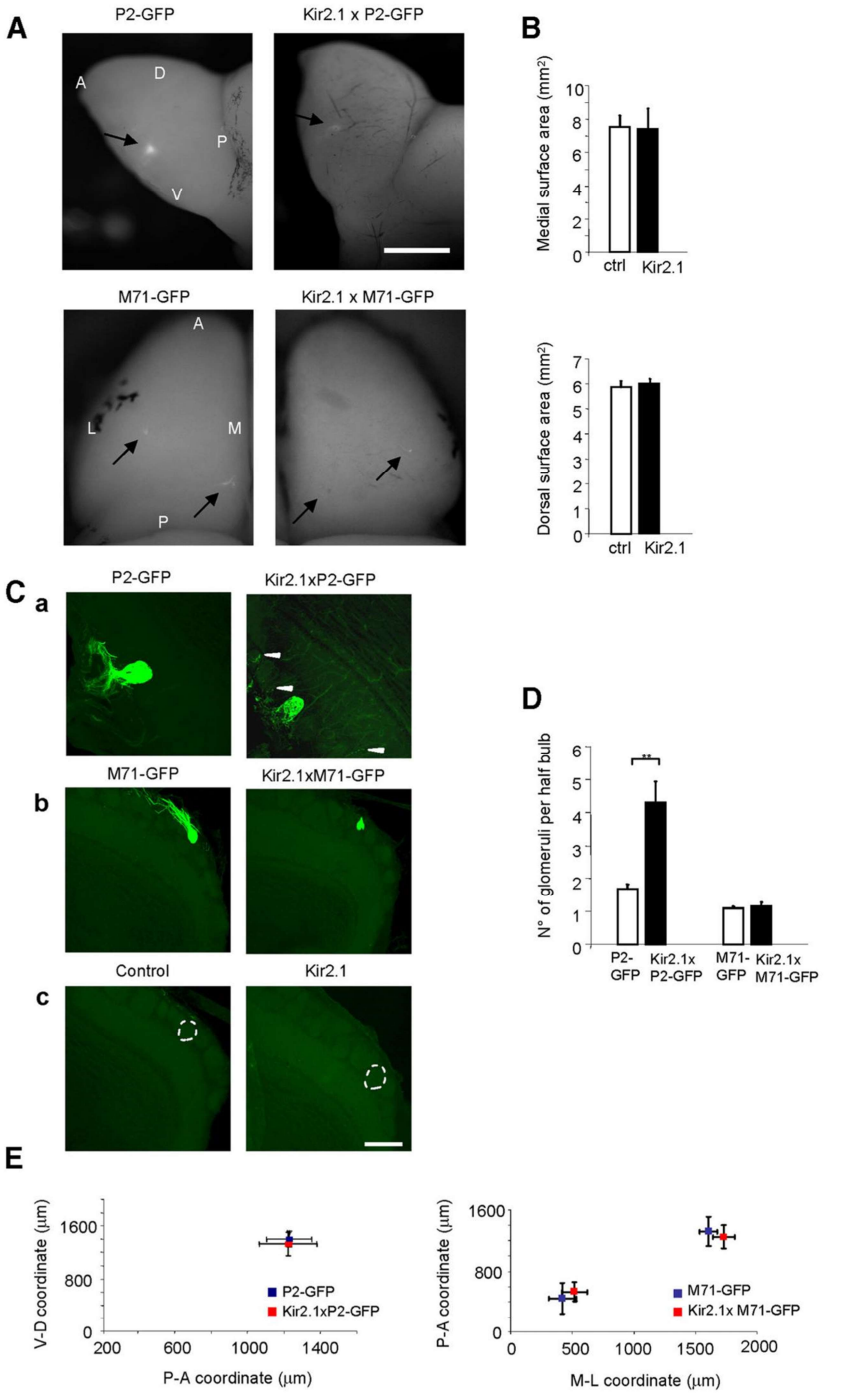

Figure 2. Additional glomeruli in the OB of Kir2.1 mice. ***A***, Top, Medial aspect of the OB in P2-GFP, left, and Kir2.1 × P2-GFP mice, right. Bottom, Dorsal views of the OB of M71-GFP controls, left, and Kir2.1 × M71-GFP mice, right. Arrows indicate P2-GFP and M71-GFP glomeruli. Scale bar, 1 mm. ***B***, OB size. Top, Area of medial surface (control, $n = 6$; Kir2.1, $n = 6$) and bottom area of the dorsal surface (control, $n = 7$; Kir2.1, $n = 9$) of OB in control and Kir2.1 mice. Data are presented as mean ± SD. ***C***, Number of glomeruli in the OB of control and Kir2.1 mice. ***Ca***, Examples of GFP-labeled glomeruli in horizontal sections of the OB of P2-GFP control mice (left) and of Kir2.1 × P2-GFP mice (right), of M71-GFP control mice (***Cb***, left) and Kir2.1 × M71-GFP mice (***Cb***, right). ***Cc***, Examples of glomeruli in horizontal sections of the OB in control (left) and Kir2.1 (right) mice. Dashed circles outline the profile of a single glomerulus. Scale bar, 200 μm. ***D***, Number of glomeruli per each half-bulb, and summary of results. Mice per condition: P2-GFP, $n = 7$; Kir2.1 × P2-GFP, $n = 7$. M71-GFP, $n = 7$; Kir2.1-M71-GFP, $n = 6$. t test, P2-GFP control versus Kir2.1 × P2-GFP, $^{**}p = 0.002$; M71-GFP control versus Kir2.1 × M71-GFP, $p = 0.59$. ***E***, Graph of the coordinates that define the location of the main glomeruli in the OB of P2-GFP control ($n = 5$) and Kir2.1 × P2-GFP mice, left ($n = 4$, t test controls-Kir2.1, V-D, $p = 0.3$, P-A, $p = 0.9$). Right, Graph of the coordinates that define the location of the main glomeruli in the OB of M71-GFP control mice ($n = 4$) and of Kir2.1 × M71-GFP mice ($n = 4$, t test controls-Kir2.1, lateral glomerulus P-A, $p = 0.6$; M-L, $p = 0.07$; medial glomerulus P-A, $p = 0.5$; M-L, $p = 0.24$). Blue square, P2-GFP and M71-GFP glomeruli; red square, Kir2.1 × P2-GFP and Kir2.1 × M71-GFP glomeruli. M, medial; L, lateral; A, anterior; P, posterior; V, ventral; D, dorsal. Data are presented as mean ± SD.

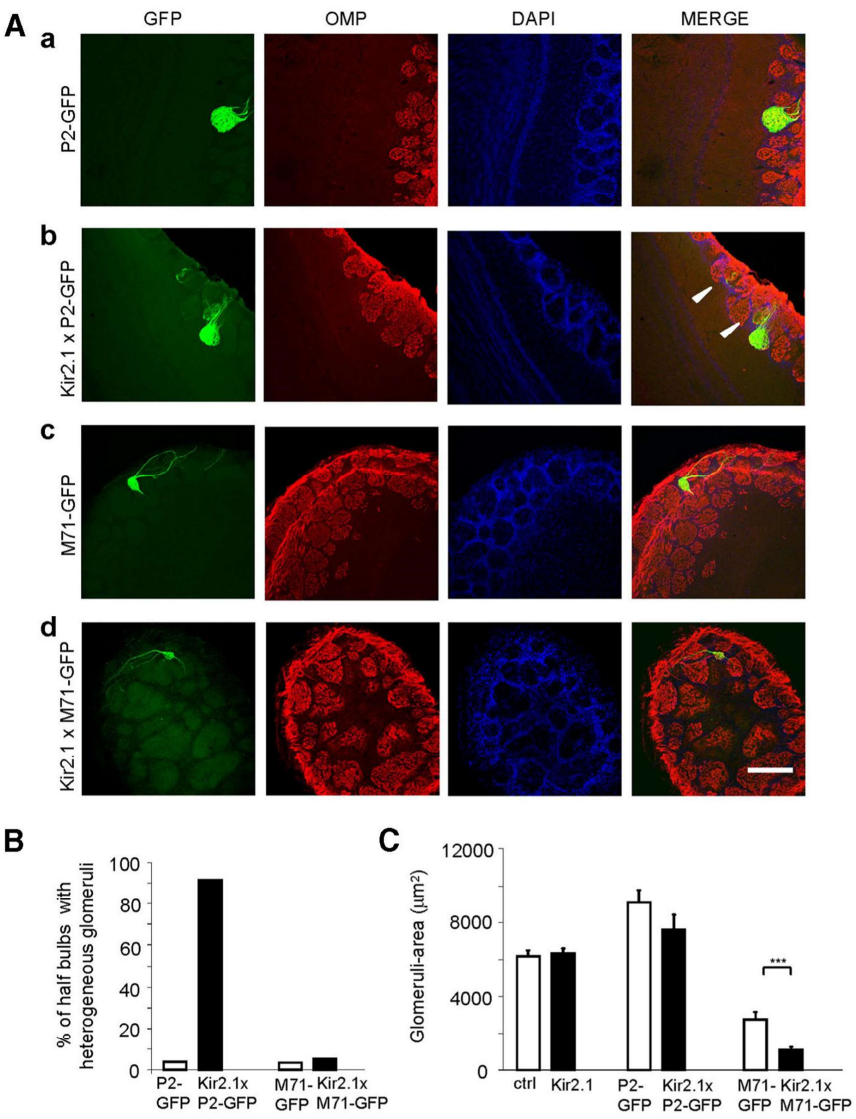

Figure 3. Organization of glomeruli in control and Kir2.1 mice. ***A***, Organization of P2 and M71glomeruli was revealed by immunolabeling horizontal sections of the OB with antibodies against the OMP (red). GFP expressed in P2 and M71-axons (green). Nuclei stained by the nuclear marker, DAPI (blue). ***Aa***, ***Ab***, P2-axons expressing both GFP and OMP coalesce to form homogeneous glomeruli in P2-GFP and in Kir2.1 × P2GFP mice. ***Ab***, P2-axons also innervate adjacent glomeruli (i.e., heterogeneous glomeruli, arrowheads) in Kir2.1 × P2-GFP mice. ***Ac***, ***Ad***, M71 glomeruli are formed by OSN axons expressing both GFP and OMP (homogeneous glomeruli) in M71-GFP mice and in most Kir2.1 × M71-GFP mice. Scale bar, 200 μm. ***B***, Percentage of half-bulb with heterogeneous glomeruli in P2-GFP ($n = 8$) and in Kir2.1 × P2-GFP ($n = 8$) and in M71-GFP ($n = 8$) and Kir2.1 × M71-GFP ($n = 8$). ***C***, Area of glomeruli in Kir2.1 × P2-GFP mice, in Kir2.1 × M71-GFP mice, and in controls. The size of glomeruli resulted in similar control and Kir2.1 mice, with the exception of M71-GFP glomeruli that were smaller. Data are presented as mean ± SEM.

OSNs (Reisert, 2010; Connelly et al., 2013). However, spontaneous firing was significantly reduced in Kir2.1 mice with respect to control, as shown Figure 1*D–F* (Mann—Whitney *U* test, one-tail, $p = 0.02^{*}$).

In response to an odor puff, the percentage of responsive neurons was similar in control (79%) and Kir2.1 (68%) mice. Odor-evoked spiking activity was very similar in OSNs in control and Kir2.1 mice (Fig. 1*G–J*), confirming the results we obtained with the Ca^{2+} imaging (see above). In particular we found that both nonsaturating (Fig. 1*G*,*H*) and saturating (Fig. 1*I*,*J*) responses to an odor puff were similar in OSNs in control and Kir2.1 mice (Fig. 1*H*,*J*). The firing rate of the evoked responses, estimated as ISI (see Materials and Methods for details), was not significantly different in OSNs in control and Kir2.1 mice (respectively, 17.1 ± 1.3 ms, $n = 8$ and 15.1 ± 1.6 ms, $n = 5$ in Kir2.1; *t* test, $p = 0.4$).

Odor-evoked activity in response to a large panel of chemically diverse odors also was recorded in glomeruli in functional imaging experiments (Fig. 1*K*). As shown in Figure 1*K* we found that evoked activity in response to odors (~0.1% saturated vapor pressure, a concentration routinely used in previous studies; Rubin and Katz, 1999; Uchida et al., 2000; Meister and Bonhoeffer, 2001; Soucy et al., 2009) could be recorded, although the functional maps were more blurred than in controls. We found that upon odor stimulation more glomeruli were activated and that each glomerulus responded to a higher number of odorants in Kir2.1 mice versus control animals (Fig. 1*L*,*M*; $n = 89$ control and 149 Kir2.1 glomeruli, $p = 0.002$, Kolmogorov–Smirnov test). The average size of the activated areas was bigger in Kir2.1 mice (Fig. 1*N*; $n = 89$ control and 149 Kir2.1 glomeruli, $p < 0.005$, Kolmogorov–Smirnov test), while the amplitude of response to a given odor was slightly smaller in Kir2.1 glomeruli than in controls (Fig. 1*O*; $n = 1531$ Kir2.1 responses, $n = 767$ control responses; $p = 0.025$, Kolmogorov–Smirnov test).

The sensory map and the organization of glomeruli in the OB of Kir2.1 mice

To study the convergence of OSNs with reduced spontaneous activity to form glomeruli in the OB, mice heterozygous for OMP-IRES-tTA/tet_o-Kir2.1-IRES-tauLacZ were crossed with mice homozygous for the P2-IRES-GFP or with M71-IRES-GFP allele (Kir2.1 × P2-GFP or Kir2.1 × M71-GFP mice). In these mice, sensory neurons expressing the odorant receptor P2 or M71 coexpress GFP. As a result of this genetic manipulation the corresponding glomeruli can be easily identified in the OB. The overall size of the OB was comparable in Kir2.1 and in control mice (Fig. 2*A*,*B*). By P30, in Kir2.1 mice, the P2-expressing axons form one or two distinct glomeruli on the medial and on the lateral side of each bulb (as in controls); however, they also projected to several adjacent glomeruli (from 3 to 9, in one case, 18, mice, $n = 7$; Fig. 2*C*,*D*). All the additional glomeruli were located in a restricted area, within five glomeruli from the main P2 glomerulus. Due to the late maturation of M71 glomeruli (Zou et al., 2004), we examined M71-GFP mice at P30 and P50. At both these temporal points, the Kir2.1 × M71-GFP mice presented one glomerulus on each side of the bulb (same as controls) although, occasionally, a few M71-expressing axons also entered one or two adjacent glomeruli ($n = 10$; Fig. 2*C*,*D*). As a result of the presence of

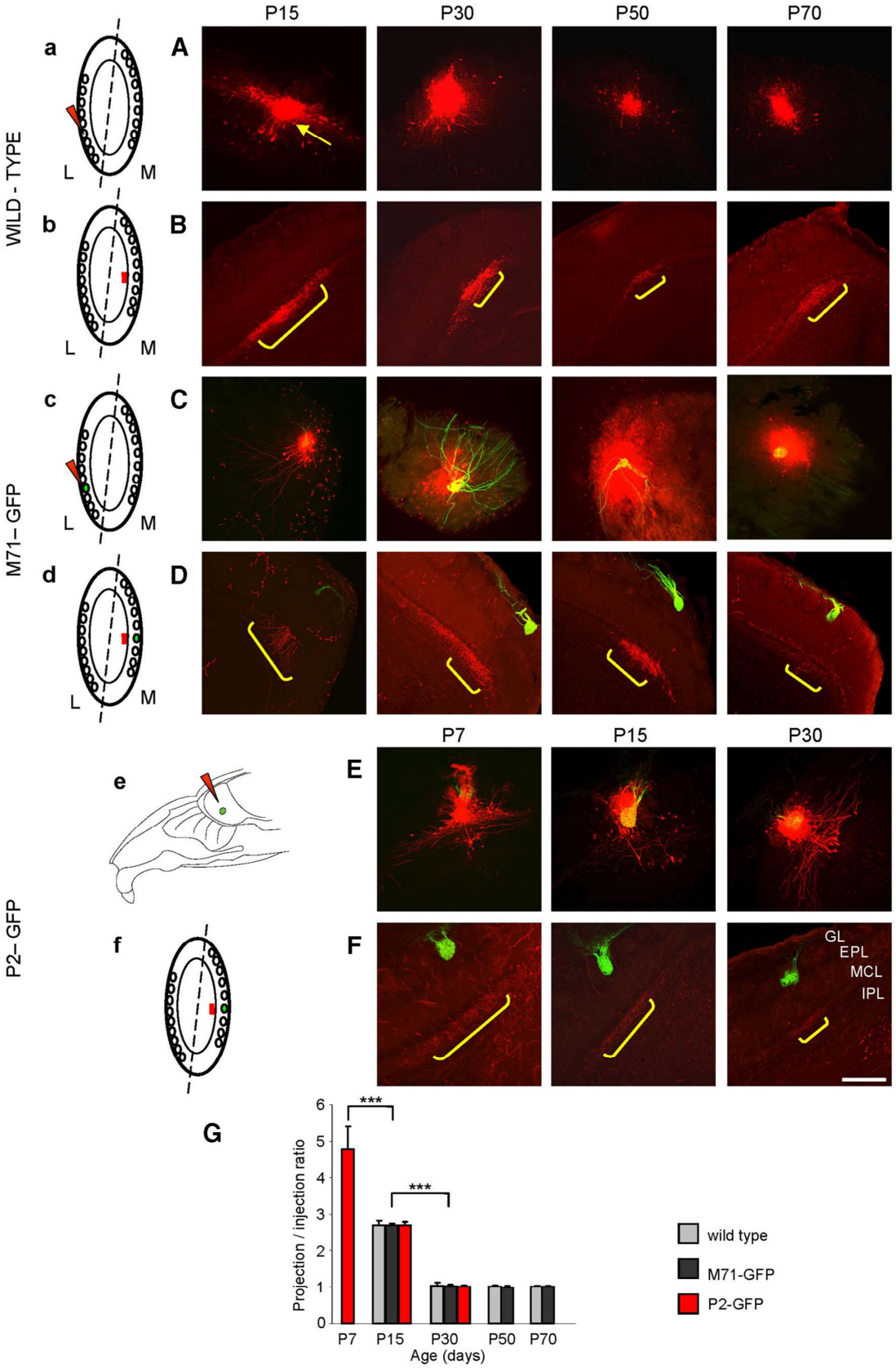

Figure 4. Development of the link between homologous glomeruli in control mice. ***a–f***, Schemes of horizontal sections of the OB. The dashed line depicts the line of symmetry between the two maps of homologous glomeruli. ***a***, ***c***, ***e***, The red arrowhead indicates the tracer injection targeted to the glomerular layer. ***b***, ***d***, ***f***, The red line indicates the ETC projection on the opposite side of the OB. ***A***, Examples of small tracer injections (red spots) targeted to the glomerular layer from P15 to P70. Arrow indicates labeled ETCs. ***B***, Axons of the ETCs labeled (*Figure legend continues.*)

additional glomeruli, the olfactory bulb resulted to have a higher number of glomeruli in Kir2.1 than in controls mice ($^*p < 0.05$; Kir2.1 mice, $n = 4$ and control mice, $n = 4$). The location of the main glomeruli for M71 and P2 was superimposable in Kir2.1 × M71-GFP and Kir2.1 × P2-GFP and control mice, as shown in Figure 2*E*.

A hallmark of mature glomeruli, which represents a key feature in the organization of the OB, is that they are innervated exclusively by fibers expressing the same OR. To assess the glomerular organization, serial sections of the OB of Kir2.1 × P2-GFP and Kir2.1 × M71- GFP mice were immunolabeled with antibodies against the OMP, a protein expressed by all mature OSNs (Danciger et al., 1989). The supernumerary glomeruli contained fibers immunopositive for both OMP and for GFP (i.e., axons expressing P2 or M71) along with axons positive only for OMP, but not for GFP (i.e., axons that express a different OR from P2 or M71; Fig. 3*Ab*,*Ad*). The main P2 and M71 glomeruli were composed exclusively of fibers positive for OMP and for GFP, i.e., P2 and M71-expressing axons, respectively (Fig. 3*Aa*,*Ac*). These data suggest that the increased number of P2 and M71 glomeruli can be accounted for by a greater number of heterogeneous glomeruli (Fig. 3*B*). The size of the main glomeruli was unaltered in most cases analyzed (Fig. 3*C*). Our data demonstrate that in Kir2.1 mice the organization of the OB in functional units defined by homogeneous glomeruli is disrupted by the presence of additional heterogeneous glomeruli.

Development of the link between homologous glomeruli

The perturbed organization of the sensory map in mice with reduced spontaneous activity in OSNs prompted us to examine the second level of topography of the bulb, the connections between homologous glomeruli. To address this question we studied the development of the connections in Kir2.1 and control mice, because our previous studies were limited to adults (Belluscio et al., 2002; Lodovichi et al., 2003). As a result of a possible incomplete refinement and/or mistargeting of the axonal projections of the external tufted cells (ETCs), the intrabulbar link could be less precise and the resulting topographic map more blurred, at early stages of development.

We first analyzed the morphology of the intrabulbar link from P15 to P70 in wild-type mice. To ascertain whether the projection was confined to a single glomerulus (size of the projection), we performed focal injections of an anterograde tracer (tetramethylrhodamine) that were largely restricted to a single glomerulus. We then calculated the ratio between the projection size and the injection size. We knew that in the mature system, analyzed in animals ≥3–4 weeks (Lodovichi et al., 2003) the ratio is 1:1. At P15, we found that a focal injection gave rise to a broad projection, not exclusively confined to the homologous glomerulus (ratio projection size/injections size = 2.7 ± 0.12, $n = 5$; Fig. 4*A*,*B*,*G*). The intrabulbar projections underwent a refinement process between P15 and P30, when they reached the point-to-point projection/injection ratio of 1:1, and remained stable throughout adulthood (ratio projection/injection size: P30, ratio = 1.04 ± 0.09, $n = 6$; P50, ratio = 1.03 ± 0.03, $n = 4$; P70, ratio = 1.03 ± 0.01, $n = 4$, *t* test: P15–P30, ratio $^{***}p < 0.001$; P30–P50, ratio $p = 0.8$; P50–P70, ratio $p = 0.9$; Fig. 4*A*,*B*,*G*).

To assess whether the projection was specifically targeted beneath the homologous glomerulus, focal dye injections were performed into the lateral GFP-labeled glomerulus in M71-GFP mice from P15 to P70 (Fig. 4*C*,*D*). We found that, at all the time points analyzed, the projection was targeted underneath the medial M71-GFP glomerulus, although at P15 the projection was not exclusively confined to the homologous glomerulus, but larger (ratio = 2.7 ± 0.35, $n = 6$; Fig. 4*C*,*D*,*G*). The refinement process was observed again between P15 and P30, when the projection size/injection size ratio was 1:1 (P30, ratio = 1.03 ± 0.04, $n = 6$; P50, ratio = 1.01 ± 0.03, $n = 3$; P70, ratio = 1.03 ± 0.001, $n = 4$; *t* test: M71 P15–P30, ratio $^{***}p < 0.001$; P30–P50, ratio $p = 0.4$; P50–P70, ratio $p = 0.9$; Fig. 4*C*,*D*,*G*). Focal tracer injections also were targeted to the P2-GFP glomeruli. In this case, due to the position of the medial glomerulus, buried deep along the medial wall of the OB, the injections were performed in hemihead explant preparations in which the medial side of the bulb was exposed while retaining its connections with the olfactory epithelium and the brain (Fig. 4*e*; Lodovichi et al., 2003). Due to the early maturation of the P2 glomeruli (Royal and Key, 1999), the size and the targeting of the intrabulbar connections were examined beginning at P7. At all the time points analyzed, again, the axonal projection of the ETCs ended just beneath the homologous glomerulus. Although at earlier stages of development the ETC projection was broader (projection size/injection size ratio at P7, 4.8 ± 0.6, $n = 3$; P15, 2.7 ± 0.09, $n = 4$; Fig. 4*E*–*G*), it reached the 1:1 projection size/injection size ratio at P30 (ratio = 1.03 ± 0.03, $n = 3$; *t* test P7–P15, ratio $^{***}p < 0.001$, P15–P30, ratio $^{***}p < 0.001$; Fig. 4*E*–*G*).

Intrabulbar circuitry in Kir2.1 mice

To analyze the intrabulbar circuitry in Kir2.1 mice, focal tracer injections were targeted to the glomerular layer in Kir2.1 mice from P30, the age at which a mature, point-to-point connection between homologous glomeruli is present in control animals (see above and Lodovichi et al., 2003) to P70. At all the time points examined, a small injection site corresponded to a projection not confined to a single glomerulus (Fig. 5*A*,*B*,*E*). Although a reduction in the projection/injection ratio was observed from P30 to P70, it never reached the value of 1:1 as in control animals (ratio P30 = 2.33 ± 0.1, $n = 9$; P50 ratio = 2 ± 0.05, $n = 5$; P70, ratio = 1.92 ± 0.13, $n = 3$; *t* test: Kir2.1 P30–P50 ratio $^{***}p < 0.001$, Kir2.1 P50–P70 ratio $p = 0.3$, P30 wt-P30 Kir2.1 ratio $^{***}p < 0.001$, P50 wt- P50 Kir2.1 ratio $^{***}p < 0.001$, P70 wt-P70 Kir2.1 ratio $^{***}p < 0.001$).

Focal tracer injection targeted to the P2 medial glomerulus in Kir2.1 × P2-GFP mice ended in a projection just beneath the homologous glomerulus (Fig. 5*C*–*E*, P30, ratio = 2.37 ± 0.08, $n = 6$, *t* test ratio P2-GFP-Kir2.1 × P2-GFP $^{***}p < 0.001$; P30, ratio Kir2.1 × P2-GFP vs Kir2.1 $p = 0.5$). Therefore the specific targeting of the anterograde projection was not affected in Kir2.1 mice. The specific targeting between M71 glomeruli in Kir2.1 × M71-GFP mice could not be examined, since identifying and targeting such small glomeruli were extremely challenging.

All together these data indicated that the connection between the main glomeruli was preserved in Kir2.1 mice, although it was not confined exclusively to isofunctional glomeruli due to the lack of refinement of the axonal projections of the ETCs.

←

(*Figure legend continued.*) by tracer injections (***A***) ended in anterograde projections (yellow brackets) on the opposite side of the OB. ***c***, ***d***, The M71-GFP glomerulus is indicated in green. ***C***, Examples of tracer injections targeted to the M71-GFP glomeruli from P15 to P70 and the corresponding projections (yellow brackets) just underneath the M71-GFP homologous glomerulus on the opposite side of the bulb (***D***). ***e***, Schematic representation of the hemi-head preparation. In green, the P2-GFP glomerulus on the medial surface of the bulb. ***E***, Examples of tracer injections targeted to the P2-GFP medial glomerulus from P7 to P30 and the corresponding projections just underneath the homologous P2-GFP glomerulus on the opposite side of the OB (***F***). GL, glomerular layer; EPL, external plexiform layer; MCL, mitral cell layer; IPL, internal plexiform layer. Scale bar, 200 μm. ***G***, Summary of results. Data are presented as mean ± SD.

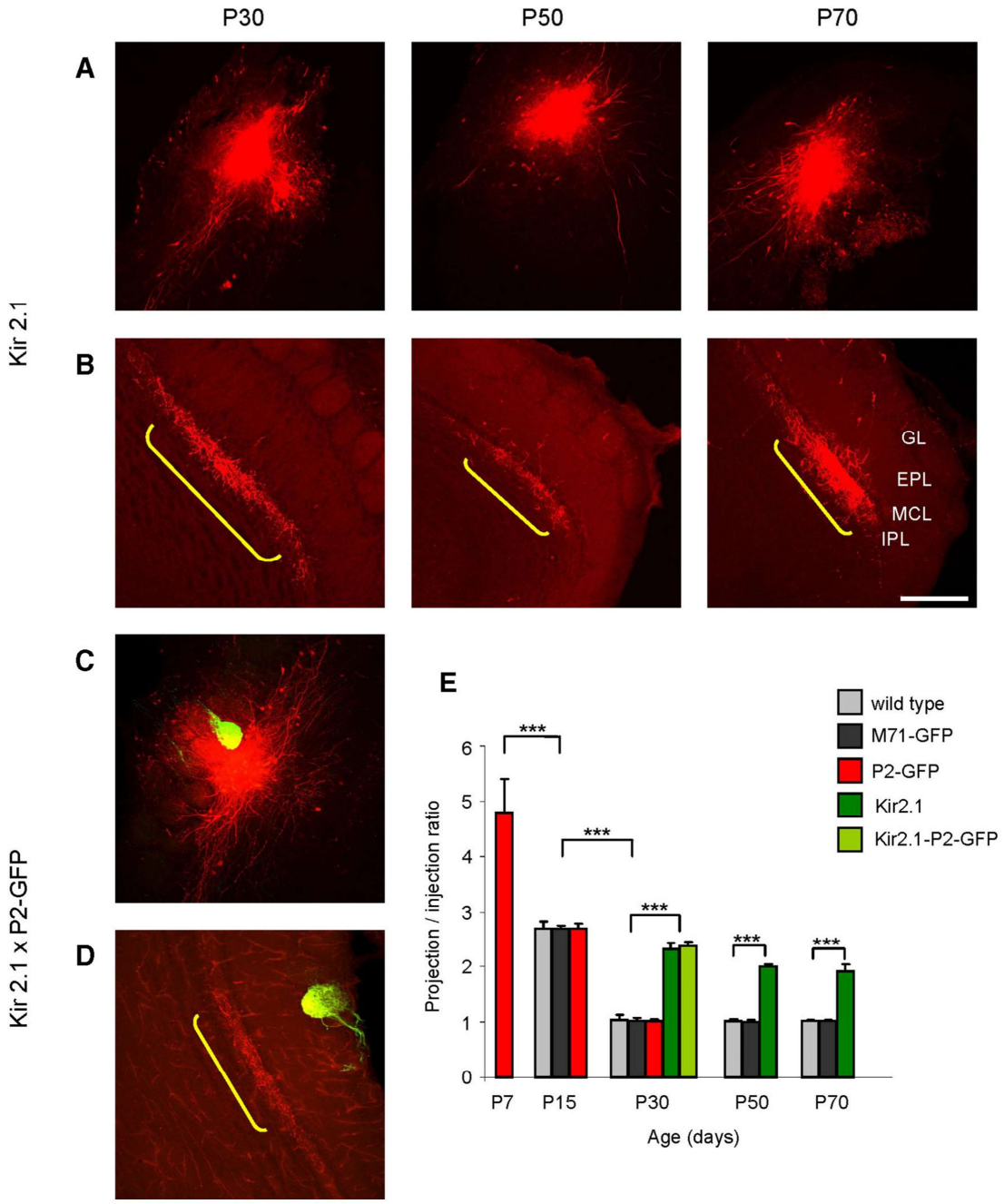

Figure 5. Unrefined intrabulbar circuitry in Kir2.1 mice. ***A***, Examples of focal tracer injections (red spots) targeted to the glomerular layer in Kir2.1 mice from P30 to P70. ***B***, ETC axons labeled in ***A*** give rise to anterograde projections (yellow brackets) on the opposite side of the bulb, which are larger than the corresponding injection sites. ***C***, Tracer injection targeted to the medial P2-GFP glomerulus and the corresponding projection underneath the homologous P2-GFP glomerulus (***D***). GL, glomerular layer; EPL, external plexiform layer; MCL, mitral cell layer; IPL, internal plexiform layer. Scale bar, 200 μm. ***E***, Summary of results. Data are presented as mean ± SD.

Development of mitral cell apical dendrite in Kir2.1 mice

We found that the developmental refinement of the OSN and ETC axonal projections is perturbed in Kir2.1 mice. We asked whether the postsynaptic targets of the OSNs, the mitral cells (MCs), exhibited any effect related to their developmental maturation in Kir2.1 mice. Mature mitral cells extend a single apical dendrite into a single glomerulus to contribute to the organization of the odor column. This single apical dendrite remains after the withdrawal of other, supernumerary dendrites, a process that is completed in the first postnatal week (Lin et al., 2000). We found no difference in the developmental remodeling of the apical dendrite of MCs in Kir2.1 mice versus controls (from P6 to P8 mice). At this developmental stage, indeed, most MCs presented a single apical dendrite as in controls (MCs with single apical dendrite at P6 = 91.6% in controls, 91% in Kir2.1 mice, at P7 = 96.7% in controls and 96.8% in Kir2.1 mice, at P8 = 98% in controls and 97% in Kir2.1 mice; Fig. 6*A–D*).

Olfactory discrimination behavior in Kir2.1 mice

The altered organization of the anatomical and functional maps of the OB could affect olfactory behavior. To address this question we studied the ability of Kir2.1mice to discriminate between

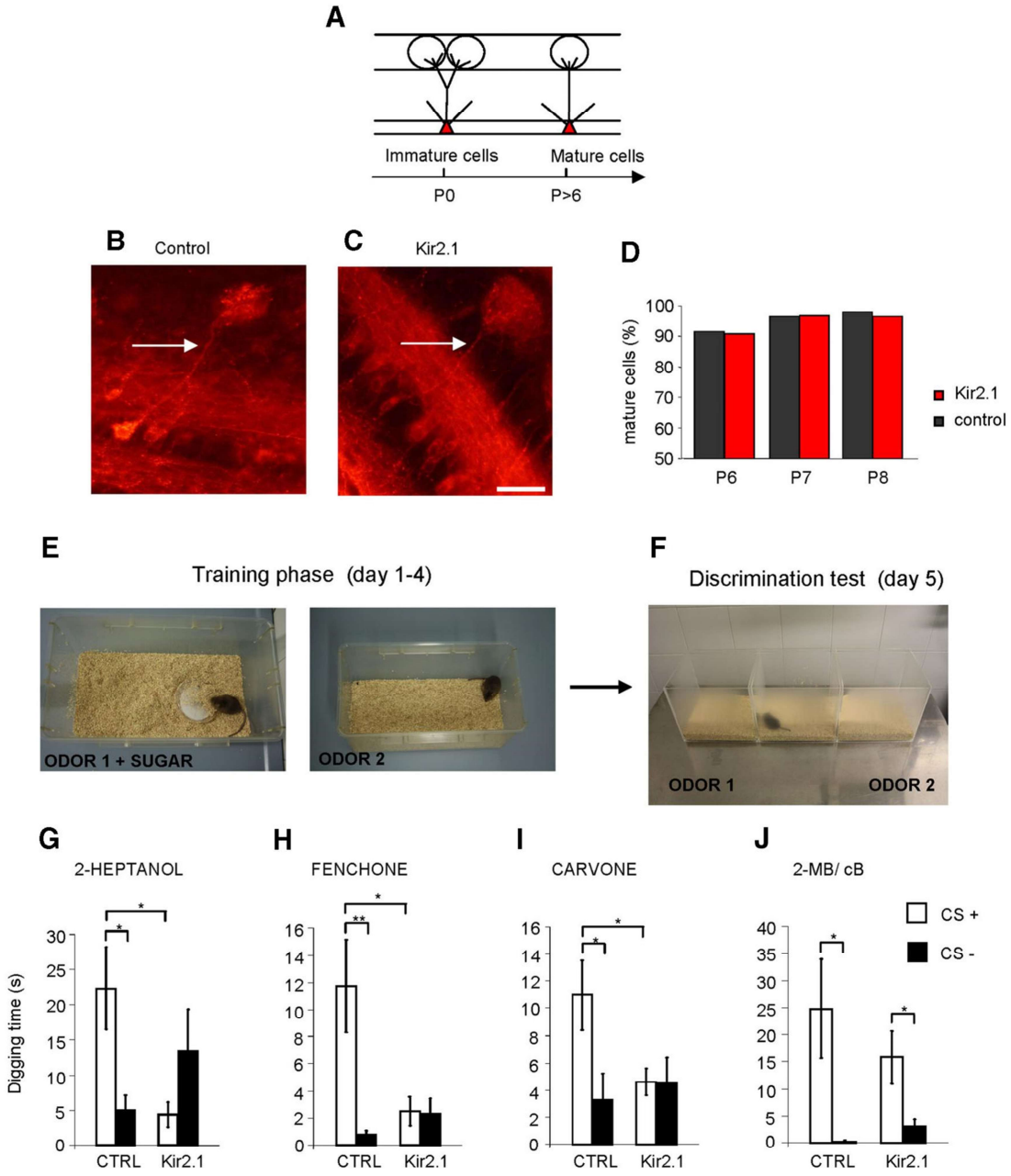

Figure 6. Developmental refinement of the apical dendrite in MCs. ***A***, Schematic representation of the developmental withdrawal of the extra apical dendrites. ***B–C***, Examples of MCs, retrogradely labeled by DiI, in horizontal sections of the OB, in control (***B***) and in Kir2.1(***C***) mice at P7. In both cases (***B***, ***C***) a single apical dendrite (arrow) ends in an apical tuft within a single glomerulus. ***D***, Summary of results (P6: Kir2.1 mice, $n = 6$, wild-type mice, $n = 4$; P7: Kir2.1 mice, $n = 5$, wild-type mice, $n = 4$; P8: Kir2.1 mice, $n = 6$, wild-type mice, $n = 4$). Scale bar, 100 μm. Odor discrimination tests in control and Kir2.1 mice. ***E***, Control and Kir2.1 mice were trained for 4 d to discriminate between the conditioned odor (odor 1 + sugar, CS+) and the unconditioned odor (odor 2, CS−). On the fifth day (***F***) the animals were tested in a three-chamber apparatus and the digging time for each odor (without sugar) of the related pair was scored. ***G–J***, Digging time for each pair of odors tested. Bars indicate SEM. *$p < 0.05$, ** $0.001 < p < 0.01$.

two odors. We found that the altered connectivity was confined around the main glomeruli, for both the sensory map and for the intrabulbar connections. We reasoned that the Kir2.1 mice could have difficulties in discriminating odorants that elicit very similar spatial maps of activated glomeruli, such as enantiomers. Enantiomers, mirror symmetric pairs of molecules that differ only in their optical activity, are represented by similar functional maps that differ for one or a few activated glomeruli located in a restricted area, in rodents. It has been shown that the spatial pattern of glomerular activity provide sufficient information to discriminate molecular shapes (Linster et al., 2001; Rubin and Katz, 2001; Kobayakawa et al., 2007; Clarin et al., 2010; Mori and Sakano, 2011; Murthy, 2011).

To assess the discrimination capabilities of Kir2.1 mice, we performed an olfactory discrimination test (Schellinck et al., 2001) using four different couples of odorants. Mice were trained for 4 d to associate either of the two related odors to a food reward (sugar). On the fifth day, the sugar reward was removed and the animal ability to discriminate between the two related odors was tested. The lengths of time the mouse spent investigating, digging, and sniffing the odorants were measured (see methods for details). If the animal spends most of the time investigating the

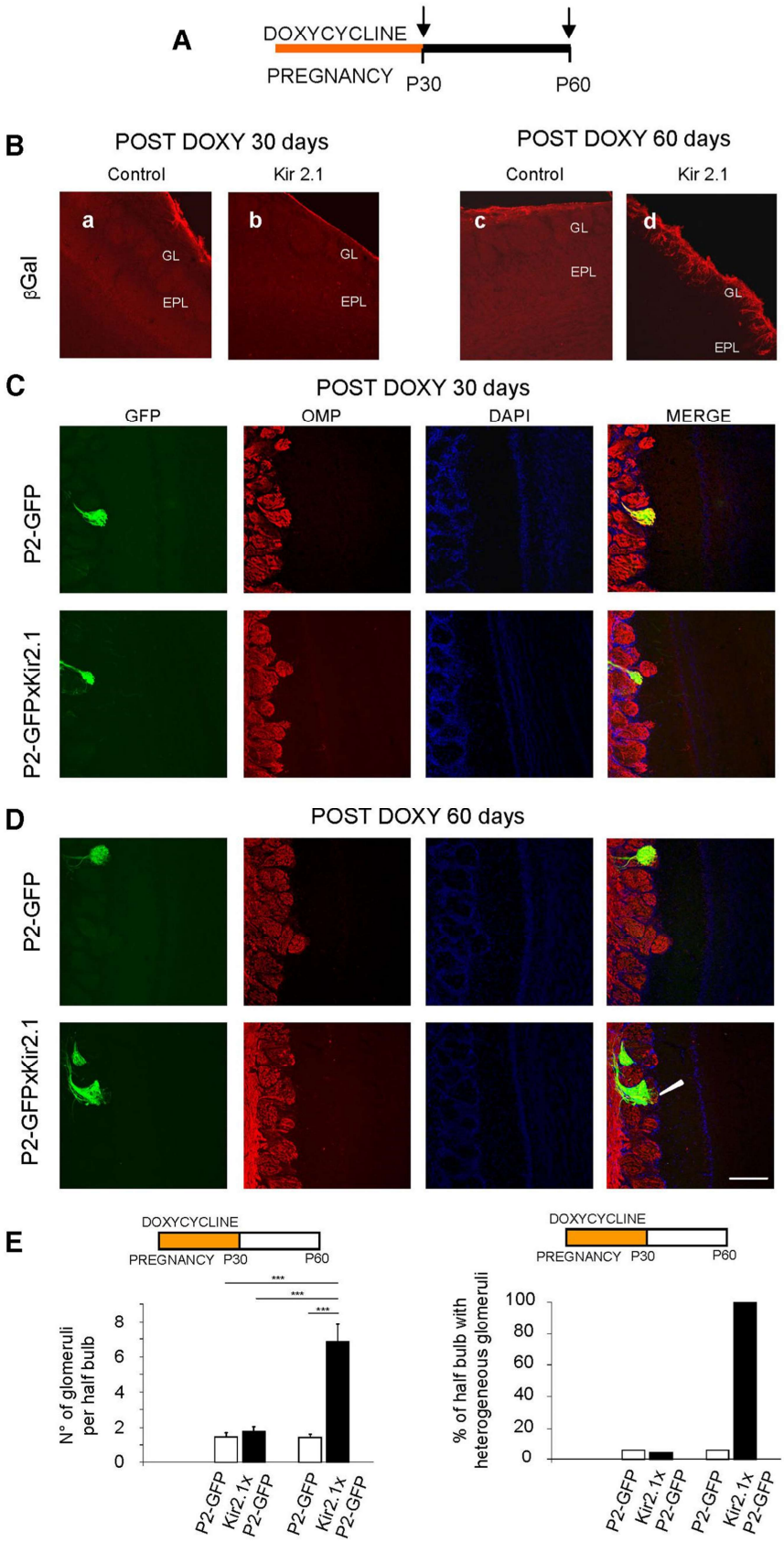

Figure 7. Sensory map plasticity in Kir2.1 mice. ***A***, Schematic of the experimental strategy. Doxycycline is supplied with the food throughout the gestation and in newborn mice until P30. The sensory map is analyzed at P30 (***C***) and at P60 (***D***). In the latter case, Kir2.1 is re-expressed from P30 to P60. ***B***, Horizontal sections of the OB immunostained with antibodies against β-gal in wild-type control (***Ba***) and in Kir2.1 (***Bb***) mice, both treated with doxycycline until P30 (***Ba***, ***Bb***). In the Kir2.1 mice (***Bb***), β-gal (i.e., Kir2.1) expression is abolished, due to the doxycycline administration. ***Bc***, ***Bd***, Horizontal sections of the OB immunostained with antibodies against β-gal in wild-type control (***Bc***) and in Kir2.1 (***Bd***) mice, analyzed at P60. In Kir2.1 mice β-gal is clearly re-expressed. ***C***, Organization of P2 glomeruli was revealed by immunolabeling horizontal sections of the OB with antibodies against OMP (red). GFP expressed in P2 axons (green). Nuclei stained by the nuclear marker, DAPI (blue). Upon doxy administration, at P30, P2-axons converge into a single homogeneous glomerulus in control and Kir2.1 mice. ***D***, At P60, P2-axons converge into a single glomerulus in control and Kir2.1 mice; however, they also project to adjacent heterogeneous glomeruli in Kir2.1 mice (arrowhead). Scale bar, 200 μm. ***E***, Summary of results. As indicated by the schematic on top in each graph: left, results at P30; right, results at P60.

conditioned odor, this indicates that the animal is able to discriminate the two odors.

We found that Kir2.1 mice were unable to discriminate between odors that elicit very similar spatial patterns of activation, such as the couples of the enantiomers 2-heptanol (+) and (−), fenchone (+) and (−), carvone (+) and (−), but retained the ability to distinguish between odorants that presented a more distinct spatial pattern of activated areas, such as 2-MB acid and cb acid (Figure 6*E–J*).

Overexpression of Kir2.1 in adults disrupted the already refined connectivity

Spontaneous activity has always been thought to play a prominent role in early stages of development (Goodman and Shatz, 1993; Huberman et al., 2008). Once the sensory systems become responsive to sensory stimuli, evoked activity contributes to the stabilization and further refinement of neuronal connections (Shatz, 1996; Hensch, 2004). Whether spontaneous activity can modulate synaptic connections in adult life remains largely unknown.

To address this point we took advantage of the inducible nature of the Kir2.1 construct. In one group of experimental animals, the expression of the Kir2.1 channel was suppressed by doxycycline administration in the food, during gestation, and in the first 30 d of postnatal life (P30) in Kir2.1 mice (Fig. 7*A*). In a second group of animals, at P30 the administration of doxycycline was suspended, allowing the Kir2.1 channel to be expressed until P60 (Fig. 7*A*).

We analyzed the effect of suppression/re-expression of Kir2.1 on both levels of the topographic organization of the olfac-

tory bulb, namely the glomerular map and the intrabulbar connections. We found that doxycycline administration until P30 completely abolished the expression of Kir2.1 (Fig. 7*B*). Analyzing the sensory map at P30, we found that the stereotypical pattern of convergence of the P2 OSN axons was restored (control mice, $n = 3$; Kir2.1 mice, $n = 3$; t test, $p = 0.4$; Fig. 7*C*,*E*). Studying the sensory map at P60, in mice that expressed Kir2.1 gene from P30 to P60, we found that P2-axons converge to form not only the main homogenous glomeruli, but they also targeted several additional heterogeneous glomeruli (Fig. 7*D*,*E*; control mice, $n = 3$; Kir2.1 mice, $n = 4$, control-Kir2.1 P60 t test, $^{***}p < 0.0001$; Kir 30-Kir 60 t test, $^{***}p < 0.0001$; Fig. 7*D*,*E*).

We then analyzed the intrabulbar connections. In the first experimental design, a small tracer injection targeted to the glomerular layer in Kir2.1 mice at P30 ended in a small projection, confined to a single glomerulus (as in controls), on the opposite side of the bulb (Fig. 8*A*–*E*,*K*; wild-type controls + doxy, P30, mice, $n = 3$, ratio $= 1.01 \pm 0.03$, Kir2.1 mice + doxy, P30, mice, $n = 3$, ratio $= 1.1 \pm 0.09$, t test ratio Kir2.1-wt mice, $p = 0.2$).

A focal tracer injection targeted to the glomerular layer at P60 in Kir2.1 mice that overexpressed Kir2.1channel from P30 to P60, gave rise to a projection that was broader than in controls (Fig. 8*F*–*K*; wild-type control mice: $n = 3$, ratio $= 1.1 \pm 0.09$; Kir2.1 mice: $n = 3$, ratio $= 1.8 \pm 0.2$; t test ratio Kir2.1-controls (P60), $^{**}p = 0.002$). The projection size/injection size ratio was smaller at P60 in Kir2.1 mice treated with doxycycline until P30 than in Kir2.1 mice at P30 ($^{***}p \leq 0.001$).

Discussion

Perturbed neural wiring and functional maps in Kir2.1 mice

In this paper we studied circuit formation and function in the OB of mice genetically modified to have reduced spontaneous activity in OSNs (Kir2.1 mice; Yu et al., 2004). We found that the basal spiking activity was significantly reduced in OSNs of Kir2.1 mice with respect to controls. In response to odor stimulation, however, the Ca^{2+} response and the firing pattern were superimposable in control and Kir2.1 mice. These data suggest that odorant stimuli, at all the concentrations tested, were capable of overcoming the hyperpolarization of OSNs in Kir2.1 mice. It is worth noting that OSNs have high input impedance (Lynch and Barry, 1989; M. Ma et al., 1999; Grosmaitre et al., 2006) and small odor-evoked currents may be sufficient to cause suprathreshold depolarization. Consistent with our results, previous studies have shown that although basal activity is reduced in neurons expressing Kir2.1, once threshold is reached, stimulus-evoked activity in control and overexpressing Kir2.1 neurons is similar (Burrone et al., 2002). These data indicate that Kir2.1 mice are a useful model to dissect the role of spontaneous activity in the topographic and functional organization of the OB.

Odor-evoked activity also was clearly recorded in glomeruli of Kir2.1 mice although the functional maps were coarser than in controls. A recent paper (L. Ma et al., 2014) reported that methyl valerate did not elicit responses in the OB of Kir2.1 mice, in contrast to our extensive data. It is not clear what the difference is, but we note that our study used a large suite of odorants (97 chemically diverse odorants, including ethyl valerate, an odor similar to methyl valerate). Our *in vivo* data are also corroborated by *in vitro* recordings demonstrating clear odor response in Kir2.1overexpressing OSNs.

We found a higher number of active spots to stimuli that resulted in a larger overall area of response, compared with controls. Each glomerulus was responsive to a higher number of odorants, although the odor responses were smaller in amplitude in Kir2.1 glomeruli than in controls. It has been shown that the spots of the activated area correspond to single glomeruli and they derived primarily from the activation of the sensory neuron axons (Meister and Bonhoeffer, 2001; Belluscio et al., 2002; Soucy et al., 2009). A hallmark of mature glomeruli is that they are innervated exclusively by sensory axons expressing the same OR (Treloar et al., 2002). We found that OSN axons expressing the same OR project to multiple adjacent glomeruli in Kir2.1 mice, a proper feature of early stage of development (Royal and Key, 1999; Lodovichi and Belluscio, 2012). This pattern of projection can explain the higher number of activated glomeruli in response to a given odorant. The spatial vicinity of these additional heterogeneous glomeruli is likely to account for the larger size of the spots. The heterogeneous organization of glomeruli can explain the smaller amplitude of the response, since not all the fibers within a given glomerulus are responsive to a given odorant. Having different types of ORs, each glomerulus is responsive to a higher number of odors, resulting in wider molecular receptive range. These data suggest that the functional alterations reflected with remarkable precision the unrefined connectivity of the sensory map of Kir2.1 mice.

In addition, we found that in Kir2.1 mice the intrabulbar connections, although preserved, did not undergo the refinement process that takes place between P15 and P30 in control animals, resulting in spread of connections. The axonal projections of the ETCs also were coarser in the absence of sensory experience due to naris occlusion (Marks et al., 2006) although the defects were more severe in that case. The absence of evoked activity appears to cause a significant enlargement of the ETC projections while reduced spontaneous activity prevents their refinement. Our data show that reduced spontaneous activity in Kir2.1 mice affects the refinement process of both levels of topography in the OB.

Although the mechanism underlying neural circuit refinement remains to be clarified, different scenarios can be envisioned. (1) Disrupted spontaneous activity is likely to influence the levels of second messengers such as cyclic nucleotides and Ca^{2+} that are known to play a critical role in axon targeting in several systems (Song et al., 1997; J.Q. Zheng and Poo, 2007) including the OS (Maritan et al., 2009; Lodovichi and Belluscio, 2012). (2) Spontaneous firing could facilitate the action of factors, such as neurotrophic factors, in the activity-dependent competition that operates on branch stability or formation (Thoenen, 1995; Bonhoeffer, 1996). It has been shown that the action of neurotrophins has to be coupled to afferent spontaneous activity to modulate neuronal plasticity in the developing visual cortex (Caleo et al., 1999). In addition, the action of trophic factors on axon growth in retinal ganglion cell is dramatically enhanced by activity (Goldberg et al., 2002). It is worth noting that the OR is thought to determine not only odor-evoked activity but also specific pattern of spontaneous activity, in OSNs in *Drosophila* (Hallem and Carlson, 2004) and also in mice (Connelly et al., 2013). Therefore, an activity-based competition could modulate the response of OSN and ETC axons to trophic factors and/or guidance molecules present in the bulb, favoring the refinement, pruning, and stabilization of axon arbors.

Altered odor discrimination ability in Kir2.1 mice

Analyzing the olfactory behavior, we found that Kir2.1 mice were not able to discriminate odorants that elicited similar spatial maps of activated glomeruli but retained the ability to discriminate odorants that activated a more distinct spatial pattern of glomeruli. These results could be explained by the alterations we found in the anatomical and functional maps of the OB in Kir2.1

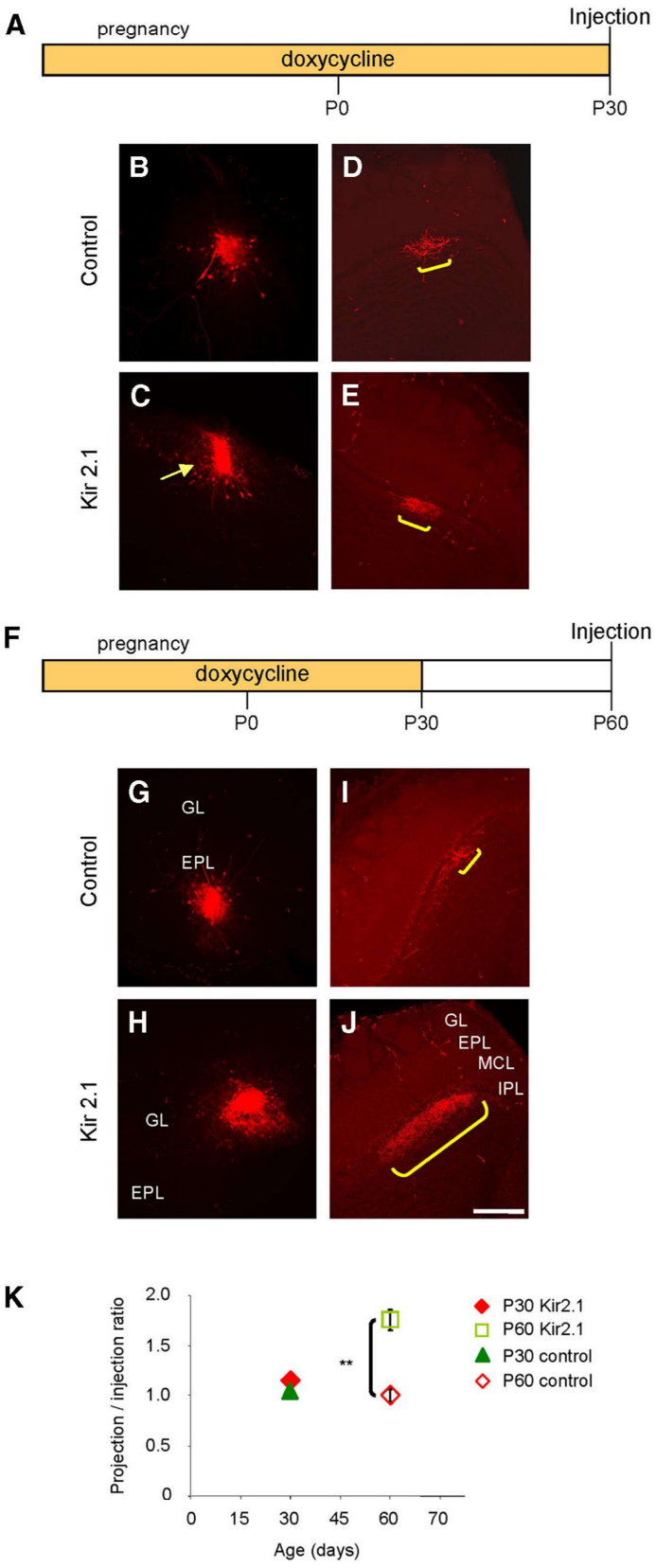

Figure 8. Plasticity of the intrabulbar link in Kir2.1 mice. ***A***, Schematic of experimental strategy. ***B***, ***C***, Examples of focal tracer injections targeted to the glomerular layer of control (***B***) and Kir2.1 (***C***) mice (supplied with doxycycline). Arrow, labeled ETCs. ***D***, ***E***, The patchy corresponding projections (yellow bracket) on the opposite side of the OB. ***F***, Schematic representation of the experimental strategy. Doxycycline administration is suspended at P30 and tracer injection targeted to the glomerular layer in control and Kir2.1 mice at P60. Between P30 and P60 no doxycycline is supplied to allow overexpression of the Kir2.1. ***G***, ***H***, Examples of focal injections in the glomerular layer in control (***G***) and in Kir2.1 (***H***) mice and the corresponding projections (yellow bracket) on the opposite side of the bulb in control (***I***) and Kir2.1 (***J***) mice. In Kir2.1 mice (***J***) the projection is clearly broader. Scale bar, 200 μm. GL, glomerular layer; EPL, external plexiform layer; MCL, mitral cell layer; IPL, internal plexiform layer. ***K***, Summary of results. Data are presented as mean ± SD $^{**}0.001 < p < 0.01$.

mice. The functional maps elicited by the (−) or (+) element of each pair of the enantiomers (Linster et al., 2001; Rubin and Katz, 2001; Clarin et al., 2010) differ for a few glomeruli located in a restricted region. That region is superimposable to the area where we found additional heterogeneous glomeruli and a broader link between homologous glomeruli. Therefore the specific spatial pattern that contributes to the neural representation of enantiomers appears to be disrupted by the unrefined connectivity of the OB in Kir2.1 mice. Discrimination of odorants that are represented by glomeruli scattered in more distinct locations in the bulb was not significantly affected. Our data corroborate the view that spatial maps in the OB contribute to the neural representation of different odor molecules (Rubin and Katz, 2001; Kobayakawa et al., 2007).

Neuronal plasticity in the olfactory bulb

Sensory experience modulates the development of neuronal circuitry mostly within a defined period of time (the critical period) during which the brain is particularly plastic (Hensch, 2004). Beyond this critical period the wiring of neural circuitry is hardly affected by changes in evoked activity. Unlike other sensory modality, it has been shown that neural circuits in the OB, namely the link between homologous glomeruli, remain sensitive to manipulation of evoked activity also in adulthood (Cummings and Belluscio, 2010).

The effect of the spontaneous activity on mature neuronal circuits has been scarcely examined. Indeed the role of spontaneous activity is generally thought to be confined to the early phase of development (Shatz, 1996; McLaughlin et al., 2003; Spitzer, 2006; Huberman et al., 2008). Our data demonstrated that the OB differs significantly from this paradigm. We found that the re-expression of Kir2.1 in adult animals induces a regression of the already refined connectivity of the glomerular map and of the link be-

tween homologous glomeruli to a coarser status. These results indicate that the neuronal wiring in the OB, when formed correctly, remained sensitive to afferent spontaneous activity manipulations in adults.

Although the mechanisms underpinning the formation of the intrabulbar connections and its relationship with the development of the glomerular map remain to be clarified, it is likely that the coarser link between homologous glomeruli could reflect the coarser glomerular map. The lack of afferent spontaneous activity seems to freeze the system at an early stage, during development and to induce a regression of the already refined connectivity to a coarser status, in adulthood.

In recent papers (L. Ma et al., 2014; Tsai and Barnea, 2014), using different types of transgenic mice, (including the Kir2.1mice) found that the stereotypical pattern of OSN convergence can be restored when the transgene expression is abolished during pregnancy and/or in the early postnatal days, as we observed in our procedure. However, they found that if the map develops abnormally, because the transgene expression is only suppressed after the early days of life, the map continued to be perturbed. It seems that a memory of the disrupted sensory map also is maintained when the transgene expression is later abolished. The mechanisms underlying these results, as well as their relation to the intrabulbar maps, remain to be explained, in a system with such a high degree of plasticity.

Overall, our data indicate that spontaneous afferent activity plays a critical role in the refinement and in the maintenance of the topographic organization of the OB, that in turn, affects odor information processing and olfactory behavior.

References

Belluscio L, Gold GH, Nemes A, Axel R (1998) Mice deficient in G(olf) are anosmic. Neuron 20:69–81. CrossRef Medline

Belluscio L, Lodovichi C, Feinstein P, Mombaerts P, Katz LC (2002) Odorant receptors instruct functional circuitry in the mouse olfactory bulb. Nature 419:296–300. CrossRef Medline

Bonhoeffer T (1996) Neurotrophins and activity-dependent development of the neocortex. Curr Opin Neurobiol 6:119–126. CrossRef Medline

Bozza TC, Kauer JS (1998) Odorant response properties of convergent olfactory receptor neurons. J Neurosci 18:4560–4569. Medline

Burrone J, O'Byrne M, Murthy VN (2002) Multiple forms of synaptic plasticity triggered by selective suppression of activity in individual neurons. Nature 420:414–418. CrossRef Medline

Caleo M, Lodovichi C, Maffei L (1999) Effects of nerve growth factor on visual cortical plasticity require afferent electrical activity. Eur J Neurosci 11:2979–2984. CrossRef Medline

Clarin T, Sandhu S, Apfelbach R (2010) Odor detection and odor discrimination in subadult and adult rats for two enantiomeric odorants supported by c-fos data. Behav Brain Res 206:229–235. CrossRef Medline

Connelly T, Savigner A, Ma M (2013) Spontaneous and sensory-evoked activity in mouse olfactory sensory neurons with defined odorant receptors. J Neurophysiol 110:55–62. CrossRef Medline

Cossart R, Ikegaya Y, Yuste R (2005) Calcium imaging of cortical networks dynamics. Cell Calcium 37:451–457. CrossRef Medline

Cummings DM, Belluscio L (2010) Continuous neural plasticity in the olfactory intrabulbar circuitry. J Neurosci 30:9172–9180. CrossRef Medline

Danciger E, Mettling C, Vidal M, Morris R, Margolis F (1989) Olfactory marker protein gene: its structure and olfactory neuron-specific expression in transgenic mice. Proc Natl Acad Sci U S A 86:8565–8569. CrossRef Medline

Delay R, Restrepo D (2004) Odorant responses of dual polarity are mediated by cAMP in mouse olfactory sensory neurons. J Neurophysiol 92:1312–1319. CrossRef Medline

Feinstein P, Bozza T, Rodriguez I, Vassalli A, Mombaerts P (2004) Axon guidance of mouse olfactory sensory neurons by odorant receptors and the beta2 adrenergic receptor. Cell 117:833–846. CrossRef Medline

Feldheim DA, O'Leary DD (2010) Visual map development: bidirectional signaling, bifunctional guidance molecules, and competition. Cold Spring Harb Perspect Biol 2:a001768. CrossRef Medline

Gogos JA, Osborne J, Nemes A, Mendelsohn M, Axel R (2000) Genetic ablation and restoration of the olfactory topographic map. Cell 103:609–620. CrossRef Medline

Goldberg JL, Espinosa JS, Xu Y, Davidson N, Kovacs GT, Barres BA (2002) Retinal ganglion cells do not extend axons by default: promotion by neurotrophic signaling and electrical activity. Neuron 33:689–702. CrossRef Medline

Goodman CS, Shatz CJ (1993) Developmental mechanisms that generate precise patterns of neuronal connectivity. Cell 72 [Suppl]:77–98. CrossRef Medline

Grienberger C, Konnerth A (2012) Imaging calcium in neurons. Neuron 73:862–885. CrossRef Medline

Grosmaitre X, Vassalli A, Mombaerts P, Shepherd GM, Ma M (2006) Odorant responses of olfactory sensory neurons expressing the odorant receptor MOR23: a patch clamp analysis in gene-targeted mice. Proc Natl Acad Sci U S A 103:1970–1975. CrossRef Medline

Hallem EA, Carlson JR (2004) The odor coding system of *Drosophila*. Trends Genet 20:453–459. CrossRef Medline

Hensch TK (2004) Critical period regulation. Annu Rev Neurosci 27:549–579. CrossRef Medline

Huberman AD, Feller MB, Chapman B (2008) Mechanisms underlying development of visual maps and receptive fields. Annu Rev Neurosci 31:479–509. CrossRef Medline

Kerr JN, Greenberg D, Helmchen F (2005) Imaging input and output of neocortical networks in vivo. Proc Natl Acad Sci U S A 102:14063–14068. CrossRef Medline

Kobayakawa K, Kobayakawa R, Matsumoto H, Oka Y, Imai T, Ikawa M, Okabe M, Ikeda T, Itohara S, Kikusui T, Mori K, Sakano H (2007) Innate versus learned odour processing in the mouse olfactory bulb. Nature 450:503–508. CrossRef Medline

Lin DM, Wang F, Lowe G, Gold GH, Axel R, Ngai J, Brunet L (2000) Formation of precise connections in the olfactory bulb occurs in the absence of odorant-evoked neuronal activity. Neuron 26:69–80. CrossRef Medline

Linster C, Johnson BA, Yue E, Morse A, Xu Z, Hingco EE, Choi Y, Choi M, Messiha A, Leon M (2001) Perceptual correlates of neural representations evoked by odorant enantiomers. J Neurosci 21:9837–9843. Medline

Lodovichi C, Belluscio L (2012) Odorant receptors in the formation of the olfactory bulb circuitry. Physiology 27:200–212. CrossRef Medline

Lodovichi C, Belluscio L, Katz LC (2003) Functional topography of connections linking mirror-symmetric maps in the mouse olfactory bulb. Neuron 38:265–276. CrossRef Medline

Lynch JW, Barry PH (1989) Action potentials initiated by single channels opening in a small neuron (rat olfactory receptor). Biophys J 55:755–768. CrossRef Medline

Ma L, Wu Y, Qiu Q, Scheerer H, Moran A, Yu CR (2014) A developmental switch of axon targeting in the continuously regenerating mouse olfactory system. Science 344:194–197. CrossRef Medline

Ma M, Chen WR, Shepherd GM (1999) Electrophysiological characterization of rat and mouse olfactory receptor neurons from an intact epithelial preparation. J Neurosci Methods 92:31–40. CrossRef Medline

Maritan M, Monaco G, Zamparo I, Zaccolo M, Pozzan T, Lodovichi C (2009) Odorant receptors at the growth cone are coupled to localized cAMP and Ca2+ increases. Proc Natl Acad Sci U S A 106:3537–3542. CrossRef Medline

Marks CA, Cheng K, Cummings DM, Belluscio L (2006) Activity-dependent plasticity in the olfactory intrabulbar map. J Neurosci 26:11257–11266. CrossRef Medline

McLaughlin T, Torborg CL, Feller MB, O'Leary DD (2003) Retinotopic map refinement requires spontaneous retinal waves during a brief critical period of development. Neuron 40:1147–1160. CrossRef Medline

McQuiston AR, Katz LC (2001) Electrophysiology of interneurons in the glomerular layer of the rat olfactory bulb. J Neurophysiol 86:1899–1907. Medline

Meister M, Bonhoeffer T (2001) Tuning and topography in an odor map on the rat olfactory bulb. J Neurosci 21:1351–1360. Medline

Mombaerts P (1996) Targeting olfaction. Curr Opin Neurobiol 6:481–486. CrossRef Medline

Mori K, Sakano H (2011) How is the olfactory map formed and interpreted

in the mammalian brain? Annu Rev Neurosci 34:467–499. CrossRef Medline

Murthy VN (2011) Olfactory maps in the brain. Annu Rev Neurosci 34: 233–258. CrossRef Medline

Nunemaker CS, DeFazio RA, Moenter SM (2003) A targeted extracellular approach for recording long-term firing patterns of excitable cells: a practical guide. Biol Proced Online 5:53–62. CrossRef Medline

Pietrobon M, Zamparo I, Maritan M, Franchi SA, Pozzan T, Lodovichi C (2011) Interplay among cGMP, cAMP, and Ca2+ in living olfactory sensory neurons *in vitro* and *in vivo*. J Neurosci 31:8395–8405. CrossRef Medline

Reisert J (2010) Origin of basal activity in mammalian olfactory receptor neurons. J Gen Physiol 136:529–540. CrossRef Medline

Ressler KJ, Sullivan SL, Buck LB (1994) Information coding in the olfactory system: evidence for a stereotyped and highly organized epitope map in the olfactory bulb. Cell 79:1245–1255. CrossRef Medline

Ronnett GV, Parfitt DJ, Hester LD, Snyder SH (1991) Odorant-sensitive adenylate cyclase: rapid, potent activation and desensitization in primary olfactory neuronal cultures. Proc Natl Acad Sci U S A 88:2366–2369. CrossRef Medline

Rospars JP, Lánský P, Duchamp A, Duchamp-Viret P (2003) Relation between stimulus and response in frog olfactory receptor neurons in vivo. Eur J Neurosci 18:1135–1154. CrossRef Medline

Royal SJ, Key B (1999) Development of P2 olfactory glomeruli in P2-internal ribosome entry site-tau-LacZ transgenic mice. J Neurosci 19: 9856–9864. Medline

Rubin BD, Katz LC (1999) Optical imaging of odorant representations in the mammalian olfactory bulb. Neuron 23:499–511. CrossRef Medline

Rubin BD, Katz LC (2001) Spatial coding of enantiomers in the rat olfactory bulb. Nat Neurosci 4:355–356. CrossRef Medline

Sakano H (2010) Neural map formation in the mouse olfactory system. Neuron 67:530–542. CrossRef Medline

Savigner A, Duchamp-Viret P, Grosmaitre X, Chaput M, Garcia S, Ma M, Palouzier-Paulignan B (2009) Modulation of spontaneous and odorant-evoked activity of rat olfactory sensory neurons by two anorectic peptides, insulin and leptin. J Neurophysiol 101:2898–2906. CrossRef Medline

Schellinck HM, Forestell CA, LoLordo VM (2001) A simple and reliable test of olfactory learning and memory in mice. Chem Senses 26:663–672. CrossRef Medline

Schoenfeld TA, Marchand JE, Macrides F (1985) Topographic organization of tufted cell axonal projections in the hamster main olfactory bulb: an intrabulbar associational system. J Comp Neurol 235:503–518. CrossRef Medline

Shatz CJ (1996) Emergence of order in visual system development. Proc Natl Acad Sci U S A 93:602–608. CrossRef Medline

Shepherd GM (2004) The synaptic organization of the brain. Oxford: Oxford UP.

Song HJ, Ming GL, Poo MM (1997) cAMP-induced switching in turning direction of nerve growth cones. Nature 388:275–279. CrossRef Medline

Soucy ER, Albeanu DF, Fantana AL, Murthy VN, Meister M (2009) Precision and diversity in an odor map on the olfactory bulb. Nat Neurosci 12:210–220. CrossRef Medline

Spitzer NC (2006) Electrical activity in early neuronal development. Nature 444:707–712. CrossRef Medline

Tan J, Savigner A, Ma M, Luo M (2010) Odor information processing by the olfactory bulb analyzed in gene-targeted mice. Neuron 65:912–926. CrossRef Medline

Thoenen H (1995) Neurotrophins and neuronal plasticity. Science 270: 593–598. CrossRef Medline

Treloar HB, Feinstein P, Mombaerts P, Greer CA (2002) Specificity of glomerular targeting by olfactory sensory axons. J Neurosci 22:2469–2477. Medline

Tsai L, Barnea G (2014) A critical period defined by axon-targeting mechanisms in the murine olfactory bulb. Science 344:197–200. CrossRef Medline

Uchida N, Takahashi YK, Tanifuji M, Mori K (2000) Odor maps in the mammalian olfactory bulb: domain organization and odorant structural features. Nat Neurosci 3:1035–1043. CrossRef Medline

Vassar R, Chao SK, Sitcheran R, Nuñez JM, Vosshall LB, Axel R (1994) Topographic organization of sensory projections to the olfactory bulb. Cell 79:981–991. CrossRef Medline

Yu CR, Power J, Barnea G, O'Donnell S, Brown HE, Osborne J, Axel R, Gogos JA (2004) Spontaneous neural activity is required for the establishment and maintenance of the olfactory sensory map. Neuron 42:553–566. CrossRef Medline

Zhang LI, Poo MM (2001) Electrical activity and development of neural circuits. Nat Neurosci 4 [Suppl]:1207–1214. CrossRef Medline

Zheng C, Feinstein P, Bozza T, Rodriguez I, Mombaerts P (2000) Peripheral olfactory projections are differentially affected in mice deficient in a cyclic nucleotide-gated channel subunit. Neuron 26:81–91. CrossRef Medline

Zheng JQ, Poo MM (2007) Calcium signaling in neuronal motility. Annu Rev Cell Dev Biol 23:375–404. CrossRef Medline

Zou DJ, Feinstein P, Rivers AL, Mathews GA, Kim A, Greer CA, Mombaerts P, Firestein S (2004) Postnatal refinement of peripheral olfactory projections. Science 304:1976–1979. CrossRef Medline

4.2 - A role for the Ca^{2+}-activated Cl^- channel in olfaction

Manuscript submitted

Gianluca Pietra, Michele Dibattista, Anna Menini, Johannes Reisert, Anna Boccaccio

A role for the Ca^{2+}-activated Cl^- channel in olfaction

Gianluca Pietra[1]*, Michele Dibattista[2]*, Anna Menini[1#], Johannes Reisert[2#], Anna Boccaccio[3#]

[1]Neurobiology Group, SISSA, Scuola Internazionale Superiore di Studi Avanzati, Trieste, Italy

[2]Monell Chemical Senses Center, Philadelphia, PA, USA

[3]Institute of Biophysics, CNR, Genova, Italy,

*equal contribution

corresponding authors

Key words: ANO2, TMEM16B, transduction, calcium-activated chloride channels, signal amplification, olfaction

4.2.1 - Abstract (max 150 words)

A large portion of odor-evoked transduction currents in olfactory sensory neurons (OSNs) is due to Ca^{2+}-activated Cl^- currents (CaCCs). It has been reported that disruption of the *TMEM16b/Ano2* gene in mice completely abolished CaCCs in OSNs but did not produce any other major change in olfaction. Here, we re-addressed the question of the role of TMEM16B in olfaction. Responses to stimulation of individual OSNs showed transient bursts of action potentials significantly longer in TMEM16B knockout (KO) than in wild type (WT) mice. Lack of TMEM16B caused a markedly reduced basal spiking activity in OSNs expressing the I7 odorant receptor. Axonal targeting to the olfactory bulb was also altered, leading to the appearance of supernumerary I7 glomeruli. Furthermore, TMEM16B KO mice showed behavioral deficits in odor-guided food finding ability, an effect that diminished after several trials. Altogether, these results show that TMEM16B has a relevant role in normal olfaction.

4.2.2 - Introduction

The olfactory system detects small volatile molecules, odorants, which enter the nasal cavity via the inhaled air during normal breathing or sniffing. Odorants bind to odorant receptors (ORs) located on the cilia of olfactory sensory neurons (OSNs). Cilia are embedded in the mucus covering the epithelium and are the site of olfactory transduction: odorant molecules, once bound to ORs, activate a G protein-coupled transduction cascade, leading to the production of cAMP and culminating in the opening of two types of ion channels, cyclic nucleotide-gated (CNG) and Ca^{2+}-activated Cl^- channels. The primary inward current through CNG channels is mainly due to Ca^{2+} entry, which triggers the activation of a large secondary Cl^- current (Kleene, 1997, 1993; Kurahashi and Yau, 1993; Kleene and Gesteland, 1991; Lowe and Gold, 1993; Zhainazarov and Ache, 1995; Firestein and Shepherd, 1995; Reisert et al., 2005; Boccaccio and Menini, 2007). In electrophysiological recordings from isolated OSNs, Ca^{2+}-activated Cl^- currents (CaCCs) account for up to 90% of the transduction current (Boccaccio and Menini, 2007; Lowe and Gold, 1993). CaCCs are depolarizing currents as a result of the active Cl^- ions accumulation inside OSNs. This process is mainly mediated by the Na^+-K^+-$2Cl^-$–cotransporter NKCC1, which elevates Cl^- inside the cilia up to the same range as the Cl^- concentration present in the embedding mucus (Kaneko et al., 2004; Nickell et al., 2006; Reuter et al., 1998; Reisert et al., 2005). Additionally, the presence of the excitatory Cl^- current steepens the dependence of the transduction current on the stimulus amplitude, contributing to narrowing the neuron's dynamic range (Lowe and Gold, 1993; Boccaccio et al., 2006; Kleene, 2008).

The transduction current elicited by odorants produces a depolarization leading to generation of action potentials (APs) that are conducted to the olfactory bulb (OB) along the OSN axon. OSNs not only generate APs following odorant activation of the transduction current, but also fire APs in the absence of stimulation (O'Connell and Mozell, 1969; Trotier and MacLeod, 1983; Frings and Lindemann, 1991; Reisert and Matthews, 2001a; Reisert, 2010). It has been shown that spontaneous firing in OSNs is driven by the constitutive activity of the expressed OR (Reisert, 2010; Connelly et al., 2013), and that it is greatly suppressed by blocking CaCCs, indicating that the Cl^- current contributes to the basal firing activity of OSNs (Reisert, 2010). A change in spontaneous firing of OSNs expressing the same OR may have very important consequences at the level of the OB. Indeed, it is well known that not only all OSNs expressing the same OR do send their axons to specific glomeruli in the OB, but also OSN spontaneous firing plays a critical role to establish and maintain a correct glomerular targeting (Nishizumi and Sakano, 2015a; Yu et al., 2004; Lorenzon et al., 2015; Lodovichi and Belluscio, 2012; Nakashima et al., 2013).

Interestingly, although CaCCs were first observed in the early nineties (Kleene and Gesteland, 1991; Kleene, 1993; Lowe and Gold, 1993; Kurahashi and Yau, 1993), their molecular identity has been elusive for over two decades, hindering the possibility to better understand the role of CaCCs in the olfactory system. After ruling out several possible candidates, the channels expressed in OSN cilia responsible for CaCCs were finally identified as TMEM16B/Anoctamin2 (Stephan et al., 2009; Pifferi et al., 2009; Sagheddu et al., 2010;

Billig et al., 2011; Pifferi et al., 2012), a member of the *Tmem16* (*Anoctamin*) gene family (Pedemonte and Galietta, 2014). Disruption of the *TMEM16b* (*Ano2*) gene in mice (Billig et al., 2011) completely abolished CaCCs in OSNs. However, TMEM16B KO mice were reported not to have any obvious olfactory deficit, leading to the conclusion that CaCCs are dispensable for olfaction, and suggesting that odorant-evoked CNG currents, which remain in OSNs of TMEM16B KO mice, are sufficient to encode odorant information and supported near-normal olfactory function (Billig et al., 2011). As this first (and until now only) study on TMEM16B KO mice raised serious doubts about a relevant role of Ca^{2+}-activated Cl^- channels in olfaction (Billig et al., 2011), we sought to re-examine this question by further extending the experimental analysis and comparing additional aspects of olfactory function in TMEM16B KO vs WT mice.

As the role of TMEM16B in OSN firing has not been investigated yet, we measured both spontaneous and stimulus-induced firing activity. We found a decrease in spontaneous firing activity in randomly chosen OSNs in TMEM16B KO compared to WT mice. To reduce the variability due to the expression of different ORs in randomly chosen OSNs, we analyzed firing activity of OSNs expressing the I7 OR. To identify I7 OSNs we used I7-IRES-tauGFP (Bozza et al., 2002) mice crossed with TMEM16B KO mice. In I7 OSNs, we measured a reduction of spontaneous firing activity in the absence of TMEM16B compared to control mice. Moreover, we identified a dramatic change in the firing pattern in response to heptanal, a well-known agonist for the I7 OR. This change was manifested as a prolonged odorant response and a higher number of APs per response in I7 OSNs from TMEM16B KO compared to WT mice. Axonal targeting of I7 OSNs to the OB was also altered, as indicated by the presence of supernumerary I7 glomeruli in TMEM16B KO mice. Furthermore, from a behavioral point of view, TMEM16B KO mice showed a reduction in the ability to use olfactory cues to locate previously unknown buried food compared to WT mice. Our results demonstrate that the Ca^{2+}-activated Cl^- channel plays a physiological role in olfaction, showing that it is not simply dispensable for all aspects of olfaction but it is required for certain olfactory-driven behaviors. Moreover, in contrast to previous findings showing normal axonal targeting of OSNs expressing the P2 or M72 ORs, we find that axons of I7-expressing OSNs target an abnormally large number of glomeruli in the olfactory bulb. Importantly, TMEM16B had an influence on OSN action potential firing rates.

4.2.3 - RESULTS

4.2.3.1 - TMEM16B KO mice display altered olfactory ability in finding buried food

We used an odor-guided food-seeking test where mice have to use their olfactory ability to locate a food item buried under the bedding chips in the cage. We run the test for 5 consecutive days. On the first day of testing, when mice were naïve with respect to the food item and its odor (a piece of Oreo cookie), we observed that close to a fourth of TMEM16B KO mice (3 out of 13) failed to locate the food within the 10-min test time whereas none of the WT exceeded 10 min. On average, KO mice were significantly slower in locating the piece of Oreo (Fig. 1A, Mann-Whitney U-test, $p<0.05$). During the following 4 days of testing both WT and KO mice began to locate the food faster and, in the end, KO mice could perform the task as quickly as WT. TMEM16B KO mice did not show any gross motor, metabolic or motivational deficits as they performed equally well as WT mice when the food was presented visually on top of the bedding and not buried underneath it (Fig. 1A). Since the differences between TMEM16B KO and WT mice were prominent on the very first day of the experiment, we hypothesized that KO mice may not be able to reliably recognize new odors. We tested this hypothesis by giving the animals a week of rest and recovery and following the 8th day exposed them daily to new sources of odors (and new kind of food). The first day of this second set of experiments, mice were challenged to retrieve the same known kind of Oreo cookie used in the first set and both WT and KO performed equally (Fig. 1B). This suggests that mice retained the effect of the previous sessions of experiments and the identity of the odor. Over the following two days peanut or cheese were buried and TMEM16B KO mice displayed greater latencies in locating the source of the odor. Indeed, in both cases KO mice were around 2 fold slower than WT. These results confirm that, even when the task was already known, KO mice did not locate the food as fast as WT when exposed to new food odors (Fig. 1B, Mann-Whitney U-test, peanut $0.001<p<0.01$ and cheese $p<0.001$). When challenged to find chocolate (Fig. 1B), both strains performed equally fast, even though we observed a tendency for the KO to perform slower than

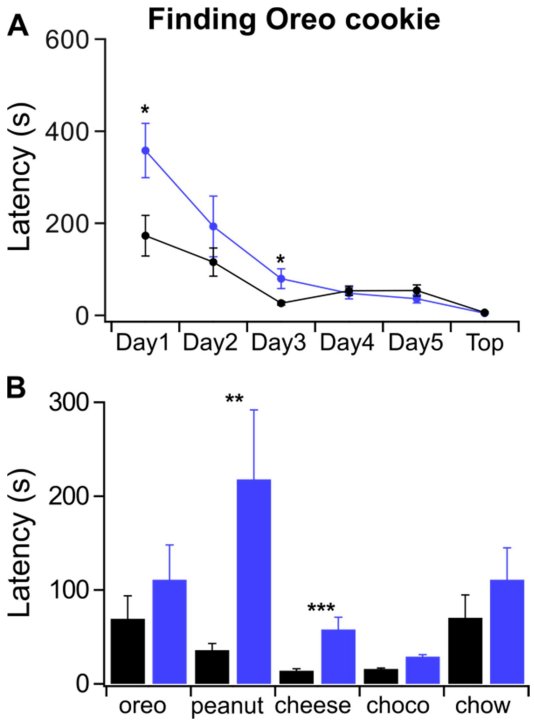

Figure 1: Behavioral deficits in TMEM16B KO mice.
(A): WT and KO mice had to locate an Oreo cookie buried in the bedding of their cage. Experiments were performed once a day over 5 days, on the 6th day the cookie was placed on top of the bedding. (B): Mice were exposed to a series of odors which were known (Oreo and chow) or novel (peanut, cheese, chocolate) to them. WT black and KO blue symbols. Mann-Whitney U-test * = $p<0.05$, ** = $p<0.01$, *** = $p<0.001$. Mean ± sem. Mice n=11 WT and n=13 KO.

the WT. Possibly a "floor" effect occurred, diminishing the difference between WT and KO mice. It is also possible that mice used cocoa which is also present in the Oreo cookie to locate the source of odor, thus making chocolate not an entirely new odor to them. The last day of the experiment mice had to locate a familiar source of odor (and food), their standard chow, and differences between WT and KO vanished. Also, with a new and naïve set of mice we repeated the same type of experiments but this time used cheese as the food item to be found for the first five consecutive days. Again, KO mice were significantly slower to locating the cheese on the first two days, but were equally fast for the remaining three. After a week of rest we tested the new cohort of mice for their ability to locate new sources of odor. Now WT and KO mice could locate the cheese equally fast, but KO performed significantly slow on the now new Oreo odor. Altogether, these experiments suggest that TMEM16B KO might have deficits in recognizing or locating the source of odors that are novel to them.

4.2.3.2 - Ca^{2+}-activated Cl^- currents are absent in OSNs from TMEM16B KO mice

Given the olfactory deficits we observed, we focused on comparing the electrophysiological properties of OSNs in the absence and in the presence of TMEM16B. First, similar to experiments previously reported for OSNs in tissue slices (Billig et al., 2011), we investigated Cl^- currents in OSNs isolated from WT and TMEM16B KO mice using flash photolysis of caged 8-Br-cAMP combined with patch-clamp recordings, a technique we used extensively to characterize transduction currents in isolated OSNs (Boccaccio et al., 2006; Boccaccio and Menini, 2007). We measured the whole-cell patch clamp current evoked by photorelease of 8-Br-cAMP inside the cilia-knob region of OSNs at various holding potentials (Fig. 2). At +50 mV, the current is mainly due to the cationic efflux through CNG channels directly activated by 8-Br-cAMP. As little Ca^{2+} enters the cilia at this holding potential, no Cl^- current was activated. In contrast, at -50 mV, the influx of Ca^{2+} through CNG channels activated a large secondary CaCC (Fig. 2A). OSNs from TMEM16B KO did not show the secondary large component at -50 mV, while they retained a similar outward current amplitude at +50 mV (Fig. 2A). Indeed, mean values for current amplitudes in WT and KO neurons were significantly different at -50 mV (Mann-Whitney U-test $0.01<p<0.05$) but not at +50 mV (Fig. 2B). Thus, we confirmed that CaCCs are

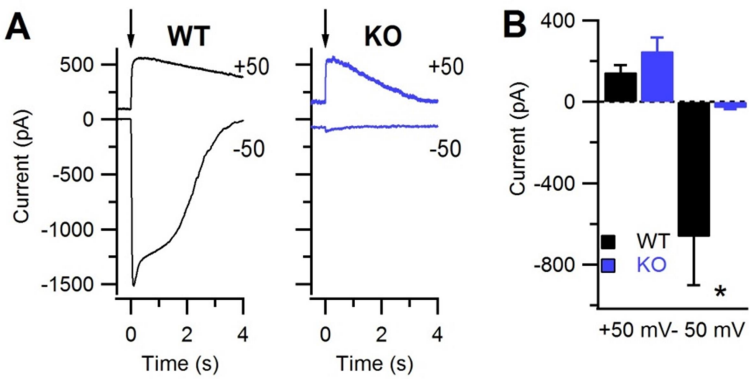

Figure 2: Transduction current elicited by 8-Br-cAMP photorelease recorded in isolated olfactory neurons.
(A): Representative whole cell response to photorelease of 8-Br-cAMP at a holding potential of -50 mV and +50 mV for WT and KO OSNs. (B): Summary of the average maximal current ± sem (n= 5 WT, n=3 KO; 1 tail t-test, * $0.01<p<0.05$).

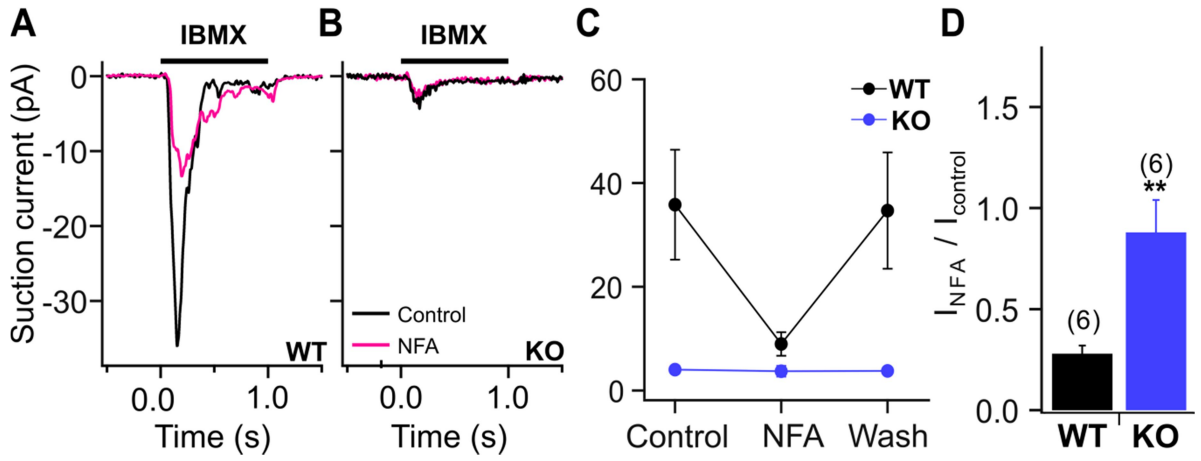

Figure 3: Transduction current recorded with the suction pipette technique from isolated OSNs (A-B): Single-cell suction electrode recordings from a dissociated WT (A) and KO (B) OSN stimulated with a 1 s pulse of 1 mM IBMX in Ringer's solution and in the presence or absence of 300 μM NFA, a Cl^- channel blocker. (C-D): Suction peak currents measured in control, in the presence of NFA and after washout (C) and ratio of the response in the presence and absence of NFA (D). Mean ± sem, n=6 for WT and KO. (** $p<0.01$ unpaired t-test)

absent in isolated OSNs from TMEM16B KO mice as previously shown by flash photolysis of caged Ca^{2+} and caged 8-Br-cAMP (Billig et al., 2011). As stated previously (Billig et al., 2011), the small residual current in KO OSNs at -50 mV was likely due to CNG cationic currents, further demonstrating that in isolated OSNs the transduction current is largely carried by CaCCs through TMEM16B channels (Billig et al., 2011).

We also investigated the contribution of CaCCs to stimulus-induced responses using the suction pipette technique in isolated OSNs (Fig. 3). We stimulated OSNs with the phosphodiesterase inhibitor IBMX, a feasible alternative to odorant stimulation (Reisert et al., 2007). Currents elicited by 1 mM IBMX (1 s application) were greatly reduced by application of the Cl^- current blocker niflumic acid (NFA, 300 μM) in WT OSNs (Fig. 3A, C, D). In OSNs from TMEM16B KO mice, IBMX application produced a significantly smaller current in KO compared to WT mice (Fig. 3B-C). This small current could not be further reduced by the application of NFA (Fig. 3B-D), a result consistent with the presence of a residual CNG current.

4.2.3.3 - IBMX-evoked firing in OSNs

The OSN transduction current evoked by a stimulus (e.g. IBMX or odorants) produces a depolarization that elicits APs, which are sent to the OB along the OSN axon. Up to now, AP firing of TMEM16B KO OSNs has not been investigated. In a first set of experiments, we compared AP firing in isolated OSNs from WT and KO mice stimulated by 1 s application of 1 mM IBMX using suction electrode recordings. In this recording configuration both transduction current and APs, which are generated as the voltage is free to vary, can be simultaneously recorded using a large bandwidth filter setting (see Methods). In WT OSNs we recorded AP firing during the early rising phase of the IBMX-stimulated transduction current (Fig. 4A). Surprisingly,

TMEM16B KO OSNs fired APs during the entire IBMX transduction current (Fig. 4B). On average, the number of spikes was significantly higher, and the spike train duration (measured as the time from the first to the last spike of the train to occur) was significantly longer in TMEM16B KO compared to WT mice (Fig. 4 A-B insets, C-D). Other parameters, such as the delay of the first action potential (Fig. 4E) and the maximal firing frequency (Fig. 4F) were not significantly different in KO and WT mice. These results show that the lack of CaCCs altered the firing behavior in response to IBMX by increasing the number of spikes and prolonging the duration of the spike train in isolated OSNs from TMEM16B KO mice.

In a second set of experiments, we recorded from OSNs *in situ* by using an intact olfactory epithelium preparation instead of dissociated OSNs. In this preparation OSNs still retain a large portion of their axons and are surrounded by a more physiological environment, including supporting cells. We recorded

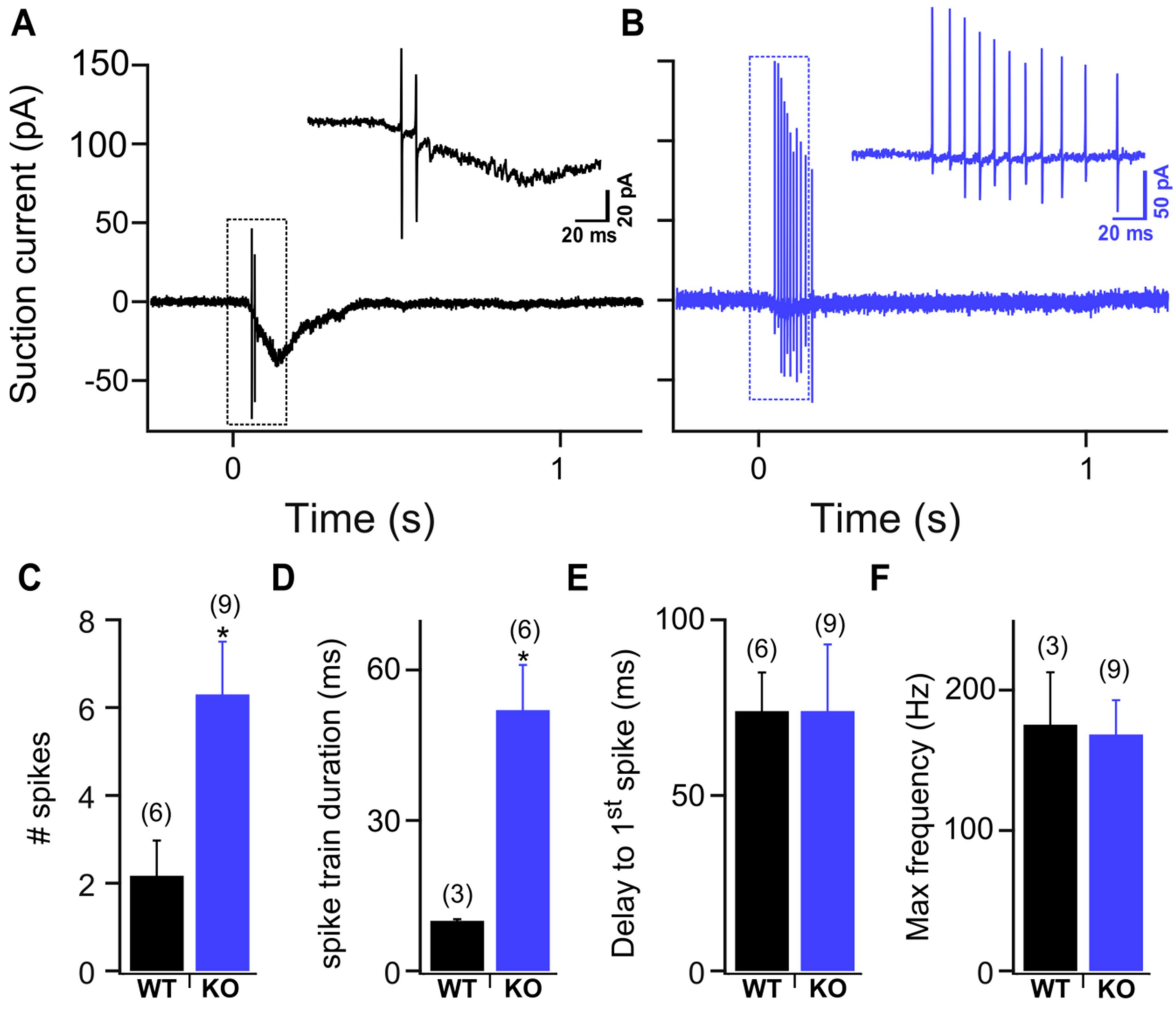

Figure 4: Evoked activity recorded with the suction pipette technique in OSNs from WT and KO mice.

(A-B): Single-cell suction electrode recordings from a dissociated WT (A) and KO (B) OSN stimulated with a 1 s pulse of 1 mM IBMX. Insets show responses on an expanded time scale. The recording bandwidth was 0-5000 Hz to display action potentials. (C-F): Differences in the response was quantified for the number of spikes (C), the duration of the train of elicited spikes (D), the delay of the first spike (E), maximal firing frequency (F). Mean ± sem, number of experiments is indicated in parenthesis. *p<0.05 unpaired t-test.

responses to IBMX using the loose-patch configuration from the dendritic knobs of OSNs. Figure 5A shows representative responses to a 50 ms puff of 100 µM IBMX of two OSNs from WT mice. The IBMX responses of both OSNs consisted of an initial burst of APs of rapidly declining amplitude followed by a silent period (Fig 5A, lower traces).

The amplitude of the spikes progressively recovered after the silent time or spikes reappeared at full

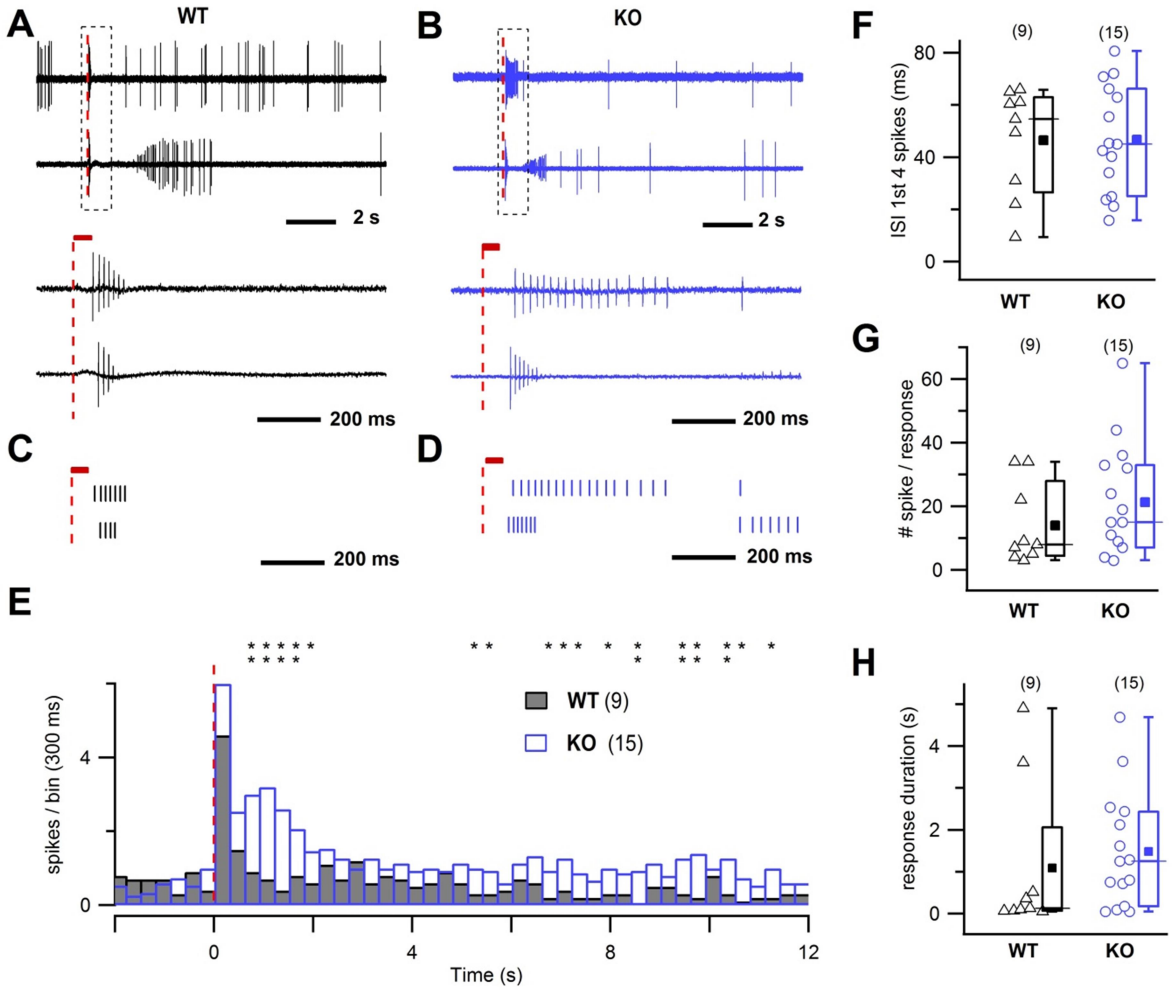

Figure 5: Evoked activity in WT and KO OSNs.

(A-B): Representative responses to 100 µM IBMX stimulation (50 ms) for two different OSNs from WT (A) and KO mice (B). Data represents loose patch recordings from dendritic knobs of OSNs located in the septum. The bottom panels show the regions enclosed by the dashed box on an expanded time scale. Broken red line represents the onset of IBMX stimulation, and the red bar in the bottom panel its duration. (C-D): Raster plots on an enlarged time scale for the same cells showed in panel (A) and (B). (E): Averaged responses to IBMX as in panel (A) and (B), normalized to the number of neurons (n=9 / 7 WT mice, n=15 / 8 KO mice; bin 300 ms). Broken red line represents the onset of stimulation and data belongs to WT and KO PSTH distributions. * and ** indicate 0.01<p<0.5 and p<0.01 respectively. (F-H): Scatter and boxplots of interspike interval (ISI) of the first four spikes (F, 47 ± 21 ms in WT, 47 ± 21 ms in KO), of the total number of spikes (G), 14± 13 spike/response in WT, 21 ± 18 spike/response in KO) and of the response duration (H, 1.1± 1.8 s in WT, 1.5 ± 1.4 spike/response in KO; mean ± SD). In the box plots the square represents the mean, lines represent the median, upper and lower box boundaries represent the 25th and 75th percentile, upper and lower whiskers represent the 5th and 95th percentiles. Data were not statistically different (one tail t-test for data in panel (F), Mann-Whitney U test, one tail, p>0.05 for data in panels (G-H). The number of experiments is indicated in parenthesis.

magnitude (Fig 5A, traces at the top) as previously described (Trotier, 1994, 1998; Duchamp-Viret et al., 2000; Reisert and Matthews, 2001a; Savigner et al., 2009; Lorenzon et al., 2015; Connelly et al., 2013). Overall, the responses to IBMX of OSNs from KO mice had broadly similar properties to WT OSNs, with a spike burst, silent period, and spike reappearance, as illustrated by two representative KO OSNs (Fig. 5B). The comparison between the cumulative responses normalized to the number of neurons (multi-cell PSTH or peristimulus time histogram; Fig. 5E) shows the presence of a second broad peak in KO OSNs, indicating an increase in firing activity compared to WT OSNs. The asterisks in the figure represents the bins with significantly higher firing rates in KO respect to WT OSNs (analysis according to (Dorrscheidt, 1981)).

To quantitatively characterize the responses we constructed raster plots (Fig. 5C-D), quantified the interspike interval (ISI) of the first four spikes (Fig. 5F), the total number of spikes in the response (Fig. 5G), and the response duration (Fig. 5H). Although the PSTH distribution differed between KO and WT mice these parameters were not significantly different, probably due to the high variability observed in this preparation.

Altogether our results show that both isolated and *in situ* OSNs from TMEM16B KO mice are able to fire APs in response to a stimulus, although displayed an altered evoked firing pattern. In particular, isolated OSNs from KO mice responded to IBMX with an increased number of APs and a spike train that lasted longer compared to WT OSNs. The spike train distribution recorded from OSNs *in situ* differed between KO and WT mice, with a higher firing activity of the former group.

4.2.3.4 - Heptanal-induced firing in I7 OSNs

The effectiveness of the IBMX stimulus has large variations among OSNs expressing different ORs (Reisert, 2010), potentially masking potential differences among evoked activity in OSNs from WT and KO mice. Therefore, we analyzed in detail the odorant-induced firing activity of OSNs that express the I7 OR by crossing I7-IRES-tauGFP (Bozza et al., 2002) with TMEM16B KO mice. Since the mouse I7 gene is expressed mostly in the ventro-lateral zone (zone 1) of the olfactory epithelium, we increased the probability of recording from an I7 OSNs using a coronal slice preparation from P0-P4 mice, which includes the epithelium attached to the turbinates where I7 OSNs are highly present. Responses to the I7 ligand heptanal (Bozza et al., 2002; Zhao, 1998) were recorded from the dendritic knobs of OSNs with the loose-patch configuration. The stimulation consisted of a 50 ms puff of 500 μM heptanal, a stimulus evoking a robust response in I7 OSNs. Figure 6A and B shows the responses of two representative OSNs for each WT and KO mice. In the WT, responses to heptanal were similar to those recorded with IBMX (Fig 5 A-B), i.e. characterized by a short burst of spikes of reducing amplitude, a period of silence, and a rebound of spikes of increasing amplitude (Fig. 6A-B), as previously described (Tan et al., 2010; Connelly et al., 2013). However, KO OSNs showed longer rebound periods, which added to the overall duration of the response (see Methods) compared to WT OSNs (Fig. 6A-D). A quantitative characterization of the heptanal responses showed that

ISI of the first four spikes did not significantly differ in WT and KO mice (Fig. 6F), whereas the overall number of spikes and response durations were significantly different (12 ± 10, spike/response and 2.3 ± 1.3 s for WT, and 70 ± 57 spike/response and 8.1 ± 7 s for KO, mean ± SD, Mann-Whitney U-test, 1 tail, $p<0.01$). Thus, I7 OSNs from KO mice showed a prolonged response to heptanal stimulation with a higher number of spikes in the response compared to I7 OSNs from WT mice. The difference between WT and KO I7 OSNs is also highlighted by the cumulative response normalized to the number of neurons (PSTH, Fig. 6E): the initial

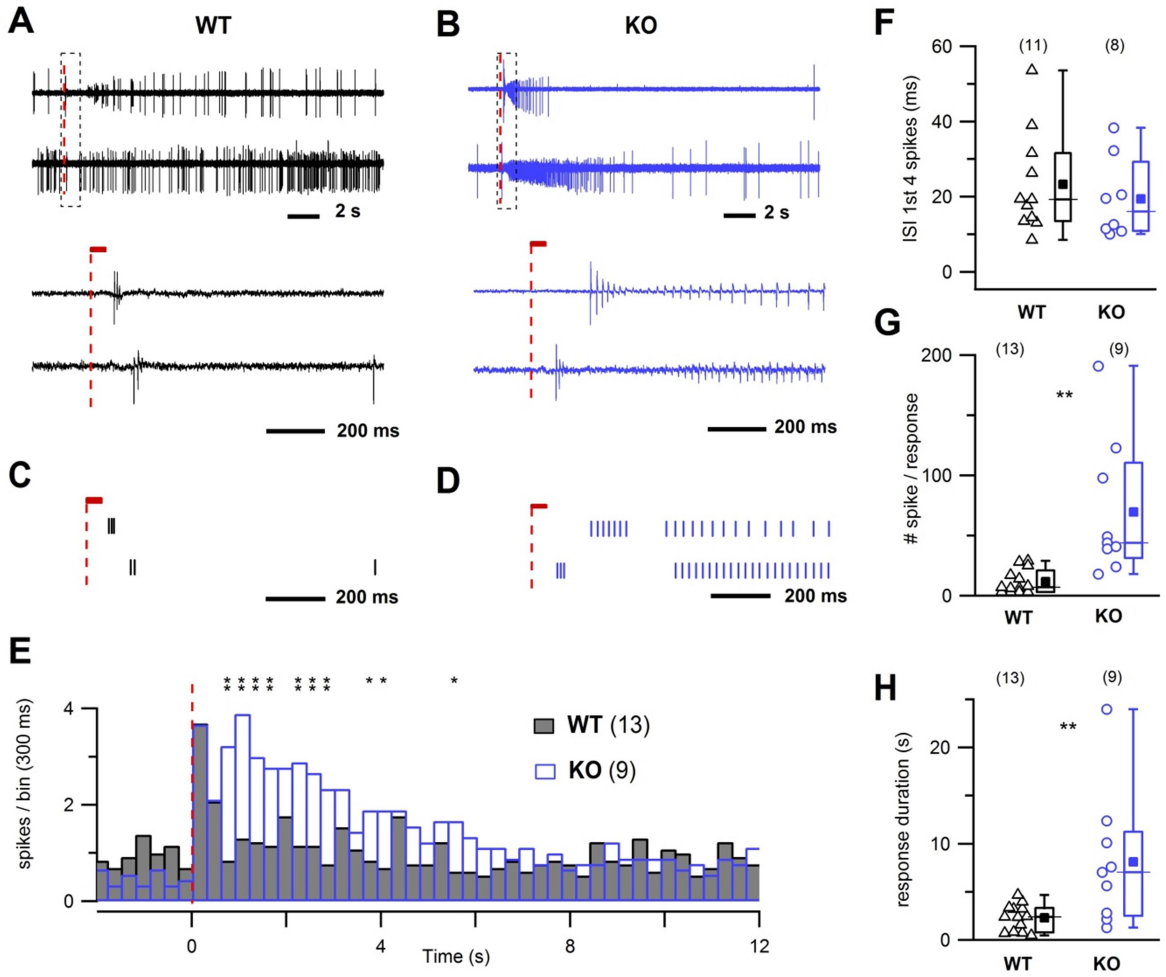

Figure 6: Evoked activity in OSNs in I7-GFP WT and KO mice for TMEM16B.
(A-B): Representative recordings of responses to a puff of 50 ms of 500□M heptanal for two different OSNs from WT (A) and KO mice (B). The bottom panels show the regions enclosed by the dashed box on an expanded time scale. (C-D): Raster plots on an enlarged time scale for the same cells showed in panel (A) and (B). Broken red line represents the onset of heptanal stimulation, and the red bar in the bottom panel its duration. (E): Averaged responses to the same odorant puff as panel (A) and (B), normalized to the number of neurons (n=13 / 7 WT mice, n=9 / 5 KO; bin 300 ms). Broken red line represents the onset of stimulation and data belongs to WT and KO PSTH distributions. * and ** indicate $0.01<p<0.5$ and $p<0.01$ respectively. (F-H): Scatter plot of interspike interval (ISI) of the first four spikes (F, 23 ± 13 ms in WT, 20 ± 11 ms in KO; mean ± SD; Mann-Whitney U test, one tail, $p>0.05$), of the total number of spikes (G, 12 ± 10 spike/response in WT, 70 ± 57 spike/response in KO; Mann-Whitney U test, one tail **$p<0.01$) and of the response duration (H, 2.3 ± 1.3 s in WT, 8.1 ± 7.0 s in KO; Mann-Whitney U test, 1 tail **$p<0.01$). In the box plots the square represents the mean, lines represent the median, upper and lower box boundaries represent the 25th and 75th percentile, upper and lower whiskers represent the 5th and 95th percentiles. The number of experiments is indicated in parenthesis.

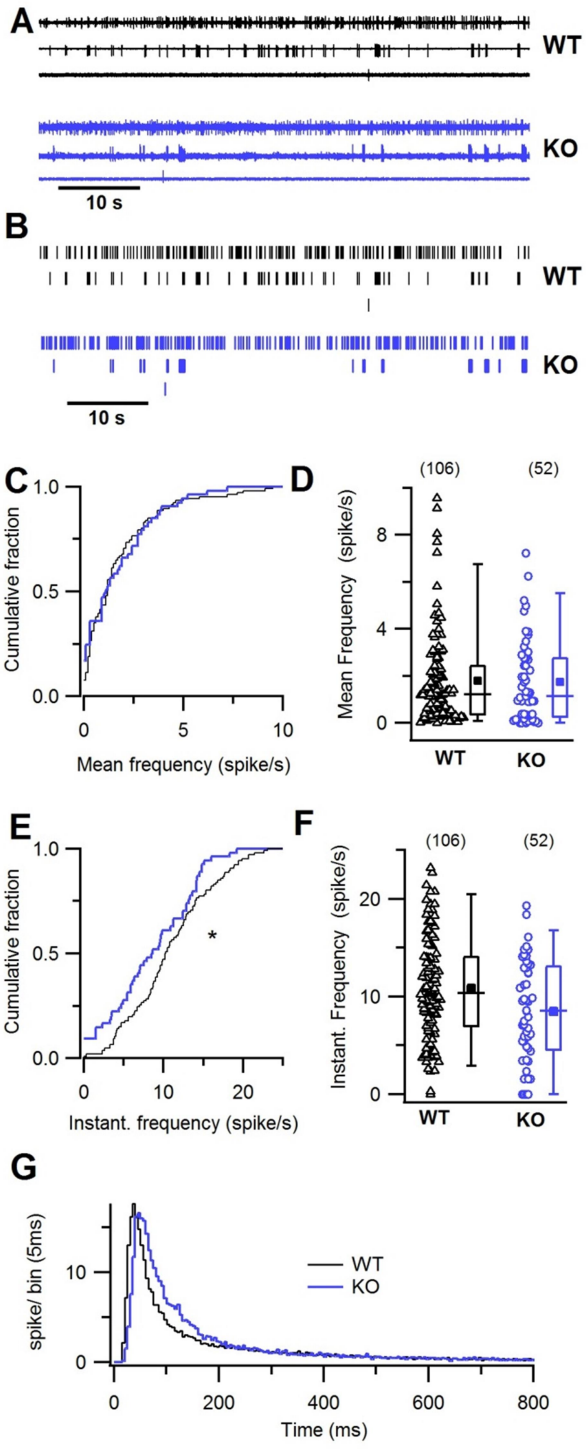

peak of activity is followed by a broader one of similar amplitude that is reflecting a prolonged and more intense firing activity in KO with respect to WT I7 OSNs (as quantified in Fig. 6G-H). The asterisks in the Fig. 6E represents bins with significantly higher firing rates in KO respect to WT OSNs (analysis according to (Dorrscheidt, 1981)). It is worth noting that a similar effect, with an initial peak of activity followed by a broader one, although smaller in amplitude, has been described in Fig. 5E for IBMX-evoked responses from *in situ* OSNs.

In summary, by taking advantage of recordings from OSNs expressing the I7 OR, we showed that the lack of CaCCs altered the firing behavior in response to heptanal by increasing the number of spikes and prolonging the duration of the response in isolated OSNs from TMEM16B KO with respect to WT.

4.2.3.5 - Spontaneous firing activity in OSNs

Different OSNs have different levels of basal firing activity, depending on the spontaneous activation of the expressed OR that is driving basal transduction activity (Reisert, 2010; Connelly et al., 2013). Since CaCCs contribute to basal transduction currents (Reisert, 2010), we investigated whether the lack of TMEM16B has

Figure 7: Spontaneous activity in OSNs in WT and KO mice.
(A-B): Loose-patch recordings (A, 60 s recordings) and raster plots (B) of the spontaneous activity in three WT OSNs (top) and three KO OSNs (bottom). (C-E): Cumulative plot of spontaneous mean (C) and instantaneous (E) firing frequency, bin of 0.1 Hz, in control (black line) and TMEM16B KO mice (blue line). (Mann-Whitney U-test, one-tail $p>0.05$ for C, * $0.01<p<0.05$ for E). (D-F): Box and scatter plots of spontaneous mean (D) and instantaneous (E) firing activity in OSNs in WT and KO mice. In the box plots, the inner square represents the mean, lines represent the median, upper and lower box boundaries represent the 25th and 75th percentile, upper and lower whiskers represent the 5th and 95th percentiles. (G): Interspike interval distribution (ISI) histogram (bin=5 ms) normalized to the number of recorded neurons in WT (black line, n=106 / 47 mice) and KO mice (blue line, n=52 / 22 mice).

an effect on the spontaneous spiking activity of OSNs. Spontaneous activity was recorded with on-cell loose-patch recordings from dendritic knobs of OSNs in the intact olfactory epithelium. OSNs showed a wide range of spontaneous firing rates as illustrated by representative recordings of three different WT and KO OSNs, and by the corresponding raster plots (Fig. 7 A,B). In WT mice, the pattern of OSNs' spike activity was highly variable and confirmed previous reports (Connelly et al., 2013; Reisert, 2010; Lorenzon et al., 2015). A comparison among OSNs from WT and KO mice showed that the mean firing frequency for each neuron, calculated over 2 to 5 minutes recording, ranged from 0.0087 to 9.582 in WT and from 0 to 7.22 spikes/s in KO, with mean values of 1.79 ± 1.98 and 1.93 ± 1.93 spikes/s respectively (mean ± SD, Fig. 7D). The cumulative distribution of firing frequencies did not reveal any difference between WT and KO OSNs (Mann-Whitney U-test, 1 tail, not statistically different; Fig. 7C). To further investigate the pattern of firing activity, we analyzed the instantaneous firing frequency, calculated as the inverse of the interspike interval (ISI) between consecutive spikes. The average instantaneous firing frequencies were 10.85 ± 5.28 and 8.57 ± 5.22 spikes/s (mean ± SD) respectively in WT and KO mice (Fig. 7F). The cumulative distribution showed a shift of the instantaneous firing frequency to lower frequencies for KO compared to WT OSNs (Fig. 7E, statistically significant, Mann-Whitney U-test, 1 tail, p=0.0102). Figure 7G shows the distribution of interspike intervals normalized to the number of recorded neurons. The peak of the KO distribution was slightly shifted to the right compared to WT, reflecting the lower instantaneous frequency for KO compared to WT. Despite the observed variability in spontaneous firing pattern, we found an indication that instantaneous firing frequencies may be reduced in KO OSNs. The large variability most likely originated from the fact that we recorded from randomly picked OSNs expressing a wide variety of ORs with different basal activities, as better shown in experiments obtained from the identified I7 OR (Fig. 8).

4.2.3.6 - Spontaneous firing activity of I7 OSNs decreases in TMEM16B KO mice

To restrict OSN variability we analyzed spontaneous firing activity of OSNs that express the I7 OR, crossing I7-IRES-tauGFP (Bozza et al., 2002) with TMEM16B KO mice (same mice used for heptanal-induced responses in Fig. 6). Spontaneous activity was recorded with on-cell loose-patch recordings from dendritic knobs of OSNs in coronal slices from P0-P4 mice. Although expressing the same I7 OR, these OSNs also showed some variability in spike activity, as shown by three different WT OSNs in Fig. 8A, and in agreement with previous reports (Connelly et al., 2013; Reisert, 2010). The mean firing activity of OSNs was significantly lower in KO compared to WT mice (Mann-Whitney U-test, 1-tail, $p<0.01$), as shown by the cumulative distributions (Fig. 8C) and by the scatter plot (Fig. 8D) (mean value ± SD, WT 3.19± 1.90 spikes/s, KO 1.68± 1.40 spikes/s). Additionally, the instantaneous frequency showed a significant reduction in KO compared to WT OSNs (mean value ± SD, WT 10.2 ± 3.64 spikes/s, KO 4.05 ± 2.28 spikes/s, Mann-Whitney U-test, 1tail, $p<0.001$; Fig. 8E,F). The plot of the distribution of interspike intervals normalized to the

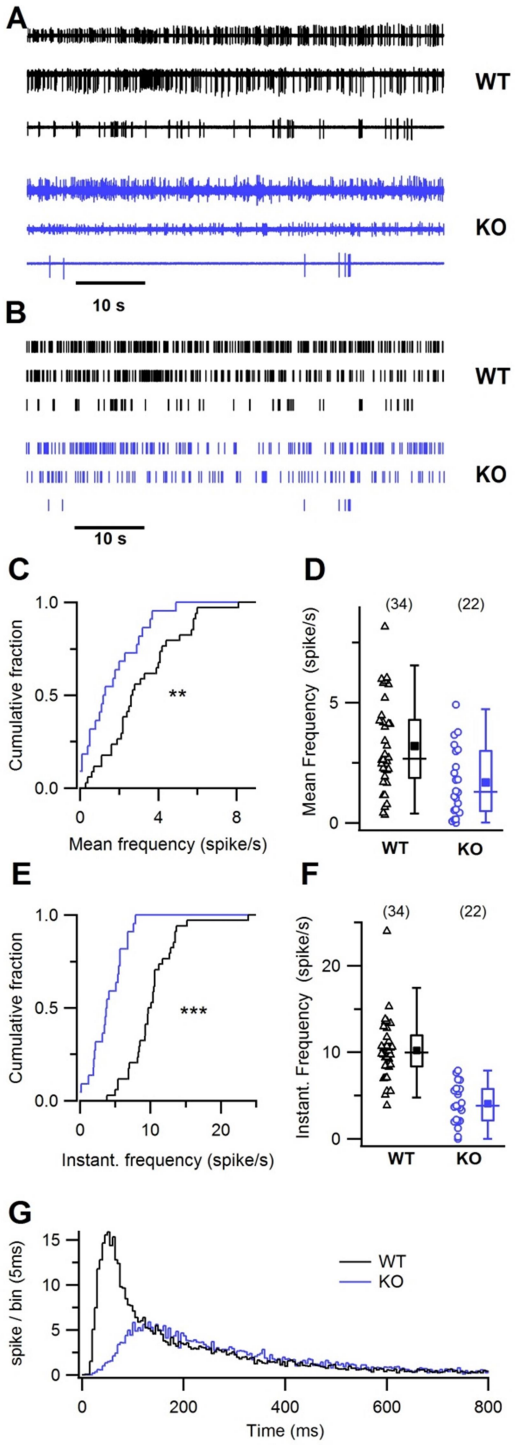

number of recorded neurons reveals that brief ISIs were missing in TMEM16B KO neurons compared to WT and that their distribution was shifted to longer ISIs (Fig. 8G).

The above data clearly show that, despite the high variability, the spontaneous firing is significantly reduced in I7-OR expressing neurons lacking TMEM16B.

4.2.3.6 - Axonal convergence of I7 OSNs is modified in TMEM16B KO mice

Our electrophysiological data show a reduced spontaneous activity in I7-expressing OSNs in TMEM16B KO compared to WT mice. It is well known that spontaneous OSN spiking activity is required for correct targeting of OSN axons to their glomeruli in the OB and for the establishment and maintenance of the olfactory sensory map (Lodovichi and Belluscio, 2012). For example, recent publications showed that overexpression of the inward rectifying potassium channel (Kir2.1) in OSNs diminishes the excitability of OSNs and indeed severely disrupts the formation of the glomerular map (Yu et al., 2004; Lorenzon et al., 2015). To investigate if the altered spiking behavior in I7 OSNs from TMEM16B KO mice affects the fidelity of axonal targeting, we analyzed axonal innervation into glomeruli in the OB by comparing results from sagittal sections of WT and TMEM16B KO OBs. Figure 9A shows images of a

Figure 8: Spontaneous activity in OSNs from I7-GFP WT and KO mice for TMEM16B.
(A-B): Loose patch recordings (A, 60 s recordings) and raster plots (B) of the spontaneous firing activity from three WT OSNs (top) and three KO mice (bottom). (C-E): Cumulative plot of spontaneous mean (C) and instantaneous (E) firing frequency, bin of 0.1 Hz, in control (black line) and TMEM16B KO mice (blue line). (Mann-Whitney U-test, one-tail ** p <0.01 in C and *** p<0.001 in E). (D-F): Box and scatter plots of spontaneous mean (D) and instantaneous (E) firing activity in OSNs in WT and KO mice. In the box plots, the inner square represents the mean, lines represent the median, upper and lower box boundaries represent the 25th and 75th percentile, upper and lower whiskers represent the 5th and 95th percentiles G Interspike interval distribution (ISI) histogram (bin=5 ms) normalized to the number of recorded neurons in control (continuous line, n=34 /19 mice) and KO mice (dotted line, n=22 / 9 mice).

single I7 glomerulus from a WT I7-IRES-tauGFP mouse (Fig. 9A, top row) and multiple glomeruli in I7-IRES-tauGFP mice KO for TMEM16B (Fig. 9A, bottom row).

In WT mice, typically one single I7 glomerulus was observed for each side of the OB, whereas in TMEM16B KO mice multiple I7 glomeruli were observed in consecutive sagittal sections (see Fig. 9A where up to 5 glomeruli are visible). In WT, we identified an average of 4 I7 glomeruli per mouse in the ventral side of the OB (1 lateral and 1 medial per bulb, Fig. 9B). In KO mice, the average number of I7 glomeruli almost doubled compared to WT (Fig. 9B). The supernumerary glomeruli in TMEM16B KO were evenly scattered in the ventral area of both lateral and medial locations. In addition, some I7 OSN axons innervated additional glomeruli (heterogeneous glomeruli) with a trend towards more glomeruli in TMEM16B KO compared to WT mice, even though this difference did not reach statistical significance (Fig. 9C).

In conclusion, our results show that TMEM16B contributes to the glomerular formation and refinement of I7-expressing OSNs in the OB.

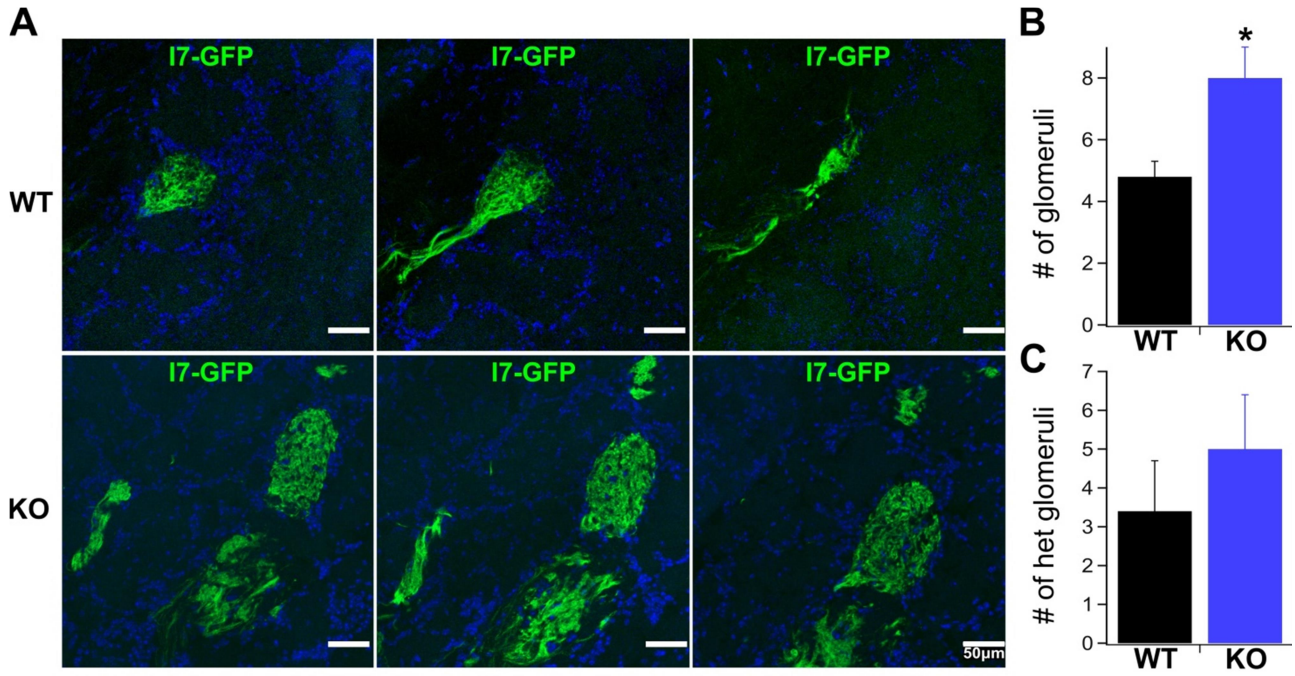

Figure 9: The number of I7-GFP glomeruli increased in TMEM16B KO mice.
(A): Top row shows a series of three consecutive sagittal sections where a single I7-GFP glomerulus is present in a WT mouse. Bottom row shows a series of consecutive sections from a KO mouse, where several glomeruli were observed. (B): Bar plot representing the total number of glomeruli per animal, that significantly increased in the KO (8 ± 1, n=7 mice) compared to WT (4.8±0.5, n=7 mice) * $0.01<p<0.05$ unpaired t-test. (C): bar plot representing the number of heterogeneous glomeruli in WT (black bar, 3.4±3, n=7 mice) and in KO mice (blue bar, 5±1.4, n=7 mice).

4.2.4 - DISCUSSION

The involvement of CaCCs in odor transduction has been described in the early nineties (Kleene, 1997, 1993; Kurahashi and Yau, 1993; Kleene and Gesteland, 1991; Lowe and Gold, 1993). CaCCs constitute up to 90% (Lowe and Gold, 1993; Boccaccio and Menini, 2007) of the transduction current and Cl^- channels may be 8 times more numerous than CNG channels in olfactory cilia (Reisert et al., 2003). The cooperative nature of the current activation by Ca^{2+} significantly contributes to set the dynamic range of OSNs (Lowe and Gold, 1993; Boccaccio et al., 2006). Despite its proposed importance to OSN physiology, the molecular identity of the Ca^{2+}-activated Cl^- channel has been identified as TMEM16B/Anoctamin2 channel only in 2009 (Stephan et al., 2009; Pifferi et al., 2009; Sagheddu et al., 2010). A loss of function approach unequivocally demonstrated that indeed the olfactory Cl^- channel was TMEM16B, but intriguingly it was reported to be dispensable for near-normal olfactory function (Billig et al., 2011). This raises the question what the purpose of such densely-expressed TMEM16B channels in the cilia of OSNs might be.

4.2.4.1 - Odor-guided food-finding ability

An essential behavior for animal survival is the capability to find food and olfaction plays a very important role in food location. We addressed a possible olfactory-driven behavioral deficit in TMEM16B KO mice by using an odor-guided food-seeking test, which has been largely used to test olfactory acuity in mice (Stephan et al., 2012; Li et al., 2013). The test does not rely on any specific mouse training, e.g. learning of an operant-conditioning task, but instead mice have to rely on their naïve sense of smell to locate the odor source of food. When confronted with novel odors, TMEM16B KO required longer times to locate the food compared to WT mice, while for odors already known to the mice, e.g. re-testing with the same food, they performed equally well. KO mice required longer times to find novel foods even when they performed equally well on known odors, suggesting that the observed difference between WT and KO is not a simple lack of motivation, deficit in locomotion or inability to perform the task. It is tempting to speculate that the observed glomerular mistargeting and/or altered AP firing in TMEM16B KO mice may be the underlying causes for the observed olfactory-driven behavioral deficit, an issue that future experiments will have to address.

4.2.4.2 - TMEM16B channel is responsible for the generation Ca^{2+}-activated Cl^- currents in OSN cilia and shortens evoked firing in OSNs

In agreement with a previous report (Billig et al., 2011), we confirmed here that CaCCs were absent in isolated OSNs from TMEM16B KO mice (Figs. 2, 3), further supporting the notion that the CaCC is the major contributor to the transduction current in isolated OSNs. Moreover, since NFA, a blocker of the CaCC, did not further block the remaining current in KO OSNs, we could exclude that it might have had unspecific effects on other currents in isolated OSNs. Thus we confirm that TMEM16B is responsible for CaCCs in OSN cilia.

Importantly, AP firing along OSN axons transfers information about odors to the OB. Here, we first investigated the ability of TMEM16B KO OSNs to generate APs in response to a stimulus. In a first set of experiments, we compared AP firing in OSNs from WT and KO mice using suction electrode recordings from isolated OSNs (Fig. 4). Despite the strong reduction of the transduction current in isolated TMEM16B KO OSNs, on average we measured longer trains and a higher number of APs in response to the phosphodiesterase inhibitor IBMX compared to WT OSNs (Fig. 4), suggesting that TMEM16B contributes to shorten IBMX-evoked firing activity.

We also extended our experiments to OSNs recorded *in situ* (Fig. 5) in the intact olfactory epithelium, a situation more closely resembling the physiological OSN conditions. The cumulative distribution of the evoked responses indicated an increase in firing activity in KO with respect to WT mice (IBMX in Fig. 5E, heptanal in Fig.6E). The contribution of CaCC was more evident in the heptanal responses of OSNs expressing the I7 OR, probably due to lower intrinsic variability as in this case we recorded from a defined set of OSNs expressing one know OR.

APs are generated during the rising phase of the receptor current and display a progressive loss of amplitude during the spike train down to zero levels at which APs firing is absent (Reisert and Matthews, 2001a; Savigner et al., 2009), leading to a shortening of the spike train. This spike disappearance originates from progressive inactivation of voltage-gated Na^+ and Ca^{2+} channels during prolonged and strong depolarization (Trotier, 1994). The lack of a substantial transduction current, as observed in isolated TMEM16B KO OSNs (Fig. 3), likely affects the depolarization of OSNs, causing a reduced or slower inactivation of voltage-gated channels, allowing for more spikes to be generated over a longer time window. Thus, although the presence of CNG currents is necessary and sufficient to generate APs in response to a stimulus, CaCCs contribute to regulating firing duration and number of spikes.

4.2.4.3 - TMEM16B increases the spontaneous firing rate in OSNs

It is well established that spontaneous activity in OSNs significantly contributes to the development and physiology of the olfactory system (Nakashima et al., 2013; Lorenzon et al., 2015). Moreover, different ORs have various basal activities (Reisert, 2010), which stimulate the signal transduction cascade to drive basal cAMP fluctuations, opening of CNG channels followed by TMEM16B channels and AP generation. Here the availability of TMEM16B KO mice gave us the possibility to directly investigate how the absence of CaCCs affects the spontaneous activity in OSNs. On average, OSNs expressing random ORs showed a mild decrease in the instantaneous firing frequency in TMEM16B KO compared to WT mice (Fig. 7E). Interestingly, OSNs expressing the I7 OR, a receptor known to have a relatively high spontaneous activity ((Reisert, 2010) in dissociated neurons, (Connelly et al., 2013) *in situ*), showed a strong reduction of both instantaneous and mean firing frequencies in the absence of TMEM16B (Fig. 8 C,E). Thus CaCCs contribute to the spontaneous firing activity of I7 OSNs by amplifying the current through CNG channels, which itself is

driven by baseline cAMP fluctuations. It is likely that OSNs expressing ORs with a basal activity lower than that of I7 would not be affected by the lack of TMEM16B as much as the I7 OR. Indeed, OSNs expressing random ORs did not show a reduced mean firing activity (Fig. 7C), but only a decrease in the instantaneous firing frequency (Fig. 7E).

Thus the small activation of CaCCs likely occurring in basal conditions contributes to neurons' depolarization and supports spontaneous spike generation.

4.2.4.4 - Proper glomerular formation in the OB requires the presence of TMEM16B

Axons from OSNs expressing the same OR coalesce together in the OB where they typically form one laterally and one medially located glomerulus in each bulb. The process of glomerular formation and refinement is highly dependent by the OR type an OSN expresses (Nakashima et al., 2013; Nishizumi and Sakano, 2015a). On top of activity-independent mechanisms, neuronal activity is important for circuitry formation in visual and auditory systems (Huberman et al., 2008; Wang et al., 2015) as well as in the olfactory system (Lodovichi and Belluscio, 2012; Yu et al., 2004; Lorenzon et al., 2015; Nakashima et al., 2013), where it is involved in segregation of axons into glomerular structures (see (Nishizumi and Sakano, 2015b) for review).

Hitherto glomerular targeting in TMEM16B KO mice has been investigated for the P2 and M72 ORs (Billig et al., 2011) and no apparent lack of axonal coalescence into glomeruli was observed, while the number of innervated glomeruli in WT and KO animals remained unclear. Here, we investigated axonal targeting for the I7 OR and demonstrated that nearly twice as many glomeruli were formed in TMEM16B KO compared to WT mice (Fig. 9). This indicates that TMEM16B plays a relevant role for glomerular targeting of OSNs expressing the I7 OR. Furthermore, TMEM16B may be necessary for proper glomerular targeting of some, but not all ORs, possibly by regulating basal and/or odorant-induced activity. This is consistent with previous observations where in the same genetically modified animal models different ORs showed different glomerular targeting or mis-targeting phenotypes (Zheng et al., 2000; Lorenzon et al., 2015; Yu et al., 2004; Mobley et al., 2010). Interestingly, OSNs of Kir2.1 knock-in mice have a reduced spontaneous firing activity compared to WT and also show some supernumerary glomeruli (Lorenzon et al., 2015), similarly to what we observed in TMEM16B KO mice.

In conclusion, we found that the Ca^{2+}-activated Cl^- channel TMEM16B modulates olfactory function in unexpected ways by increasing spontaneous firing activity, but reducing and shortening stimulus-induced firing, and by ensuring correct glomerular targeting of I7-receptor expressing OSNs. In TMEM16B KO mice, the impaired ability of forming a proper glomerular map along with the altered action potential firing in response to odorants may contribute to the olfactory-driven impairment in food-finding behavior that we

observed, thus making the Ca^{2+}-activated Cl^- currents relevant for the OSN physiology and for the functioning of the olfactory system as a whole.

4.2.5 - METHODS

Animals

Mice were handled in accordance with the Italian Guidelines for the Use of Laboratory Animals (Decreto Legislativo 27/01/1992, no. 116) and European Union guidelines on animal research (No. 86/609/EEC), under a protocol approved by the ethic committee of SISSA, or in accordance with methods approved by the Animal Care and Use Committees of the Monell Chemical Senses Center (conforming to NIH guidelines). In this study we used TMEM16B KO and WT mice derived from breeder pairs kindly provided by Dr. Thomas Jentsch (Leibniz-Institut für Molekulare Pharmakologie/Max-Delbrück-Centrum für Molekulare Medizin, Berlin, Germany)(Billig et al., 2011). To record from OSNs expressing an identified OR and for immunohistological experiments TMEM16B KO mice were crossed with I7-IRES-tauGFP, a mouse line in which OSNs expressing the I7 OR also expressed GFP (Bozza et al., 2002) with control mice obtained from the I7-IRES-tauGFP mouse line. I7-IRES-tauGFP mouse strain was a generous gift from Dr. Peter Mombaerts (Max Planck Research Unit for Neurogenetics, Frankfurt, Germany).

Odor-guided food seeking test.

A small piece of food was buried below the surface of the cage bedding so that it constituted a purely olfactory cue and the time taken by a mouse to find the food item was recorded. All mice of either sex were maintained on a 12:12 light/dark cycle, and tested in the light phase. Mice were food deprived overnight with ad libitum access to water. Every morning, each mouse was placed in a novel test cage (standard mouse cage, L * H *W, 24 cm * 12 cm * 15 cm) in which a ~3 g piece of cookie (Oreo^{TM}, Nabisco) had been buried under fresh bedding. The latency of the animal to retrieve the cookie was recorded with a stopwatch and by an experimenter that was blinded to the animal's genotype. Retrieving the cookie was defined as digging it up with forepaws, picking it up and placing it in the mouth. We set a 10 minutes limit within which the animals had to find the cookie, after that the time was stopped and the cookie was exposed so that the mouse could have access to and eat it. The position of the buried cookie was randomly changed every day so that the animal could not rely on spatial information to find it. This was repeated for 5 days. Mice were weighed every morning prior to experiments to monitor their body weight. 1.5 grams of standard chow (Tekland rodent diet 8604) was given every day after testing to maintain body weight. If a mouse was found to have lower than 80 % starting body weight, additional food was given to maintain a healthy body weight. On the 6th day the Oreo was placed on top of the bedding. We repeated this same type of experiment with a second set of mice and cheese (Craft Cracker Barrel Extra Sharp Cheddar Cheese stick) had been buried under fresh bedding.

Mice were returned to normal food for 1 week. After one week mice were again food deprived overnight and the following 5 food items were hidden in the bedding over the next 5 days, one food was tested each

day: Oreo, peanut (Select Whole Peanuts in Shell. Deshelled), cheese (Craft Cracker Barrel Extra Sharp Cheddar Cheese stick), chocolate (Hersheys Milk Chocolate King size) and standard chow. The time the mice took to retrieve the food was recorded and the limit to perform the task was 15 min. The second set of mice which had previously performed the cheese seeking task was exposed, after a week of rest, to cheese, peanut (Select Whole Peanuts in Shell. Deshelled), Oreo, chocolate (Hersheys Milk Chocolate King size) and standard chow hidden in the bedding over the next 5 days, one food was tested each day.

Preparation of dissociated olfactory sensory neurons

Mice (3-5 weeks of either sex) were anesthetized with CO_2 inhalation, decapitated, and the head was hemisected sagittally along the septum. The olfactory epithelium was removed and OSNs were dissociated either mechanically for suction pipette recordings (Ponissery Saidu et al., 2012) or enzymatically, with a papain–cystein treatment, for uncaging-patch clamp experiments (Boccaccio et al., 2011, 2006; Lagostena and Menini, 2003).

Patch clamp experiments and photorelease of caged 8-Br-cAMP.

Currents were measured from dissociated OSNs with an Axopatch 200B patch-clamp amplifier (Axon Instruments, Union City, CA) in the whole-cell voltage-clamp mode.

For flash photolysis, we used a xenon flash-lamp system JML-C2 (Rapp OptoElectronic, Hamburg, Germany) coupled into the epifluorescence port of the microscope with a quartz light guide (Boccaccio et al., 2011, 2006). The spot of light had a diameter of about 15 µm that could cover only the ciliary region and in some cases, also part of the dendrite. The flash duration was 1.5 ms. We used [6,7-Bis(carboxymethoxy)coumarin-4-yl]methyl-8-bromoadenosine-3', 5'-cyclic monophosphate (BCMCM-caged 8-Br-cAMP), dissolved in DMSO at 10 mM and added to the intracellular solution at a final concentrations of 50 µM. The compound was a generous gift from V. Hagen (Leibniz-Institut für Molekulare Pharmakologie, Berlin, Germany).

Patch pipettes were pulled from borosilicate glass and filled with the intracellular solution containing (in mM): 140 KCl, 4 $MgCl_2$, 0.5 EGTA, 10 HEPES, pH 7.4 and additionally 50 µM BCMCM-caged 8-Br-cAMP. Bath mammalian Ringer solution contained (in mM): 140 NaCl, 5 KCl, 1 $CaCl_2$, 1 $MgCl_2$, 10 HEPES, 10 glucose, and 1 Na-pyruvate, pH 7.4. All experiments were carried out at room temperature (20–22°C).

Suction pipette recordings

Recordings from isolated OSNs were made using the suction pipette technique as described previously (Lowe and Gold, 1991; Ponissery Saidu et al., 2012). Briefly, a freshly-dissociated OSN was gently drawn inside the tip of the recording pipette so that its knob and cilia remained exposed to bath and/or stimulus solutions. In this recording configuration the intracellular voltage is free to vary and action potentials (APs)

are recorded as fast biphasic transients. The recorded suction current was filtered at DC – 5000 Hz (-3dB, 8-pole Bessel filter) to display the fast APs and the underlying receptor current was isolated by low-pass filtering at 50 Hz (-3dB, 8-pole Bessel filter). The recorded suction current was sampled at 10 kHz. Currents were recorded with a Warner PC-501A patch clamp amplifier, digitized using Power1401 II A/D converter and Signal acquisition software (Cambridge Electronic Design, U.K.).

Solutions and solution exchange in the suction experiments

Mammalian Ringer's solution contained (in mM) 140 NaCl, 5 KCl, 1 $MgCl_2$, 2 $CaCl_2$, 0.01 EDTA, 10 HEPES, and 10 glucose. The pH was adjusted to 7.5 with NaOH. Niflumic acid and 3-isobutyl-1-methylxanthine (IBMX) were used at concentrations of 300 μM and 1 mM respectively, by dissolving them directly into Ringer's without the use of DMSO.

Fast solution changes and odorant exposures were achieved by transferring the tip of the recording pipette containing the OSN across the interface of neighboring streams of solutions using the Perfusion Fast-Step solution changer (Warner Instrument Corporation). All experiments were performed at mammalian body temperature (37°C). Solutions were heated just before entering the solution changer by a solution heater based on Matthews (Matthews, 1999).

Intact mouse olfactory epithelium preparation

Mice (4 to 12 weeks) were anesthetized with CO_2 inhalation, decapitated and the head was immediately transferred to ice-cold artificial cerebrospinal fluid (ACSF) bubbled with 95% O2 and 5% CO_2. ACSF contained (in mM): 120 NaCl, 5 KCl, 1 $MgSO_4$, 1 $CaCl_2$, 25 $NaHCO_3$, 10 glucose, 10 HEPES, osmolarity before oxygenation was 310 mOsm, pH = 7.2. The nasal septum was dissected en bloc and the bone with the two attached epithelia was placed in a recording chamber at room temperature (21-24 °C) that was continually perfused by bubbled ACSF.

Mouse nose coronal slice preparation

Coronal slices were prepared from olfactory epithelia of mouse pups (P0-P4). Mice were directly decapitated and the nose was dissected en bloc and glued into a small hole in a cube of boiled carrot. A vibratome was used to cut coronal slices of 300 μm of thickness. During the cutting the tissue was completely submerged in ACSF continually oxygenated and kept near 0° C. After sectioning, coronal slices were allowed to recover for at least 30 minutes in ACSF continually oxygenated and kept near 0° C.

Loose-patch extracellular recordings

Dendritic knobs of individual OSNs in the olfactory epithelium were visualized using an upright microscope (Olympus BX51WI) equipped with infrared differential contrast optics, a camera (DFK Imaging Source, Germany) and a X40 water-immersion objective with an additional X2 auxiliary lens.

Extracellular recordings from dendritic knobs of OSNs in the intact olfactory epithelium were obtained in the loose-patch configuration with seal resistances of 20-40 MΩ (Nunemaker et al., 2003; Delay and Restrepo, 2004) in both coronal slices and intact olfactory epithelia preparations. Pipette solution was ACSF, as the bath solution, and the recordings were made in voltage-clamp mode with a holding potential of 0 mV. Data were low-pass filtered at 1 kHz and sampled at 5 kHz.

The experiments were performed at room temperature (21-24°C) using a Multiclamp 700B amplifier controlled by Clampex 9.2 via a Digidata 1322A (Molecular Devices, Union City, CA, USA). Patch pipettes were pulled from borosilicate capillaries (WPI, Sarasota, FL, USA) with a Narishige PC-10 puller and had resistances of 5-10 MΩ. OSNs expressing the I7 OR were stimulated by adding 500 μM Heptanal to ACSF, one of the main ligands of I7 receptor (Krautwurst et al., 1998; Hall et al., 2004). Heptanal was dissolved at 100 mM in (DMSO) and stored at -20°C.

3-isobutyl-1-methyl-xanthine (IBMX) was prepared in a 20 mM stock solution containing 5% DMSO and diluted to the final concentration of 100 μM before use.

The stimulus, either odorant or IBMX, was delivered through a pipette by pressure ejection (10-15 psi) using a Picospritzer II (Parker, USA). Stimulation delivering was visually controlled by adding fluorescein to the odorant solution. The stimulation intensity was modulated changing the puff duration. The stimulation pipette was placed at least 20 μm from the recorded OSN to avoid any mechanical response (Grosmaitre et al., 2007).

Data analysis of loose-patch extracellular recordings

Spontaneous firing activity was characterized from mean and instantaneous firing frequencies evaluated in a time window of 2 to 5 minutes. Mean spontaneous firing frequency was calculated as the number of spikes divided by the duration of the recording, and the instantaneous firing frequency as the inverse of the inter-spike interval (ISI) between consecutive spikes (second to first, third to second, and so forth). Sometimes very high frequency spontaneous firing activity followed by complete silencing of the recorded OSN showed clear evidence of neural damage or loss of cell integrity, such units were routinely discarded. For spike detection the raw data were filtered 2-1000 Hz.

Odorant-evoked firing activity was detected on top of the spontaneous background activity using an established protocol for OSN response analysis (Rospars et al., 2003; Savigner et al., 2009; Lorenzon et al., 2015). Briefly, neuronal spiking activity was defined as a presumptive response to odorant when, within 1.25 s after stimulus presentation, at least 3 consecutive spikes presented an instantaneous frequency (IF,

1/ISI) higher than the mean instantaneous frequency plus 1.5 Hz in the 30 s before stimulation (IF > avgIF + 1.5 Hz). If a presumptive response was detected, its instantaneous firing frequency distribution was compared using the Mann-Whitney U-test with the instantaneous firing frequency distribution occurring before stimulation. When the two distributions were found significantly different at a level of 1% the presumptive response was considered a true response, otherwise it was discarded.

Strong stimulations often produced a marked increment in firing frequency correlated with a progressive decrease of the AP amplitude. We defined a response as saturating when it was composed by APs which decreased their amplitude up to baseline, producing a silencing period which sometimes was followed by a high frequency burst. During the rebound burst the amplitude of APs increased and the frequency progressively decreased towards the spontaneous firing activity level (similarly to (Rospars et al., 2003; Savigner et al., 2009)).

To construct the normalized cumulative response (PSTH, peristimulus time histogram), we summed single responses obtained from several cells stimulated with an identical stimulus. We optimized the bin size by calculating a cost function, following Shimazaki and Shinomoto (Shimazaki and Shinomoto, 2007). In order to analyze the difference between PSTH from KO and WT cell, we applied the statistical procedure reported by Dorrscheidt (Dorrscheidt, 1981), with the *null hypothesis* that the two PSTHs derive from the same group of neurons and they consequently have the same firing rate.

The firing rate of the odorant-evoked response was estimated as an interspike interval (ISI) of the first four spikes. Moreover, the response intensity was visualized by a cumulative spike distribution histogram normalized by the number of responses, and it was quantified measuring the total number of spikes in the response and its duration. For saturating responses the response duration referred to the time between the first and last spike recognized as part of the response, including the silent period and the firing rebound.

Data in Figs. 5-8 are presented as mean value and boxplots in which the inner square represents the mean, lines represent the median, upper and lower box boundaries represent the 25th and 75th percentile, upper and lower whiskers represent the 5th and 95th percentiles . Spontaneous and evoked firing frequency data were not in all cases normally distributed (Kolmogorov-Smirnov test or Shapiro-Wilkinson test) and statistical significance was determined using Mann-Whitney U-test. P-values <0.05 were considered statistically significant.

Olfactory bulb histochemistry

Mice (2-4 months old) were sacrificed by cervical dislocation, decapitated, the head was immediately transferred to ice-cold ACSF solution and the OBs were extracted. The fresh tissue was left overnight in a solution of 4% of paraformaldehyde (PFA) diluted in phosphate buffer saline (PBS). After the fixation it was placed in 30% (w/v) sucrose and left overnight at 4°C for cryoprotection. 16 µm thick sagittal sections were

cut on a cryostat and stored at −20°C. Tissue sections washed in 0.1% (v/v) Tween 20 in PBS 30 min and rinsed with water. OB sections were incubated for 30 min with 4'-6-Diamidino-2-phenylindole (DAPI) (0.1 μg ml^{-1}) to reveal cell nuclei. Tissue sections were then washed and mounted with Vectashield (Vector Laboratories, Burlingame, CA, USA). Images were taken with a Leica SP2 confocal microscope at a resolution of 1024 X 1024 pixels. Contrast and brightness of the images in Fig. 9 were manipulated with ImageJ software (National Institutes of Health, Bethesda, MD) for the purpose of display only. Sectioning, staining and glomerular counting were performed by an experimenter who was blinded to the genotype of the mice.

Chemicals

All compounds and chemicals were obtained from Sigma-Aldrich, unless otherwise stated.

4.2.6 - ACKNOWLEDGEMENTS

We thank Dr. Thomas Jentsch, Dr Gwendolyn Billig and Jonas Münch (Leibniz-Institut für Molekulare Pharmakologie/Max-Delbrück-Centrum für Molekulare Medizin, Berlin, Germany) for providing TMEM16B KO mice, Dr. Peter Mombaerts (Max Planck Research Unit for Neurogenetics, Frankfurt, Germany) for providing I7-IRES-tauGFP mice. We also thank Dr. Thomas Jentsch and Dr. Graeme Lowe for insightful discussions and comments to the manuscript, Dr. Joachim Scholz-Starke and all members of the laboratories for discussions. We thank John Lees for expert assistance with mouse behavioral experiments. Immunohistochemistry and confocal microscopy was performed at the Monell Histology and Cellular Localization Core. Genotyping was performed at SISSA by Jessica Franzot or at the Monell Genotyping and DNA/RNA Analysis Core, which are supported, in part, by funding from the NIH-NIDCD Core Grant 1P30DC011735-01.

This study was supported by grants from the Italian Ministry of Education, University and Research (2010599KBR to AM), from the Fondazione Compagnia di San Paolo, Torino (2013.0922 to AB), from NIH (DC009613 to JR) and also from grant G20OD020296 (infrastructure improvement at the Monell Chemical Senses Center).

The authors declare no competing financial interests.

4.2.7 - AUTHOR CONTRIBUTIONS

MD performed behavioral experiments. GP and MD performed whole epithelium and single cell electrophysiological experiments respectively and conducted immunohistological experiments. AB performed uncaging patch-clamp experiments. All authors conceptualized and analyzed experiments and wrote the manuscript.

4.2.8 - REFERENCE LIST

The reference list of the paper is integrated in the reference list of the Thesis (Pag. 81).

5 - DISCUSSION AND CONCLUSIONS

OSNs respond to odorant binding to ORs with an inward transduction current that depolarizes the cell. This depolarization leads to generation of action potentials that, travelling across the axon, reach the glomeruli in the olfactory bulb mediating the olfactory information. Besides, OSNs fire action potentials also in absence of odor stimuli (O'Connell and Mozell, 1969; Trotier and MacLeod, 1983; Frings and Lindemann, 1991; Reisert and Matthews, 2001a; Reisert, 2010) and this spontaneous firing is driven by the constitutive activity of the expressed OR (Reisert, 2010; Connelly *et al.*, 2013). Basal activity regulates the development and shapes neuronal circuits of higher centers (Yu *et al.*, 2004, Nakashima *et al.*, 2013). In this Thesis I studied the effect of two genetic manipulations on the firing activity of the OSNs: the ectopic overexpression of Kir2.1 and the deletion of the *TMEM16B/Ano2* gene, that codes for the Ca^{2+}- activated Cl^- channel TMEM16B.

Kir2.1 overexpression reduces the spontaneous activity but does not alter the odor-evoked response in OSNs

The overexpression of Kir2.1 is a genetic approach used to reduce the excitability of the neurons and to decrease basal firing activity (Johns *et al.*, 1999). The overexpression of Kir2.1 channel in OSNs produced an unrefined topography of the olfactory bulb (Yu *et al.*, 2004). This modification is supposed to reduce the spontaneous firing in OSNs (Yu *et al.*, 2004), although a detailed study on basal firing activity was not performed, and its effect on odor-evoked activity remained to be clarified. To dissect thoroughly the effect of Kir2.1 expression on the spiking activity of OSNs, I recorded spontaneous and odor-evoked activity from dendritic knobs of OSNs in the intact epithelium using the loose-patch configuration.

The basal activity exhibited a high variability in the firing rate among neurons both in control and in Kir2.1 mice, consistently with previous studies (Reisert *et al.*, 2010; Connelly *et al.*, 2014). However, I found that overexpression of Kir2.1 strongly reduced the basal activity of OSNs.

I tested the ability to respond to odor stimuli of OSNs overexpressing Kir2.1 using as stimulus an odor mixture, and I found that the stimulus triggered action potential firing similarly to WT neurons, with a similar percentage of responsive neurons, 68% in Kir2.1 and 79% in WT OSNs. I analysed separately the saturating and not saturating responses and I concluded that the overexpression of Kir2.1 did not influence the ability of the OSNs to respond to the odor-stimulus.

A possible explanation of these results is that the overexpression of Kir2.1 hyperpolarizes the OSN contrasting the spontaneous OR-induced depolarization which, in the absence of odor stimuli, leads to basal spiking activity. On the other side, the outward K^+ current mediated by Kir2.1 may not be sufficient to

counteract the transduction inward current induced by odor stimulation, not affecting the odor responses. These results support the use of Kir2.1 mouse strain as model for understanding the contribution of spontaneous and sensory-evoked activity in the formation of sensory circuits.

A role for Ca^{2+}-activated Cl^- channels in olfaction

The transduction current, elicited by odor stimulation, is composed by the contribution of two types of ion channels: CNG and Ca^{2+}-activated Cl^- channels. The primary inward current through CNG channels, mainly due to Ca^{2+} entry, triggers the activation of a large secondary Cl^- current.

Interestingly, although CaCCs were first observed in the early nineties (Kleene and Gesteland, 1991; Kleene, 1993; Lowe and Gold, 1993; Kurahashi and Yau, 1993), their molecular identity has been elusive for two decades, hindering the possibility to better understand the role of CaCCs in the olfactory system. After ruling out several possible candidates, the channels expressed in OSN cilia and responsible for CaCCs were finally identified as TMEM16B/Anoctamin2 (Stephan *et al.*, 2009; Pifferi *et al.*, 2009; Sagheddu *et al.*, 2010; Billig *et al.*, 2011). Disruption of the TMEM16B (*Ano2*) gene in mice (Billig *et al.*, 2011) completely abolished CaCCs in OSNs. However, TMEM16B KO mice were reported unexpectedly not to have any obvious olfactory deficit, concluding that CaCCs are dispensable for olfaction.

As this first and unique study on TMEM16B KO mice raised serious doubts about the role of Ca^{2+}-activated Cl^- channels in olfaction (Billig *et al.*, 2011), we re-addressed the question performing new behavioral tests and analyzing the ability of single neurons to respond to odor stimulus.

Our collaborators at Monell Chemical Senses Center (Philadelphia, USA) addressed a possible olfactory-driven behavioral deficit in TMEM16B KO mice by using an odor-guided food-seeking test, which has been largely used to test olfactory acuity in mice (Stephan *et al.*, 2012; Li *et al.*, 2013). The animals required longer times compared to WT mice to locate the food marked with novel odor while they performed equally well for odors already known to the mice.

I focused on the characterization of the stimulus-evoked and basal activity of OSNs from TMEM16B KO mice that have not been studied yet. For this purpose I performed extracellular loose patch recordings from the knob of OSNs from intact septal epithelium or in slices of P0-P4 mice olfactory tissue.

The transduction current triggers the generation of action potentials, bringing the information of odor presence along the axon to the olfactory bulb. Although the transduction current is strongly reduced in OSNs from TMEM16B KO mice, we verified that both isolated and *in situ* OSNs responded to IBMX stimuli, similarly to WT, with a burst of action potentials.

However suction electrode recordings from isolated OSNs revealed that neurons from KO animals responded with longer trains and a higher number of APs in response to IBMX compared to WT OSNs, suggesting that TMEM16B contributes to shorten IBMX-evoked firing activity.

Loose patch recordings from the knobs of KO mice OSNs *in situ*, showed an enhancement of the evoked firing activity, but not a significant increase in the response duration, probably due to the intrinsic high variability.

To overcome the variability, we recorded the heptanal induced response in OSNs expressing I7 OR. We confirmed that TMEM16B deletion caused an increase in I7 OSNs firing activity, characterized by longer response durations and higher number of spikes.

Large transduction currents produce a depolarization which may inactivate the voltage-gated Na^+ and Ca^{2+} channels reducing the action potential amplitude (Trotier, 1994). Strong stimuli can even produce a silencing period of the OSNs firing evoked-activity (Reisert and Matthews 2001b; Savigner *et al.*, 2009). A reduction of the transduction current, as observed in isolated OSNs from TMEM16B KO, may decrease the OSNs depolarization producing a reduced inactivation of the voltage-gated channels leading to an increase of the number of action potentials for strong stimuli.

Thus, although the presence of CNG currents is necessary and sufficient to generate action potentials in response to a stimulus, CaCCs contribute to modulate firing duration and number of spikes.

It is well established that spontaneous activity in OSNs significantly contributes to the development and physiology of the olfactory system (Nakashima *et al.*, 2013). We tested whether the absence of CaCC influenced also the basal activity of OSNs. Different ORs have various basal activities (Reisert, 2010), leading to different sporadic activations of the transduction cascade. On average, the lack of CaCC mildly decreased the instantaneous firing frequency in TMEM16B KO compared to WT mice and did not alter the mean frequency. Contrarily, in OSNs expressing I7 OR, characterized by a high basal activity (dissociated cells, Reisert *et al.*, 2010; *in situ*, Connelly *et al.,* 2014), the lack of TMEM16B induced a pronounced reduction of both the mean and the instantaneous firing frequency. Since a sustained basal activity may be induced by a higher sporadic activation of the transduction cascade, with the contribution of CaCC, the pronounced difference observed in I7 expressing OSNs, but not in random OR expressing neurons, may be due to the relatively higher I7 basal activity.

Neuronal activity is important for circuitry formation of the olfactory system (Lodovichi and Belluscio, 2012; Yu *et al.*, 2004; Lorenzon *et al.*, 2015; Nakashima *et al.*, 2013) where it is involved in segregation of axons into glomerular structures (for review; Nishizumi and Sakano, 2015a). Since lack of CaCC influenced the basal activity of I7-expressing OSNs, we investigated axonal targeting for the I7 OR and demonstrated that nearly twice as many glomeruli were innervated in TMEM16B KO compared to WT mice. Given that the reduction of spontaneous activity has been reported to influence the organization of olfactory bulb (Yu *et al.*, 2004; Lorenzon *et al.*, 2015), it is likely that this effect was caused by the reduction of basal activity in I7 expressing OSNs. This data would be in agreement with previous reporting that the glomerular targeting of P2 and M71 expressing OSNs are not influenced in TMEM16B KO mice (Billig *et al.*, 2011).

The results of this Thesis show that OSN from TMEM16B KO are able to respond to odors with trains of action potentials, although the firing activity is overall increased. This finding justifies the lack of an evident olfactory phenotype in TMEM16B KO animals (Billig *et al.*, 2011).

Additionally TMEM16B regulates basal activity and glomerular targeting for I7 expressing neurons. Since this modulation of firing activity is much smaller in OSNs expressing random ORs, less spontaneously active OSNs may be less affected by the lack of the CaCCs since their basal firing activity is already very low. These data show that CaCC has a regulatory effect on OSNs firing activity and reopen the question of its importance in odor detection.

In conclusion, a new role for the Ca^{2+}-activated Cl^- channel in olfaction emerges, suggesting that it is not dispensable for olfaction but is required for correct action potentials generation, axonal targeting and behavior.

6 - REFERENCES

Adipietro, K. a., Mainland, J. D., and Matsunami, H. (2012). Functional Evolution of Mammalian Odorant Receptors. *PLoS Genet*, *8*(7), e1002821–e1002821.

Amjad, A., Hernandez-Clavijo, A., Pifferi, S., Maurya, D. K., Boccaccio, A., Franzot, J., Rock, J., Menini, A. (2015). Conditional knockout of TMEM16A/anoctamin1 abolishes the calcium-activated chloride current in mouse vomeronasal sensory neurons. *The Journal of General Physiology*, *145*(4), 285–301.

Asan, E., and Drenckhahn, D. (2005). Immunocytochemical characterization of two types of microvillar cells in rodent olfactory epithelium. *Histochemistry and Cell Biology*, *123*(2), 157–168.

Barnea, G., O'Donnell, S., Mancia, F., Sun, X., Nemes, a, Mendelsohn, M., and Axel, R. (2004). Odorant receptors on axon termini in the brain. *Science (New York, N.Y.)*, *304*(5676), 1468–1468.

Belluscio, L., Gold, G. H., Nemes, A., and Axel, R. (1998). Mice deficient in G(olf) are anosmic. *Neuron*, *20*(1), 69–81.

Berardi, N., Pizzorusso, T., Ratto, G. M., and Maffei, L. (2003). Molecular basis of plasticity in the visual cortex. *Trends in Neurosciences*, *26*(7), 369–378.

Billig, G. M., Pál, B., Fidzinski, P., and Jentsch, T. J. (2011). Ca2+-activated Cl− currents are dispensable for olfaction. *Nature Neuroscience*, *14*(6), 763–769.

Boccaccio, A., Lagostena, L., Hagen, V., and Menini, A. (2006). Fast adaptation in mouse olfactory sensory neurons does not require the activity of phosphodiesterase. *The Journal of General Physiology*, *128*(2), 171–184.

Boccaccio, A., and Menini, A. (2007). Temporal development of cyclic nucleotide-gated and Ca2+ -activated Cl- currents in isolated mouse olfactory sensory neurons. *Journal of Neurophysiology*, *98*(1), 153–160.

Boccaccio, A., Sagheddu, C., and Menini, A. (2011). Flash photolysis of caged compounds in the cilia of olfactory sensory neurons. *Journal of Visualized Experiments: JoVE*, (55), e3195.

Boekhoff, I., Kroner, C., and Breer, H. (1996). Second-Messenger Signalling in Olfactory Cilia. *Science*, *8*(3), 167–171.

Bozza, T., Feinstein, P., Zheng, C., and Mombaerts, P. (2002). Odorant receptor expression defines functional units in the mouse olfactory system. *The Journal of Neuroscience : The Official Journal of the Society for Neuroscience*, *22*(8), 3033–3043.

Bradley, J., Bönigk, W., Yau, K.-W., and Frings, S. (2004). Calmodulin permanently associates with rat olfactory CNG channels under native conditions Channels Under Native Conditions. *Nature Neuroscience*, *7*(7), 705–710.

Brann, J. H., and Firestein, S. J. (2014). A lifetime of neurogenesis in the olfactory system. *Frontiers in Neuroscience*, *8*(June), 1–11.

Breipohl, W., Laugwitz, H. J., and Bornfeld, N. (1974). Topological relations between the dendrites of olfactory sensory cells and sustentacular cells in different vertebrates. An ultrastructural study. *Journal of Anatomy*, *117*(Pt 1), 89.

Bronshtein, and Leontev. (1972). Sodium and potassium content in the mucus of the olfactory lining of vertebrates. *Zhurnal Evoliutsionnoĭ Biokhimii I Fiziologii*, *8*(6), 580–5.

Brunet, L. J., Gold, G. H., and Ngai, J. (1996). General anosmia caused by a targeted disruption of the mouse olfactory cyclic nucleotide-gated cation channel. *Neuron*, *17*(4), 681–693.

Brunner, J. D., Lim, N. K., Schenck, S., Duerst, A., and Dutzler, R. (2014). X-ray structure of a calcium-activated TMEM16 lipid scramblase. *Nature*, *516*(7530), 207–212.

Buck, L., and Axel, R. (1991). A novel multigene family may encode odorant receptors: A molecular basis for odor recognition. *Cell*, *65*(1), 175–187.

Caputo, A., Caci, E., Ferrera, L., Pedemonte, N., Barsanti, C., Sondo, E., Pfeffer, U., Ravazzolo, R., Zegarra-Moran, O., Galietta, L. J. V. (2008). TMEM16A, a membrane protein associated with calcium-dependent chloride channel activity. *Science*, *322*(5901), 590–4.

Carter, L. a. (2004). Olfactory Horizontal Basal Cells Demonstrate a Conserved Multipotent Progenitor Phenotype. *Journal of Neuroscience*, *24*(25), 5670–5683.

Chao, A. C., Dix, J. A., Sellers, M. C., and Verkman, A. S. (1989). Fluorescence measurement of chloride transport in monolayer cultured cells. Mechanisms of chloride transport in fibroblasts. Biophysical Journal, 56(6), 1071–1081.

Chen, T.-Y., and Yau, K.-W. (1994). Direct modulation by Ca^{2+}–calmodulin of cyclic nucleotide-activated channel of rat olfactory receptor neurons. *Nature*, *368*(6471), 545–548.

Chung, M.-K., Güler, A. D., and Caterina, M. J. (2008). TRPV1 shows dynamic ionic selectivity during agonist stimulation. *Nature Neuroscience*, *11*(5), 555–564.

Connelly, T., Savigner, A., and Ma, M. (2013). Spontaneous and sensory-evoked activity in mouse olfactory sensory neurons with defined odorant receptors. *Journal of Neurophysiology*, *110*(1), 55–62.

Connelly, T., Yu, Y., Grosmaitre, X., Wang, J., Santarelli, L. C., Savigner, A., Qiao, X., Wang, Z., Storm, D., Ma, M. (2014). G protein-coupled odorant receptors underlie mechanosensitivity in mammalian olfactory sensory neurons. *Proceedings of the National Academy of Sciences of the United States of America*, 1–6.

Cygnar, K. D., Stephan, A. B., & Zhao, H. (2010). Analyzing responses of mouse olfactory sensory neurons using the air-phase electroolfactogram recording. *Journal of Visualized Experiments: JoVE*, (37).Fsth

Crumling MA, Gold GH. (1998). Ion concentrations in the mucus covering the olfactory epithelium in rodents. Soc Neurosci Abstr. 24:2099.

Dahl, A. R., and Hadley, W. M. (1991). Nasal Cavity Enzymes Involved in Xenobiotic Metabolism: Effects on the Toxicity of Inhalants. *Critical Reviews in Toxicology*, *21*(5), 345–372.

Delay, R., and Restrepo, D. (2004). Odorant responses of dual polarity are mediated by cAMP in mouse olfactory sensory neurons. *Journal of Neurophysiology*, 1312–1319.

Dhallan, R. S., Yau, K.-W., Schrader, K. A., and Reed, R. R. (1990). Primary structure and functional expression of a cyclic nucleotide-activated channel from olfactory neurons. *Nature*, *347*(6289), 184–187.

Dibattista, M., Amjad, A., Maurya, D. K., Sagheddu, C., Montani, G., Tirindelli, R., and Menini, A. (2012). Calcium-activated chloride channels in the apical region of mouse vomeronasal sensory neurons. *The Journal of General Physiology*, *140*(1), 3–15.

Dorrscheidt, G. H. (1981). The statistical significance of the peristimulus time histogram (PSTH). *Brain Research*, *220*(2), 397–401.

Duchamp-Viret, P., Duchamp, A., and Chaput, M. A. (2000). Peripheral odor coding in the rat and frog: quality and intensity specification. *The Journal of Neuroscience: The Official Journal of the Society for Neuroscience*, *20*(6), 2383–2390.

Duran, C., and Hartzell, H. C. (2011). Physiological roles and diseases of Tmem16/Anoctamin proteins: are they all chloride channels? *Acta Pharmacologica Sinica*, *32*(6), 685–692.

Egger, V., Svoboda, K., and Mainen, Z. F. (2003). Mechanisms of lateral inhibition in the olfactory bulb: efficiency and modulation of spike-evoked calcium influx into granule cells. *The Journal of Neuroscience: The Official Journal of the Society for Neuroscience, 23*(20), 7551–7558.

Elsaesser, R., Montani, G., Tirindelli, R., and Paysan, J. (2005). Phosphatidyl-inositide signalling proteins in a novel class of sensory cells in the mammalian olfactory epithelium. *European Journal of Neuroscience*, *21*(10), 2692–2700.

Elsaesser, R., and Paysan, J. (2007). The sense of smell, its signalling pathways, and the dichotomy of cilia and microvilli in olfactory sensory cells. *BMC Neuroscience*, *8*(Suppl 3), S1.

Firestein, S., and Werblin, F. (1989). Odor-induced membrane currents in vertebrate-olfactory receptor neurons. *Science*, *244*(4900), 79–82.

Firestein, S., Shepherd, G. M., and Werblin, F. S. (1990). Time course of the membrane current underlying sensory transduction in salamander olfactory receptor neurones. *The Journal of Physiology*, *430*, 135–158.

Firestein, S., Picco, C., and Menini, A. (1993). The relation between stimulus and response in olfactory receptor cells of the tiger salamander. *The Journal of Physiology*, *468*, 1–10.

Firestein, S., and Shepherd, G. M. (1995). Interaction of anionic and cationic currents leads to a voltage dependence in the odor response of olfactory receptor neurons. *J Neurophysiol*, *73*(2), 562–567.

Firestein, S. (2001). How the olfactory system makes sense of scents. *Nature*, *413*(6852), 211–218.

Flannery, R. J., French, D. A., and Kleene, S. J. (2006). Clustering of Cyclic-Nucleotide-Gated Channels in Olfactory Cilia. *Biophysical Journal*, *91*(1), 179–188.

Francia, S., Pifferi, S., Menini, A., and Tirindelli, R. (2014). Vomeronasal Receptors and Signal Transduction in the Vomeronasal Organ of Mammals. In C. Mucignat-Caretta (Ed.), *Neurobiology of Chemical Communication*. Boca Raton (FL): CRC Press/Taylor and Francis.

Frings, S., and Lindemann, B. (1990). Single unit recording from olfactory cilia. *Biophysical Journal*, *57*(5), 1091–1094.

Frings, S., and Lindemann, B. (1991). Current recording from sensory cilia of olfactory receptor cells in situ. I. The neuronal response to cyclic nucleotides. *The Journal of General Physiology*, *97*(1), 1–16.

Godfrey, P. A., Malnic, B., and Buck, L. B. (2004). The mouse olfactory receptor gene family. *Proceedings of the National Academy of Sciences of the United States of America*, *101*(7), 2156–2161.

Graziadei, P., and Graziadei, G. M. (1978). Continuous nerve cell renewal in the olfactory system. *Development of Sensory Systems: Handbook of Sensory Physiology*, *9*, 55–83.

Grosmaitre, X., Santarelli, L. C., Tan, J., Luo, M., and Ma, M. (2007). Dual functions of mammalian olfactory sensory neurons as odor detectors and mechanical sensors. *Nature Neuroscience*, *10*(3), 348–354.

Grosmaitre, X., Vassalli, A., Mombaerts, P., Shepherd, G. M., and Ma, M. (2006). Odorant responses of olfactory sensory neurons expressing the odorant receptor MOR23: a patch clamp analysis in gene-targeted mice. *Proceedings of the National Academy of Sciences of the United States of America*, *103*(6), 1970–1975.

Grosmaitre, X., Fuss, S. H., Lee, A. C., Adipietro, K. A., Matsunami, H., Mombaerts, P., and Ma, M. (2009). SR1, a Mouse Odorant Receptor with an Unusually Broad Response Profile. *The Journal of Neuroscience : The Official Journal of the Society for Neuroscience*, *29*(46), 14545

Hall, S. E., Floriano, W. B., Vaidehi, N., and Goddard, W. A. (2004). Predicted 3-D structures for mouse I7 and rat I7 olfactory receptors and comparison of predicted odor recognition profiles with experiment. *Chemical Senses*, *29*(7), 595–616.

Hartzell, C., Putzier, I., and Arreola, J. (2005). Calcium-Activated Chloride Channels. *Annual Review of Physiology*, *67*(1), 719–758.

Hengl, T., Kaneko, H., Dauner, K., Vocke, K., Frings, S., and Mohrlen, F. (2010). Molecular components of signal amplification in olfactory sensory cilia. *Proceedings of the National Academy of Sciences*, *107*(13), 6052–6057.

Hille, B. (2001). *Ion Channels of Excitable Membranes, Third Edition* (3rd Edition edition). Sunderland, Mass.: Sinauer Associates.

Huang, W. C., Xiao, S., Huang, F., Harfe, B. D., Jan, Y. N., and Jan, L. Y. (2012). Calcium-Activated Chloride Channels (CaCCs) Regulate Action Potential and Synaptic Response in Hippocampal Neurons. *Neuron*, *74*(1), 179–192.

Huard, J. M. T., Youngentob, S. L., Goldstein, B. J., Luskin, M. B., and Schwob, J. E. (1998). Adult olfactory epithelium contains multipotent progenitors that give rise to neurons and non-neural cells. *Journal of Comparative Neurology*, *400*(November 1997), 469–486.

Huberman, A. D., Feller, M. B., and Chapman, B. (2008). Mechanisms underlying development of visual maps and receptive fields. *Annual Review of Neuroscience*, *31*, 479–509.

Imai, T. (2014). Construction of functional neuronal circuitry in the olfactory bulb. *Seminars in Cell and Developmental Biology*, *35*, 180–188.

Jarriault, D., and Grosmaitre, X. (2015). Perforated Patch-clamp Recording of Mouse Olfactory Sensory Neurons in Intact Neuroepithelium: Functional Analysis of Neurons Expressing an Identified Odorant Receptor. *Journal of Visualized Experiments*, (101), 1–10.

Johns, D. C., Marx, R., Mains, R. E., O'Rourke, B., and Marban, E. (1999). Inducible Genetic Suppression of Neuronal Excitability. *J. Neurosci.*, *19*(5), 1691–1697.

Joshi, H., Getchell, M. L., Zielinski, B., and Getchell, T. V. (1987). Spectrophotometric determination of cation concentrations in olfactory mucus. *Neuroscience Letters*, *82*(3), 321–326.

Kaneko, H., Nakamura, T., and Lindemann, B. (2001). Noninvasive measurement of chloride concentration in rat olfactory receptor cells with use of a fluorescent dye. *American Journal of Physiology. Cell Physiology*, *280*(6), C1387–C1393.

Kaneko, H., Putzier, I., Frings, S., Kaupp, U. B., and Gensch, T. (2004). Chloride accumulation in mammalian olfactory sensory neurons. *The Journal of Neuroscience: The Official Journal of the Society for Neuroscience*, *24*(36), 7931–7938.

Khakh, B. S., Bao, X. R., Labarca, C., and Lester, H. a. (1999). Neuronal P2X transmitter-gated cation channels change their ion selectivity in seconds. *Nature Neuroscience*, *2*(4), 322–330.

Kim, S., Ma, L., and Yu, C. R. (2011). Requirement of calcium-activated chloride channels in the activation of mouse vomeronasal neurons. *Nature Communications*, *2*(May), 365–365.

Kirkby, L., Sack, G., Firl, A., and Feller, M. B. (2013). A role for correlated spontaneous activity in the assembly of neural circuits. *Neuron*, *80*(5), 1129–1144.

Kleene, S. J., and Gesteland, R. C. (1991). Calcium-activated chloride conductance in frog olfactory cilia. *J Neurosci*, *11*(11), 3624–9.

Kleene, S. J. (1993). Origin of the chloride current in olfactory transduction. *Neuron*, *11*(1), 123–132.

Kleene, S. J., and Pun, R. Y. (1996). Persistence of the olfactory receptor current in a wide variety of extracellular environments. *Journal of Neurophysiology*, *75*(4), 1386–1391.

Kleene, S. J. (1997). High-gain, low-noise amplification in olfactory transduction. *Biophysical Journal*, *73*(2), 1110–1117.

Kleene, S. J. (2008). The electrochemical basis of odor transduction in vertebrate olfactory cilia. *Chemical Senses*, *33*(9), 839–859.

Krautwurst, D., Yau, K., and Reed, R. R. (1998). Identification of ligands for olfactory receptors. *Cell*, *95*, 917–926.

Kurahashi, T. (1989). Activation by odorants of cation-selective conductance in the olfactory receptor cell isolated from the newt. *The Journal of Physiology*, *419*, 177–192.

Kurahashi, T., and Yau, K.-W. (1993). Co-existence of cationic and chloride components in odorant-induced current of vertebrate olfactory receptor cells. *Nature*, *363*(6424), 71–74.

Kurahashi, T., and Menini, A. (1997). Mechanism of odorant adaptation in the olfactory receptor cell. *Nature*, *385*(6618), 725–729.

Lagostena, L., and Menini, A. (2003). Whole-cell recordings and photolysis of caged compounds in olfactory sensory neurons isolated from the mouse. *Chemical Senses*, *28*(8), 705–716.

Larsson, H. P., Kleene, S. J., and Lecar, H. (1997). Noise analysis of ion channels in non-space-clamped cables: estimates of channel parameters in olfactory cilia. *Biophysical Journal*, *72*(3), 1193–1203.

Leinders-Zufall, T., Rand, M. N., Shepherd, G. M., Greer, C. A., and Zufall, F. (1997). Calcium entry through cyclic nucleotide-gated channels in individual cilia of olfactory receptor cells: spatiotemporal dynamics. The Journal of Neuroscience: The Official Journal of the Society for Neuroscience, 17(11), 4136–4148.

Li, F., Ponissery-Saidu, S., Yee, K., Wang, H., Chen, M.-L., Iguchi, N., Zhang, G., Jiang, P., Reisert, J., Huang, L. (2013). Heterotrimeric G protein subunit Gγ13 is critical to olfaction. *The Journal of Neuroscience : The Official Journal of the Society for Neuroscience*, *33*(18), 7975–7984.

Lindemann, B. (2001). Predicted profiles of ion concentrations in olfactory cilia in the steady state. *Biophysical Journal*, *80*(4), 1712–21.

Ling, G., Gu, J., Genter, M. B., Zhuo, X., and Ding, X. (2004). Regulation of cytochrome P450 gene expression in the olfactory mucosa. *Chemico-Biological Interactions*, *147*(3), 247–258.

Lodovichi, C., and Belluscio, L. (2012). Odorant receptors in the formation of the olfactory bulb circuitry. *Physiology (Bethesda, Md.)*, *27*(4), 200–212.

Lorenzon, P., Redolfi, N., Podolsky, M. J., Zamparo, I., Franchi, S. A., Pietra, G., Boccaccio, A., Menini, A., Murthy, V., Lodovichi, C. (2015). Circuit formation and function in the olfactory bulb of mice with reduced spontaneous afferent activity. *The Journal of Neuroscience: The Official Journal of the Society for Neuroscience*, *35*(1), 146–160.

Lowe, G., and Gold, G. H. (1991). The spatial distributions of odorant sensitivity and odorant-induced currents in salamander olfactory receptor cells. *The Journal of Physiology*, *442*, 147–168.

Lowe, G., and Gold, G. H. (1993). Nonlinear amplification by calcium-dependent chloride channels in olfactory receptor cells. *Nature*, *366*(6452), 283–286.

Lynch, J. W., and Barry, P. H. (1989). Action potentials initiated by single channels opening in a small neuron (rat olfactory receptor). *Biophysical Journal*, *55*(4), 755–68.

Ma, M., Chen, W. R., and Shepherd, G. M. (1999). Electrophysiological characterization of rat and mouse olfactory receptor neurons from an intact epithelial preparation. *Journal of Neuroscience Methods*, *92*(1-2), 31–40.

Ma, M. (2010). Multiple Olfactory Subsystems Convey Various Sensory Signals. In A. Menini (Ed.), The Neurobiology of Olfaction. Boca Raton (FL): CRC Press/Taylor and Francis.

Ma, L., Wu, Y., Qiu, Q., Scheerer, H., Moran, A., and Yu, C. R. (2014). A Developmental Switch of Axon Targeting in the Continuously Regenerating Mouse Olfactory System of Axon. *Science (New York, N.Y.)*, *194*(APRIL), 194–197.

MacVicar, B. A. (2015). Driving the Early Auditory Network the Old-Fashioned Way. *Cell*, *163*(6), 1307–1308.

Malnic, B. (2007). Searching for the ligands of odorant receptors. *Molecular Neurobiology*, *35*(2), 175–181.

Marieb, E. N., Mitchell, S. J., and Smith, L. A. (2013). Human Anatomy and Physiology Laboratory Manual, Main Version, 10th Edition (10 edition). Pearson.

Markopoulos, F., Rokni, D., Gire, D. H., and Murthy, V. N. (2012). Functional Properties of Cortical Feedback Projections to the Olfactory Bulb. *Neuron*, *76*(6), 1175–1188.

Matthews, H.R. (1999). A compact modular flow heater for the superfusion of mammalian cells. *The journal of Physiology,* 518.P, 13P.

Matsuzaki, O., Bakin, R. E., Cai, X., Menco, B. P., and Ronnett, G. V. (1999). Localization of the olfactory cyclic nucleotide-gated channel subunit 1 in normal, embryonic and regenerating olfactory epithelium. *Neuroscience*, 94(1), 131–140.

Maue, R. a, and Dionne, V. E. (1987). Patch-clamp studies of isolated mouse olfactory receptor neurons. *The Journal of General Physiology*, *90*(1), 95–125.

Maurya, D. K., and Menini, A. (2014). Developmental expression of the calcium-activated chloride channels TMEM16A and TMEM16B in the mouse olfactory epithelium. *Developmental Neurobiology*, *74*, 657–675.

Mayer, U., Küller, A., Daiber, P. C., Neudorf, I., Warnken, U., Schnölzer, M., Frings, S., Möhrlen, F. (2009). The proteome of rat olfactory sensory cilia. *Proteomics*, *9*(2), 322–34.

Menco, B. P. M., Bruch, R. C., Dau, B., and Danho, W. (1992). Ultrastructural localization of olfactory transduction components: the G protein subunit Golfα and type III adenylyl cyclase. *Neuron*, *8*(3), 441–453.

Menco, B. P. M. (1997). Ultrastructural aspects of olfactory signaling. *Chemical Senses*, *22*(3), 295–311.

Menco, B. P. M., Birrell, G. B., Fuller, C. M., Ezeh, P. I., Keeton, D. a, and Benos, D. J. (1998). Ultrastructural localization of amiloride-sensitive sodium channels and Na+,K+-ATPase in the rat's olfactory epithelial surface. *Chemical Senses*, *23*(2), 137–149.

Menco, Bp., and Morrison, E. E. (2003). Morphology of the mammalian olfactory epithelium: form, fine structure, function, and pathology. *Neurological disease and therapy*, *57*, 17–50.

Mobley, A. S., Miller, A. M., Araneda, R. C., Maurer, L. R., Müller, F., and Greer, C. A. (2010). Hyperpolarization-activated cyclic nucleotide-gated channels in olfactory sensory neurons regulate axon extension and glomerular formation. *The Journal of Neuroscience: The Official Journal of the Society for Neuroscience*, *30*(49), 16498–16508.

Mombaerts, P., Wang, F., Dulac, C., Chao, S. K., Nemes, A., Mendelsohn, M., Edmondson, J., Axel, R. (1996). Visualizing an olfactory sensory map. *Cell*, *87*(4), 675–686.

Monahan, K., and Lomvardas, S. (2015). Monoallelic Expression of Olfactory Receptors. *Annual Review of Cell and Developmental Biology*, *31*(1), 721–740.

Mori, K., and Sakano, H. (2011). How Is the Olfactory Map Formed and Interpreted in the Mammalian Brain? *Annual Review of Neuroscience*, *34*(1), 467–499.

Morrison, E. E., and Costanzo, R. M. (1990). Morphology of the human olfactory epithelium. *The Journal of Comparative Neurology*, *297*(1), 1–13.

Munger, S. D., Leinders-Zufall, T., and Zufall, F. (2009). Subsystem Organization of the Mammalian Sense of Smell. *Annual Review of Physiology*, *71*(1), 115–140.

Murphy, G. J., Darcy, D. P., and Isaacson, J. S. (2005). Intraglomerular inhibition: signaling mechanisms of an olfactory microcircuit. *Nature Neuroscience*, *8*(3), 354–364.

Nakamura, T., and Gold, G. H. (1987). A cyclic nucleotide-gated conductance in olfactory receptor cilia. *Nature*, *325*(6103), 442–444.

Nakashima, N., Ishii, T. M., Bessho, Y., Kageyama, R., and Ohmori, H. (2013). Hyperpolarisation-activated cyclic nucleotide-gated channels regulate the spontaneous firing rate of olfactory receptor neurons and affect glomerular formation in mice. *The Journal of Physiology*, *591*(7), 1749–1769.

Nickell, W. T., Kleene, N. K., Gesteland, R. C., and Kleene, S. J. (2006). Neuronal Chloride Accumulation in Olfactory Epithelium of Mice Lacking NKCC1. *Journal of Neurophysiology*, *95*(3), 2003–2006.

Nickell, W. T., Kleene, N. K., and Kleene, S. J. (2007). Mechanisms of neuronal chloride accumulation in intact mouse olfactory epithelium. *The Journal of Physiology*, *583*(3), 1005–1020.

Niimura, Y., and Nei, M. (2005). Comparative evolutionary analysis of olfactory receptor gene clusters between humans and mice. *Gene*, *346*, 13–21.

Nishizumi, H., and Sakano, H. (2015a). Developmental regulation of neural map formation in the mouse olfactory system. *Developmental Neurobiology*, *75*(6), 594–607.

Nishizumi, H., and Sakano, H. (2015b). Decoding and deorphanizing an olfactory map. *Nature Neuroscience*, *18*(10), 1432–1433.

Nomura, T., Takahashi, S., and Ushiki, T. (2004). Cytoarchitecture of the normal rat olfactory epithelium: light and scanning electron microscopic studies. *Archives of Histology and Cytology*, *67*(2), 159–170.

Nunemaker, C. S., DeFazio, R. A., and Moenter, S. M. (2003). A targeted extracellular approach for recording long-term firing patterns of excitable cells: a practical guide. *Biological Procedures Online*, *5*(1), 53–62.

O'Connell, R. J., and Mozell, M. M. (1969). Quantitative stimulation of frog olfactory receptors. *Journal of Neurophysiology*, *32*(1), 51–63.

Ottoson, D. (1955). Analysis of the electrical activity of the olfactory epithelium. *Acta Physiologica Scandinavica*. Supplementum, 35(122), 1–83.

Pedemonte, N., and Galietta, L. J. V. (2014). Structure and Function of TMEM16 Proteins (Anoctamins). *Physiological Reviews*, *94*(2), 419–459.

Pifferi, S., Boccaccio, A., and Menini, A. (2006a). Cyclic nucleotide-gated ion channels in sensory transduction. *FEBS Letters*, *580*(12), 2853–2859.

Pifferi, S., Pascarella, G., Boccaccio, A., Mazzatenta, A., Gustincich, S., Menini, A., and Zucchelli, S. (2006b). Bestrophin-2 is a candidate calcium-activated chloride channel involved in olfactory transduction. *Proceedings of the National Academy of Sciences of the United States of America*, *103*(34), 12929–34.

Pifferi, S., Dibattista, M., and Menini, A. (2009). TMEM16B induces chloride currents activated by calcium in mammalian cells. *Pflugers Archiv European Journal of Physiology*, *458*(6), 1023–1038.

Pifferi, S., Menini, A., and Kurahashi, T. (2010). Signal Transduction in Vertebrate Olfactory Cilia. In A. Menini (Ed.), The Neurobiology of Olfaction. Boca Raton (FL): CRC Press/Taylor and Francis.

Pifferi, S., Cenedese, V., and Menini, A. (2012). Anoctamin 2/TMEM16B: a calcium-activated chloride channel in olfactory transduction. *Experimental Physiology*, *97*(2), 193–199.

Pifferi, S., and Menini, A. (2015) The Olfactory System: From Odorant Molecules to Perception. In, Aromatherapy: basic mechanism and evidence based clinical use. CRCPress

Ponissery Saidu, S., Dibattista, M., Matthews, H. R., and Reisert, J. (2012). Odorant-induced responses recorded from olfactory receptor neurons using the suction pipette technique. *Journal of Visualized Experiments: JoVE*, (62), e3862.

Ponissery Saidu, S., Stephan, A. B., Talaga, A. K., Zhao, H., Reisert, J., Saidu, S. P., Stephan, A., Talaga, A., Zhao, H., Reisert, J. (2013). Channel properties of the splicing isoforms of the olfactory calcium-activated chloride channel Anoctamin 2. *The Journal of General Physiology*, *141*(6), 691–703.

Pun, R. Y. K., and Kleene, S. J. (2004). An estimate of the resting membrane resistance of frog olfactory receptor neurones. *The Journal of Physiology*, *559*(Pt 2), 535–542.

Rasche, S., Toetter, B., Adler, J., Tschapek, A., Doerner, J. F., Kurtenbach, S., Hatt, H., Meyer, H., Warscheid, B., Neuhaus, E. M. (2010). Tmem16b is specifically expressed in the cilia of olfactory sensory neurons. *Chemical Senses*, *35*(3), 239–245.

Reisert, J., and Matthews, H. R. (1999). Adaptation of the odour-induced response in frog olfactory receptor cells. *The Journal of Physiology*, *519.3*, 801–13.

Reisert, J., and Matthews, H. R. (2001a). Response properties of isolated mouse olfactory receptor cells. The Journal of Physiology, 530(1), 113–113.

Reisert, J., and Matthews, H. R. (2001b). Responses to prolonged odour stimulation in frog olfactory receptor cells. The Journal of Physiology, 534(Pt 1), 179–191.

Reisert, J., Bauer, P. J., Yau, K.-W., and Frings, S. (2003). The Ca-activated Cl Channel and its Control in Rat Olfactory Receptor Neurons. *Journal of General Physiology*, *122*(3), 349–63.

Reisert, J., Lai, J., Yau, K.-W., and Bradley, J. (2005). Mechanism of the Excitatory Cl− Response in Mouse Olfactory Receptor Neurons. *Neuron*, *45*(4), 553–561.

Reisert, J., Yau, K.-W., and Margolis, F. L. (2007). Olfactory marker protein modulates the cAMP kinetics of the odour-induced response in cilia of mouse olfactory receptor neurons. *The Journal of Physiology*, *585*(Pt 3), 731–740.

Reisert, J. (2010). Origin of basal activity in mammalian olfactory receptor neurons. *The Journal of General Physiology*, *136*(5), 529–540.

Ressler, K. J., Sullivan, S. L., and Buck, L. B. (1993). A zonal organization of odorant receptor gene expression in the olfactory epithelium. *Cell*, *73*(3), 597–609.

Restrepo, D. (2005). The ins and outs of intracellular chloride in olfactory receptor neurons. Neuron, 45(4), 481–482.

Reuter, D., Zierold, K., Schröder, W. H., and Frings, S. (1998). A depolarizing chloride current contributes to chemoelectrical transduction in olfactory sensory neurons in situ. *The Journal of Neuroscience : The Official Journal of the Society for Neuroscience*, *18*(17), 6623–30.

Rochelle, L. G., Li, D. C., Ye, H., Lee, E., Talbot, C. R., and Boucher, R. C. (2000). Distribution of ion transport mRNAs throughout murine nose and lung. *American Journal of Physiology. Lung Cellular and Molecular Physiology*, *279*(7248), L14–L24.

Rospars, J.-P., Lánský, P., Duchamp, A., and Duchamp-Viret, P. (2003). Relation between stimulus and response in frog olfactory receptor neurons in vivo. *The European Journal of Neuroscience*, *18*(5), 1135–1154.

Rowley III, J. C., Moran, D. T., and Jafek, B. W. (1989). Peroxidase backfills suggest the mammalian olfactory epithelium contains a second morphologically distinct class of bipolar sensory neuron: the microvillar cell. *Brain Research*, *502*(2), 387–400.

Sagheddu, C., Boccaccio, A., Dibattista, M., Montani, G., Tirindelli, R., and Menini, A. (2010). Calcium concentration jumps reveal dynamic ion selectivity of calcium-activated chloride currents in mouse olfactory sensory neurons and TMEM16b-transfected HEK 293T cells. *The Journal of Physiology*, *588*(Pt 21), 4189–204.

Savigner, A., Duchamp-Viret, P., Grosmaitre, X., Chaput, M., Garcia, S., Ma, M., and Palouzier-Paulignan, B. (2009). Modulation of spontaneous and odorant-evoked activity of rat olfactory sensory neurons by two anorectic peptides, insulin and leptin. *Journal of Neurophysiology*, *101*(6), 2898–2906.

Schild, D., and Restrepo, D. (1998). Transduction Mechanisms in Vertebrate Olfactory Receptor Cells. *Physiological Reviews*, *78*(2), 429–466.

Schroeder, B. C., Cheng, T., Jan, Y. N., and Jan, L. Y. (2008). Expression Cloning of TMEM16A as a Calcium-Activated Chloride Channel Subunit. *Cell*, *134*(6), 1019–1029.

Schwenk, F., Baron, U., and Rajewsky, K. (1995). A cre-transgenic mouse strain for the ubiquitous deletion of loxP-flanked gene segments including deletion in germ cells. *Nucleic Acids Research*, *23*(24), 5080–5081.

Shepherd, G. M., Greer, C. a, Mazzarello, P., and Sassoè-Pognetto, M. (2011). The first images of nerve cells: Golgi on the olfactory bulb 1875. *Brain Research Reviews*, *66*(1-2), 92–105.

Shimazaki, H., and Shinomoto, S. (2007). A method for selecting the bin size of a time histogram. *Neural Computation*, *19*(6), 1503–1527.

Smith, D. W., Thach, S., Marshall, E. L., Mendoza, M.-G., and Kleene, S. J. (2008). Mice lacking NKCC1 have normal olfactory sensitivity. *Physiology and Behavior*, *93*(1–2), 44–49.

Song, Y., Cygnar, K. D., Sagdullaev, B., Valley, M., Hirsh, S., Stephan, A., Reisert, J., Zhao, H. (2008). Olfactory CNG Channel Desensitization by Ca2+/CaM via the B1b Subunit Affects Response Termination but Not Sensitivity to Recurring Stimulation. *Neuron*, *58*(3), 374–386.

Sosulski, D. L., Lissitsyna Bloom, M., Cutforth, T., Axel, R., and Datta, S. R. (2011). Distinct representations of olfactory information in different cortical centres. *Nature*, *472*(7342), 213–216.

Spolidoro, M., Sale, A., Berardi, N., and Maffei, L. (2009). Plasticity in the adult brain: lessons from the visual system. *Experimental Brain Research*, *192*(3), 335–341.

Stephan, A. B., Shum, E. Y., Hirsh, S., Cygnar, K. D., Reisert, J., and Zhao, H. (2009). ANO2 is the cilial calcium-activated chloride channel that may mediate olfactory amplification. *Proceedings of the National Academy of Sciences of the United States of America*, *106*(28), 11776–11781.

Stephan, A. B., Tobochnik, S., Dibattista, M., Wall, C. M., Reisert, J., and Zhao, H. (2012). The Na(+)/Ca(2+) exchanger NCKX4 governs termination and adaptation of the mammalian olfactory response. Nature Neuroscience, 15(1), 131–137.

Strader, C. D., Fong, T. M., Graziano, M. P., and Tota, M. R. (1995). The family of G-protein-coupled receptors. *The FASEB Journal : Official Publication of the Federation of American Societies for Experimental Biology*, *9*(9), 745–754.

Strotmann, J., Wanner, I., Krieger, J., Raming, K., and Breer, H. (1992). Expression of odorant receptors in spatially restricted subsets of chemosensory neurones. Neuroreport, 3(12), 1053–1056.

Sullivan, Kj, R., and Lb, B. (1993). Odorant receptor diversity and patterned gene expression in the mammalian olfactory epithelium. *Progress in Clinical and Biological Research*, *390*, 75–84.

Takeuchi, H., and Kurahashi, T. (2002). Photolysis of caged cyclic AMP in the ciliary cytoplasm of the newt olfactory receptor cell. *The Journal of Physiology*, *541*(Pt 3), 825–833.

Takeuchi, H., and Kurahashi, T. (2005). Mechanism of Signal Amplification in the Olfactory Sensory Cilia. *The Journal of Neuroscience*, *25*(48), 11084–11091.

Takeuchi, H., and Sakano, H. (2014). Neural map formation in the mouse olfactory system. *Cellular and Molecular Life Sciences: CMLS*, *71*(16), 3049–3057.

Tan, J., Savigner, A., Ma, M., and Luo, M. (2010). Odor information processing by the olfactory bulb analyzed in gene-targeted mice. *Neuron*, *65*(6), 912–926.

Tirindelli, R., Dibattista, M., Pifferi, S., and Menini, A. (2009). From pheromones to behavior. Physiological Reviews, 89(3), 921–956.

Tomaru, A., and Kurahashi, T. (2005). Mechanisms determining the dynamic range of the bullfrog olfactory receptor cell. *Journal of Neurophysiology*, *93*(4), 1880–8.

Trotier, D., and MacLeod, P. (1983). Intracellular recordings from salamander olfactory receptor cells. *Brain Research*, *268*(2), 225–237.

Trotier, D. (1994). Intensity coding in olfactory receptor cells. *Semin Cell Biol*, *5*(1), 47–54.

Trotier, D. (1998). Electrophysiological properties of frog olfactory supporting cells. *Chemical Senses*, *23*(3), 363–369.

Trzaskowski, B., Latek, D., Yuan, S., Ghoshdastider, U., Debinski, a., and Filipek, S. (2012). Action of Molecular Switches in GPCRs - Theoretical and Experimental Studies. *Current Medicinal Chemistry*, *19*(8), 1090–1109.

Vassar, R., Ngai, J., and Axel, R. (1993). Spatial segregation of odorant receptor expression in the mammalian olfactory epithelium. *Cell*, *74*(2), 309–318.

Wang, H. C., Lin, C.-C., Cheung, R., Zhang-Hooks, Y., Agarwal, A., Ellis-Davies, G., Rock, J., Bergles, D. E. (2015). Spontaneous Activity of Cochlear Hair Cells Triggered by Fluid Secretion Mechanism in Adjacent Support Cells. *Cell*, *163*(6), 1348–1359.

Wong, S. T., Trinh, K., Hacker, B., Chan, G. C., Lowe, G., Gaggar, A., Xia, Z., Gold, G., Storm, D. R. (2000). Disruption of the type III adenylyl cyclase gene leads to peripheral and behavioral anosmia in transgenic mice. *Neuron*, *27*, 487–497.

Yang, Y. D., Cho, H., Koo, J. Y., Tak, M. H., Cho, Y., Shim, W.-S., Park, S., Lee, J., Lee, B., Kim, B., Raouf, R., Shin, Y., Oh, U. (2008). TMEM16A confers receptor-activated calcium-dependent chloride conductance. *Nature*, *455*(7217), 1210–1215.

Yang, C., and Delay, R. J. (2010). Calcium-activated chloride current amplifies the response to urine in mouse vomeronasal sensory neurons. *The Journal of General Physiology*, *135*(1), 3–13.

Yang, H., Kim, A., David, T., Palmer, D., Jin, T., Tien, J., Huang, F., Cheng , T., Coughlin , S., Jan, Y., Jan, L., Y., (2012). TMEM16F forms a Ca2+-activated cation channel required for lipid scrambling in platelets during blood coagulation. *Cell*, *151*(1), 111–22.

Yu, C. R., Power, J., Barnea, G., O'Donnell, S., Brown, H. E. V., Osborne, J., Axel, R., Gogos, J. a. (2004). Spontaneous neural activity is required for the establishment and maintenance of the olfactory sensory map. *Neuron*, *42*(4), 553–566.

Yu, T.-T., McIntyre, J. C., Bose, S. C., Hardin, D., Owen, M. C., and McClintock, T. S. (2005). Differentially expressed transcripts from phenotypically identified olfactory sensory neurons. *The Journal of Comparative Neurology*, *483*(3), 251–262.

Zhainazarov, A. B., and Ache, B. W. (1995). Odor-induced currents in Xenopus olfactory receptor cells measured with perforated-patch recording. *Journal of Neurophysiology*, *74*(1), 479–83.

Zhang, X., and Firestein, S. (2002). The olfactory receptor gene superfamily of the mouse. *Nature Neuroscience*, *5*(2), 124–133.

Zhao, H., Ivic, L., Otaki, J. M., Hashimoto, M., Mikoshiba, K., and Firestein, S. (1998). Functional expression of a mammalian odorant receptor. *Science (New York, N.Y.)*, *279*(5348), 237–242.

Zheng, C., Feinstein, P., Bozza, T., Rodriguez, I., and Mombaerts, P. (2000). Peripheral olfactory projections are differentially affected in mice deficient in a cyclic nucleotide-gated channel subunit. *Neuron*, *26*(1), 81–91.

Zufall, F., Shepherd, G. M., and Firestein, S. (1991). Inhibition of the Olfactory Cyclic Nucleotide Gated Ion Channel by Intracellular Calcium. *Proceedings of the Royal Society of London B: Biological Sciences*, *246*(1317), 225–230.

Zufall, F., and Leinders-Zufall, T. (2000). The cellular and molecular basis of odor adaptation. *Chemical Senses*, *25*(4), 473–481.

Acknowledgments

In these lines I would like to acknowledge the people who helped me during the last 4 years of PhD. First, I thank my advisors Dr.ssa Anna Boccaccio and Prof.ssa Anna Menini. They are enthusiastic scientists who taught me how to become a researcher. Most of the knowledge collected during the PhD derived from them. Thank you for believing in me and for being patient concerning all my personal crisis and continuous delays. A special thanks to Anna Boccaccio who, since not physically present in SISSA, was always present to encourage me in getting better. She always listened to all my ideas discussing about all strange speculations I proposed.

Special acknowledgements to all the people who spent time in SISSA in the last 4 years. They make a wonderful international environment where I have been able to express and to develop my personality. Thanks to SISSA Medialab for the possibility to improve my communication skill and express my creativity. A special acknowledgement to all people of the Neurobiology sector. Thanks to all the professors for teaching, advising and following me in PhD project. Thanks to the technician staff for continuous help in laboratory issues. Thanks to the administration staff that following all the bureaucratic aspects makes simpler our research work. Finally, thanks to all the sector students for making a community which was a wonderful and stimulating place to interact and to discuss with. Thanks to Dr. Xavier Grosmaitre and Prof. Albertino Bigiani for accepting the roles of external examiners of my Thesis.

I would like to acknowledge also all my past and present lab members for helping me during my experiments and for creating a no pressure and stimulating environment to work. A special acknowledgement to Simone Pifferi for all the critiques and advices about both scientific and socio-humanistic situations. He stimulated me not only as a scientist but also as aware person. Thanks to Stefano Stabilini for accepting me as friend and for coming me back to reality by his concreteness. Thanks to his patience, since I suppose that it is not easy being my lab-mate, office-mate and home-mate at the same time.

An acknowledgement to all people outside SISSA who made enjoyable my life in Trieste. Thanks to my volley teams, Polisportiva Prevenire and SISSA volley. They gave me the possibility to rediscover the old passion for volley, softening these years of work. Thanks to my present home-mates Alessandro, Arianna, Mattia and Stefano for not charging on me the search of a new home in this last part of PhD.

Thanks to Andrea, Dario, Orello, Pialla, Lisa and Stefano for being as a second family here in Trieste. They created a confortable and familiar home to live and to rest. Thank for being close to me during the most difficult times of these last 4 years. Thanks to Patrizio Stefano who taught me how to use some sides of my personality that I did not know. I would like also to thank Rhea Arini who believed in me during a difficult situation. Becoming one of my best counselor and friend, she taught me that every cloud has a silver lining, and that all does not have necessarily to finish, but something might only change.

I also want to acknowledge my family and friends in Tuscany. I am lucky to be surrounded by people who supported me in all my decisions and endeavors. They encourage in following my dreams even if it means to be far away from them.

Finally, a special acknowledgement to Trieste. Although it is a historical city on the boarder not only of a nation but of different cultures, it is well people-oriented not being chaotic as often multi-ethnic realities are. A place full of contradictions, from the Austro-Hungarian town center to commercial arbor, from Barcola to the iron foundry. A place where it was wonderful to live. I will never forget these last 4 years.

Trieste 28th March 2016